PARTICLE FLOW CELL FORMATION AT MINIMUM FLUIDIZATION FLOW RATES IN A RECTANGULAR GAS-FLUIDIZED BED

Michael Charles Morgan

NAVAL POSTGRADUATE SCHOOL
Monterey, California

THESIS

PARTICLE FLOW CELL FORMATION AT
MINIMUM FLUIDIZATION FLOW RATES
IN A RECTANGULAR GAS-FLUIDIZED BED

by

Michael Charles Morgan

March 1981

Thesis Advisor: P. F. Pucci

Approved for public release; distribution unlimited

SECURITY CLASSIFICATION OF THIS PAGE (When Data Entered)

REPORT DOCUMENTATION PAGE

READ INSTRUCTIONS BEFORE COMPLETING FORM

1. REPORT NUMBER	2. GOVT ACCESSION NO. / 3. RECIPIENT'S CATALOG NUMBER
4. TITLE (and Subtitle): Particle Flow Cell Formation at Minimum Fluidization Flow Rates in a Rectangular Gas-Fluidized Bed	5. TYPE OF REPORT & PERIOD COVERED: Master's Thesis; March 1981 / 6. PERFORMING ORG. REPORT NUMBER
7. AUTHOR(s): Michael Charles Morgan	8. CONTRACT OR GRANT NUMBER(s)
9. PERFORMING ORGANIZATION NAME AND ADDRESS: Naval Postgraduate School, Monterey, California 93940	10. PROGRAM ELEMENT, PROJECT, TASK AREA & WORK UNIT NUMBERS
11. CONTROLLING OFFICE NAME AND ADDRESS: Naval Postgraduate School, Monterey, California 93940	12. REPORT DATE: March 1981 / 13. NUMBER OF PAGES: 161
14. MONITORING AGENCY NAME & ADDRESS (if different from Controlling Office)	15. SECURITY CLASS. (of this report): Unclassified / 15a. DECLASSIFICATION/DOWNGRADING SCHEDULE

16. DISTRIBUTION STATEMENT (of this Report)

Approved for public release; distribution unlimited.

17. DISTRIBUTION STATEMENT (of the abstract entered in Block 20, if different from Report)

18. SUPPLEMENTARY NOTES

19. KEY WORDS (Continue on reverse side if necessary and identify by block number)

Gas-fluidization
Bed particle cell
Fluidization flow cell

20. ABSTRACT (Continue on reverse side if necessary and identify by block number)

This study was conducted at the Naval Postgraduate School to investigate the formation of particle flow cells at minimum fluidization gas flow rates in a rectangular gas-fluidized bed. The primary objective is to determine if multiple cell formation occurs as the bed width to height ratio increases. The settled bed height is maintained at a constant level for all runs. The secondary objective is to determine if the presence of external

DD FORM 1 JAN 73 1473 EDITION OF 1 NOV 65 IS OBSOLETE
S/N 0102-014-6601

SECURITY CLASSIFICATION OF THIS PAGE (When Data Entered)

plate heaters at the end walls of the particle bed will alter the particle flow cell formation patterns when energized and to what extent they affect the fluid mixing (heat transfer) flow patterns within the particle flow. Pressure measurements across the bed are used to determine minimum fluidization points and thermocouple probe measurements determined the thermal gradients within the bed for each bed configuration. Visual observations on the external bed movement are included in the determination of the results of this experimental study.

Approved for public release; distribution unlimited.

Particle Flow Cell Formation at Minimum Fluidization Flow Rates in a Rectangular Gas-Fluidized Bed

by

Michael Charles Morgan
Lieutenant Commander, United States Navy
B.S., United States Naval Academy, 1969

Submitted in partial fullfillment of the
requirements for the degree of

MASTER SCIENCE IN MECHANICAL ENGINEERING

from the

NAVAL POSTGRADUATE SCHOOL
March 1981

ABSTRACT

This study was conducted at the Naval Postgraduate School to investigate the formation of particle flow cells at minimum fluidization gas flow rates in a rectangular gas-fluidized bed. The primary objective is to determine if multiple cell formation occurs as the bed width to height ratio increases. The settled bed height is maintained at a constant level for all runs. The secondary objective is to determine if the presence of external plate heaters at the end walls of the particle bed will alter the particle flow cell formation patterns when energized and to what extent they affect the fluid mixing (heat transfer) flow patterns within the particle flow. Pressure measurements across the bed are used to determine minimum fluidization points and thermocouple probe measurements determined the thermal gradients within the bed for each bed configuration. Visual observations on the external bed movement are included in the determination of the results of this experimental study.

TABLE OF CONTENTS

LIST OF FIGURES

LIST OF TABLES

NOMENCLATURE

English Letter Symbols

a	Constant, dependent on tube orientation - Reference 30.
A_c	Cross-sectional area of bed container.
A_m	Contact area of packet and surface - Figure 18.
B	Shape factor - Reference 12.
Bi	Biot number.
C_m	Specific heat of packet or quiescent bed.
C_{pf}	Specific heat of fluid.
C_{ps}	Specific heat of solid particle.
C_R	Constant, correction for location of immersed body - Reference 34.
C_s	Specific heat of solid particle.
dp	Diameter of sphere of same specific area as that of the bed particle.
D	Diameter of the fluidized bed.
D'	Effective diameter of free area across the bed.
D_H	Diameter of an immersed heater.
D_i	Particle diameter of sieved fraction.
D_p	Particle diameter.
$\overline{D}_p$	Average particle diameter.
D_r	Distance between two successive layers - Figure 16.
D_T	Diameter of immersed tube.
D_{20}	Diameter of immersed tube being equal to 20 mm.
g	Acceleration of gravity.

G	Fluid mass velocity.
G'	Fluid mass velocity based on voidage area.
Ga	Galileo number (Archimedes number).
G_e	Hypothetical fluid mass velocity required to merely expand a bed of particles.
G_f	Fluid mass velocity through a fluidizing bed.
G_{mf}	Fluid mass velocity for minimum fluidization.
G_{opt}	Optimum fluid mass velocity giving a maximum value of the heat transfer coefficient.
G_ν	Fluid mass velocity based on kinematic viscosity.
h_c	Heat transfer coefficient for the contact resistance at the wall.
h_o	Empirical constant - Reference 44.
h_w	Heat transfer coefficient between the fluidized bed and the surface.
h_{wiL}	Instantaneous local heat transfer coefficient.
h_{wL}	Local average heat transfer coefficient.
h_{wmax}	Maximum heat transfer coefficient between fluidized bed and surface.
H_o	Superficial bubble-to-cloud heat transfer coefficient.
k_f	Fluid thermal conductivity.
k_m	Thermal conductivity of packet or quiescent bed.
k_s	Thermal conductivity of particle.
k_{sp}	Thermal conductivity of sphere.
ℓ	Distance from bed top in packet theory - Reference 47.
L	Fluidized bed height.
L_e	Expanded bed height.
L_H	Length of heat exchange surface.

L_{mf} Bed height at point of minimum fluidization.

m Slope - Figure 12.

m´ Slope - Figure 15.

N Fluidization number.

Nu Nusselt number.

Nu_{max} Maximum value of Nusselt number.

p Empirical constant - Reference 44.

P Center-to-center distance (pitch) of adjacent tubes.

Pr Prandtl number.

q Heat flux.

q_r Heat transferred into the core portion of the bed by an interchange of particles - Figure 23.

q_w Heat flow rate from the wall into a packet.

q_{wi} Instantaneous heat transfer rate.

q_z Heat taken by particles flowing parallel to the surface in a second zone of emulsion of thickness δ_e - Figure 23.

r Fluctuation ratio - highest to lowest bed level in a gas-fluidized charge.

r_{sp} Radius of sphere.

R Bed expansion ratio.

Re Reynolds number.

Re_f Reynolds number based on particle free fall velocity.

Re_m Modified Reynolds number - Reference 27.

Re_{mf} Reynolds number at minimum fluidization.

Re_{opt} Optimum value of Reynolds number giving a maximum heat transfer coefficient.

Re_t Reynolds number based on bed diameter.

s Average replacement of packets at wall by side mixing.

St Stanton number.

t Time.

T_b Bulk bed constant temperature.

T_f Fluid film temperature.

T_i Gas temperature into bed.

T_o Gas temperature out of bed.

T_w Temperature of wall or heater.

u_d Initial fluid velocity with no particle motion.

u_e Fluid velocity required for initial expansion.

u_{mf} Fluid velocity required for minimum fluidization.

u_o Superficial velocity at fluidization conditions.

u_p Particle velocity.

u_Q Fluid velocity during fluidization.

u_s Particle velocity of Packet Model.

u_t Terminal fluid velocity.

V_p Volume displaced by particles.

W Bed width.

x Axis direction - Figures 21 and 22.

x_i Weight fraction of sieved particles for D_i.

X Packet width - Figures 21 and 22.

y Horizontal pitch of tube bundle - Reference 47.

z Vertical pitch of tube bundle - Reference 47.

Greek Letter Symbols

α Constant - Reference 9.

γ Constant - Reference 9.

γ_f Specific weight of fluid.

δ Boundary layer thickness at point between two particle layers - Figure 16.

δ^+ Average boundary layer thickness at point between two points - Figure 16.

δ_e Thickness of emulsion layer.

δ_G Thickness of gas layer.

Δ Minimum distance between surfaces of adjacent tubes (gap).

Δp_d Pressure drop across bed at u_d.

Δp_e Pressure drop across bed at u_e.

Δp_{mf} Pressure drop across bed at u_{mf}.

Δp_w Ideal pressure drop across the bed calculated from the buoyant weight of the bed.

ε Void fraction at fluidization conditions.

ε_d Initial particle voidage as filled.

ε_e Particle voidage during expansion.

ε_{mf} Particle voidage at minimum fluidization.

ε_Q Void fraction at fluidization conditions.

η Fluidization efficiency.

θ Non-dimensional absolute bed temperature.

μ Fluid viscosity.

ν_{mf} Fluid kinematic viscosity at minimum fluidization.

π Constant.

ρ_f Fluid density.

ρ_m Density of packet.

ρ_{mf} Fluid density at minimum fluidization.

ρ_s Particle density.

ρ_{sb} Nonfluidized bed density.

ϕ_s Sphericity of solid particle.

ACKNOWLEDGEMENT

The author would like to express his appreciation to Dr. Paul F. Pucci, Professor of Mechanical Engineering, for his leadership, patience and technical assistance in his role as thesis advisor.

The skilled craftsmen Messrs. T. Christian, K. Mothersell, "Junior" Dames and R. Longueira who were instrumental in developing the apparatus with which to conduct this experimental investigation.

The assistance provided by Dr. Gilles Cantin, Professor of Mechanical Engineering, in taking time to review and return beneficial suggestions on the rough drafts of this thesis along with acting as a surrogate advisor during Professor Pucci's absence.

And last but not least, the assistance of my wife Connie and those of Mrs. Carol Alejo for all the typing that was required to complete the thesis requirements for this Master of Science Degree in Mechanical Engineering.

I. INTRODUCTION

If one considers a fluid flowing through a bed of solid particles, several forms of today's fluidized bed technology are created. When the particles are stationary, the process is called flow through a porous medium or fixed bed fluidization. If the fluid velocity is such that the particles become entrained by the fluid and are removed from the bed, the process is then called pneumatic conveying or entrained flow fluidization. At some point between these two conditions, the particles in mixture with the fluid are transformed into a fluid-like state causing continuous interaction between the two mediums. The bed particles in this state do not, however, leave the bed container. This state is called fluidized bed fluidization.

The technique of fluidization (all forms) is used for solid-fluid interaction processes whenever high rates of heat and mass transfer between the two constituents is required or high rates of particle transport to and from the bed is necessary. The advantages in the use of fluidization can be listed as follows: [6,12][1]

(a) The formation of an extremely large area of contact between the particles and fluid. This very large surface

[1]Numbers in brackets indicate references.

area permits the achievement of high overall rates of heat and mass transfer between the particles and the fluid.

(b) The comparative ease with which the fluidized particles can be handled.

(c) The reduction of temperature gradients to negligible proportions throughout the bulk of the bed as a result of the high degree of particle mixing that can occur in gas-fluidized systems, i.e. a very high effective internal thermal conductivity.

(d) The occurrence of high rates of heat transfer between the fluidized particles and an immersed surface.

(e) The value of the high thermal inertia of the solids in heat transfer operations within the bed as a whole.

(f) The face that the gas-fluidized systems approximate a fluid which has a low vapor pressure even at very high temperatures - as a thermodynamic fluid it lies roughly between gases and liquids.

Inherent with the fluidization techniques are also some limitations: [6,12]

(a) The process demands the expenditure of power for fluidization.

(b) Some solids cannot be fluidized because of either an excessive tendency for particle attrition or agglomeration to occur. The first will produce too many fines by degradation of the particles which will be lost from the bed. The latter will give "agglomerated" particles too large to

fluidize. Also, there are those materials of such irregular shape that they can only be handled by spouting bed techniques.

(c) Operating rates are limited to within the range over which the bed may be fluidized. If the fluid flow is too low, the bed settles; if, on the other hand, the rate is too high, there is an excessive loss of particles from the bed by carry-over.

(d) There is usually a limit to the size of the particles which can be fluidized. This limit is approximately 6.5 mm (0.25 in) down to a few microns (0.001 in). It is particularly dependent on the fluid viscosity and particle/fluid density ratio as well as the fluid flow rate.

(e) True counter flow operation is unobtainable because of the high degree of mixing that usually occurs within a fluidized bed.

(f) The general absence of thermal gradients throughout a well mixed fluidized bed is a disadvantage in those operations where thermal gradients are required.

(g) The dynamics of fluidized systems are not sufficiently well understood to permit confident scale-up to large scale units from small scale test data when reaction conditions are critical.

Up until this time the term fluid has been used in describing the transport constituent in fluidization. To be more specific there are two fluids which have received widespread use in fluidized bed technology, air (gas) and water (liquid).

The basic differences are in the dynamics and the mass and heat transfer of the solid particles suspended in the gas-fluidized or liquid-fluidized bed. This is primarily a result of the difference in the particle to fluid density ratios. In the gas-fluidized bed the ratio will usually be on the order of a thousand while in a liquid-fluidized bed the particles are only several times heavier than the fluid.

Additionally, the fluid flow characteristics will affect the overall mass and heat transfer bed characteristics. In the liquid-fluidized system, the fluidization velocities are usually of such a magnitude that the fluid inertial terms are considered insignificant. This is not the case with a gas-fluidized system, especially when large particle sizes are used. As the velocities increase the inertial fluid losses and form drag become important in determining the bed characteristics.

With the smooth manner in which liquid-fluidized beds operate, i.e. no gross instabilities in flow, the bed is sometimes referred to as a homogeneously fluidized bed or a particulately fluidized bed. The gas-fluidized beds on the other hand usually have unstable flow above some minimum fluidization condition, characterized by violent agitation of the particles accompanied by bubbling and channeling of the gas. As a result, the gas-fluidized bed is sometimes called an aggregate or bubbling fluidized bed.

The bulk of recent research has been in the area of gas-fluidized beds vice liquid-fluidized beds. Whether this trend will shift remains to be seen. Nevertheless, this investigation will be in the gas-fluidized field and all further discussions will be based on available gas-solid research data.

In a gas-fluidized bed the particles are supported above a gas distributor plate which permits the gas to enter and flow upward through the bed. As the gas flow increases, there will be a pressure drop across the bed which will eventually reach a point when it just balances the downward gravitational force of the particle bed. When this point is reached, the bed will expand and the particles separate. This is referred to as the minimum fluidization point. Further gas flow rate increases will result in bubble formation which will rise through the bed and burst at the surface not unlike a vapor bubble in a boiling liquid.

The separation of the particles creates a large particle surface in direct contact with the gas and the bubble flow induces vigorous and thorough mixing of the particles. This high gas-particle contact area results in the high heat transfer rates which have been experienced. Because the particle flow takes place in the fluidizing gas, a secondary fluid-mixing phenomenon will be induced through the particle flow pattern. The extent of this secondary mixing and its effect on heat transfer will depend on whether the particles

are dispersed in the bed more or less as individual particles or clumps of particles. As an individual particle, dispersion by the fluid mixing would be relatively small. As an agglomerate of particles, however, the result is a dragging of gas pockets through the bed resulting in perturbations to the particle flow patterns. Thus, the extent of fluid mixing is related to the mode and quality of fluidization. This is an area that has been scarcely investigated. Two properties, though, that have been established as a result of fluid mixing investigations are that:

(a) Owing to fluid back-mixing, temperature driving forces are reduced.

(b) Analogously to heat transfer, driving forces are also reduced with mass transfer.

Based on previous research the normal particle flow pattern in small diameter cylindrical gas-fluidized beds is as shown in Figure 1. For gas flow rates which are significantly greater than the minimum fluidization flow rate the solids tend to move downward at the bed walls and the passage of the individual particle is readily observed. The particles will move down the wall and then submerge into the body of the bed. Around this entry point other particles will emerge from the bed and travel down the wall until they also merge back into the bed. This process continues until the bottom of the bed is approached. At some point near the bottom of the bed an inactive or dead region will form in the particles.

The size of this region will depend on the height of the bed, fluid flow rate and bed container geometry. In deep beds the flow regions are well defined while in very shallow beds the downward flow pattern is much less clearly defined with the bed appearing to be more turbulent and in a homogenous state of agitation.

In the literature reviewed, when the term shallow bed was used it generally was referring to a particle bed whose depth was on the order of one and a half feet or less depending on the fluid inlet cross-sectional area. In general, the major features distinguishing shallow beds from deep beds can be described as: [55]

(a) Violent coalescence of bubbles taking place through the majority of the shallow bed depth.

(b) The jetting region next to the distributor plate occupying a significant proportion of the shallow bed depth.

(c) The thermal "entry region" occupying a significant proportion of the shallow bed depth.

These features would suggest that the particle motion within the shallow bed may well be significantly greater than in a deep bed and that the bubble growth will largely be completed within a very small proportion of the bed depth. Thus the residence times of the particles at the heat transfer surface would be considerably shorter than in a deep bed.

In the flow description of deep beds, the bed particles will move upward in the center of the bed either in a spouting

type pattern or in a multi-channel pattern. It should be noted that if the bed vessel is operated in a configuration such that its containment walls are not parallel to the fluid distributor plate inlet gas flow direction, then the particle flow pattern will be adversely affected. Only a few degrees of deviation from this parallel configuration will lead to particle flow pattern short-circuiting. If the operating gas velocities are further increased while this configuration is present, then slugging will initialize.

As was previously stated, fluid mixing in gas-fluidized beds will occur as a result of the particle mixing at the onset of fluidization. Unfortunately, the gas does not circulate in the smooth manner shown in Figure 2. Instead, there will be many eddies within the central core of the particle flow pattern as well as horizontal components radiating out from the core. Additionally, part of the gas may rise rapidly in the form of bubbles, rising ahead of the slower moving interstitial gas components. Therefore, Figure 2 should only be viewed as an ideal flow pattern at minimum fluidization for the bed.

To date, particle flow patterns with the resulting particle and fluid mixing criteria have been explored only in equipment of relatively small diameter (less than one foot). The experimental apparatuses that were used were circular in nature with either no external heat source or a submerged cylindrical (tube) heat source. The data obtained was

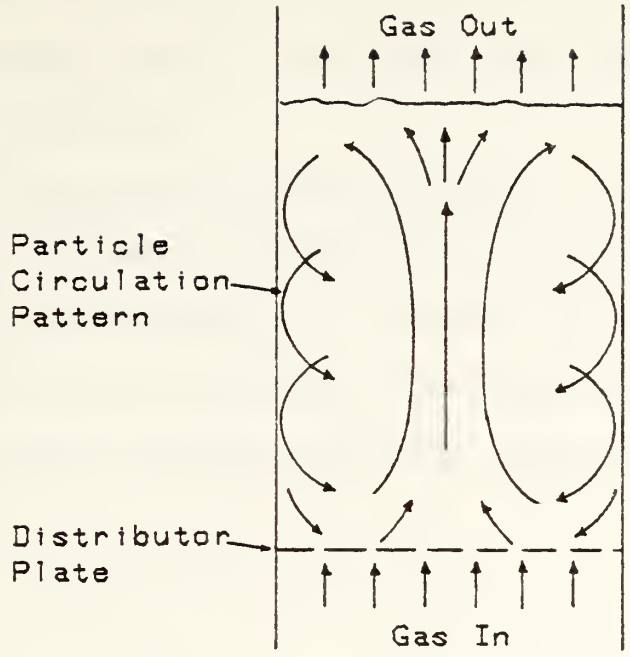

Figure 1. Observed particle circulation pattern.

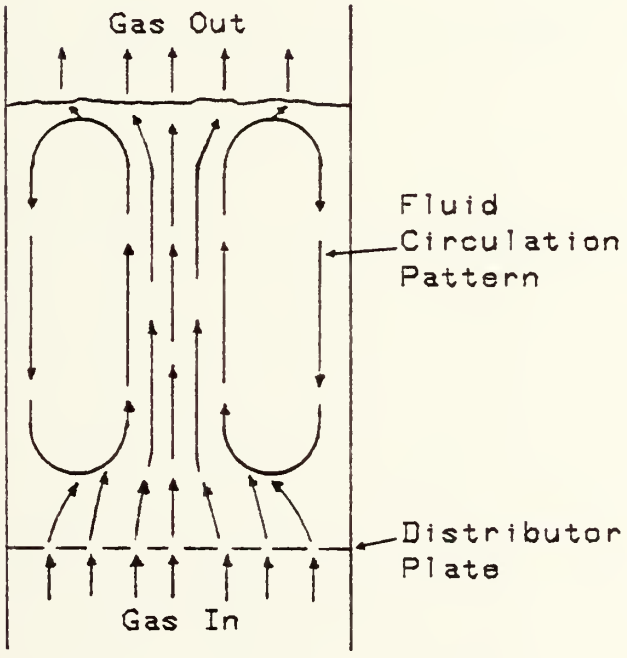

Figure 2. Greatly simplified gas flow pattern.

usually a byproduct of the investigation to determine heat transfer coefficients for fluidized beds with various heat sources and bed geometries.

This thesis investigation was conducted to determine the particle flow patterns developed in a gas-fluidized bed of variable rectangular geometry. Secondly, to determine what effect an external plate heat source has on the particle and fluid flow patterns developed within the rectangular bed.

II. OBJECTIVES AND METHOD OF APPROACH

A. GENERAL STATEMENT OF THE PROBLEM

The specific problem may be defined as an investigation into the formation of particle flow cells at minimum gas fluidization flow rates in a rectangular gas-fluidized bed. The primary objective is to determine if multiple cell formation occurs as the bed width to height (W/L_e) ratio increases. The secondary objective is to determine if the presence of plate heaters at the end walls of the particle bed will alter the particle flow cell formation patterns when energized and to what extent they affect the fluid mixing (heat transfer) flow patterns within the particle flow.

B. METHOD OF APPROACH

The methods used for this investigation were experimental and analytical. Using available research literature a determination was made of the minimum fluidizing velocity (u_{mf}) for the particular fluidized bed configuration. This value of u_{mf} was based on recorded and analytical pressure drops across the distributor plate and bed in addition to the expanded bed heights. Visual confirmation of the minimum fluidizing conditions was then compared with the analytical estimates of the required pressure drops, bed height and air

velocities. Once an initial particle flow cell was established, the bed geometry and/or activation of the plate heaters would be used in an attempt to alter its configuration. A grid of variable depth copper-constantan thermocouples was used to map the thermal distribution within the particle flow cell to determine the fluid mixing properties of the cells.

This thesis will not be involved with the heat transfer coefficient determination so prevalent in recent experimentation; rather it will focus only on how the particle flow cells relate to the bed geometry chosen and how the resulting fluid mixing affects the heat transfer within the bed. It should be noted that direct measurement of the solid particle temperatures is very unreliable and that the temperatures recorded will be considered to be that of the air at a particular point within the grid of the bed. Because of the difference in the particle to fluid density, however, the two will be considered to be at equilibrium at the point measured for this experiment.

III. SUMMARY OF PREVIOUS RESEARCH IN GAS-FLUIDIZED BED TECHNOLOGY

A. GENERAL DESCRIPTION OF GAS-FLUIDIZED BED BEHAVIOR

1. The Phenomenon of Fluidization

When the bed configuration is initially filled with particles, an initial voidage (ε_d) will result between the particles. As the fluidizing fluid, a gas in this case, is initiated at some superficial velocity (u_d) there will be no movement of the bed. However, a pressure drop (Δp_d) will occur and gradually increase at a linear rate. The magnitude of this pressure drop will be determined by the gas flow rate and the characteristics of the bed.

Eventually a condition will be reached when the gas flow rate (u_e) has increased to a point at which expansion of the bed initiates. The voidage will increase to some ε_e and the pressure drop can be calculated from the equation

$$\Delta p_e = L_e \left(1 - \varepsilon_e \right) \left(\rho_s - \rho_f \right) \qquad (3.1)$$

(Note - The units to be used with all text equations can be found in Appendix D.) While the bed is expanding, there still will have not been any particle motion taking place.

As the gas flow rate is increased further, a point will next be reached when the voidage becomes ε_{mf} and the particles are at the point of fluidization onset. The

velocity is called the minimum fluidization velocity (u_{mf}) and is critical to most bed behavior calculations. Further gas velocity increases (u_Q) will fluidize the bed causing further voidage increases (ε_Q) until a terminal velocity (u_t) is reached as defined by the bed container geometry or particle entrainment takes place. By the time u_t has been reached the particle motion will be intense although the pressure drop across the bed will remain at the level of minimum fluidization inception. This condition is referred to as dense-phase turbulent fluidization at its inception (u_Q) but degenerates to a dilute-phase when the gas rate is such that the particles become entrained in the gas. On the average the ratio of the terminal velocity (u_t) to the minimum fluidization velocity (u_{mf}) is about seventy (70). The terminal velocity is also a function of the particle diameter, shape and density as well as the properties of the fluidizing fluid.

Parent et al. [52] has characterized three types of behavior with the gas-solid mixtures in the dense-phase fluidization region. Under certain conditions, usually for small particle sizes, the gas tends to channel through the bed without causing movement of the bed. Under other conditions, such as large bed heights, large particle sizes and high gas flow rates, slugging takes place which is analogous to the turbulence observed in a boiling liquid. The third type of behavior is described as the mechanically smooth

fluidization. In this case the particles move along twisting, ever-changing paths. Occasionallly gas bubbles appear in the bed but there is no rough bumping. It is this case that the pressure drop across the bed is nearly equal to the suspension head opposing the flow (drag). A word of caution is warranted, however, in that in research conducted by Lewis et al. [42] the conclusion that the pressure drop is essentially equal to the weight of the particle bed would appear to be satisfactory only for units with small L/D ratios. It appears to be in considerable error for large L/D values or for beds having large static effects present.

Here again several researchers differ in their opinion as to the cause of this phenomenon. While Lewis et al. [42] explained it as an indication of frictional drag of the solid particles on the walls of the unit, Toomey and Johnstone [62] attribute it to kinetic energy losses caused by the collision between the particles and Wilhelm and Kwauk [76] concluded it was caused by forces which are electrostatic and/or fluid dynamic in origin. Since this thesis is operating in the shallow bed region it is not anticipated that this excess pressure drop will be of concern.

2. Voidage at Minimum Fluidization

The first bed characteristics that must be determined for an understanding of gas-fluidized bed operation is that of the bed voidage at minimum fluidization (ε_{mf}). By definition ε_{mf} is that particle separation to which the bed must

expand before particle motion, as induced by fluid flow, can initialize. There are two methods which can be used to determine this factor.

The first method is based on a collection of data from several researchers that has been graphically combined by Leva [36] and reproduced here in Figure 3. For a given particle diameter (D_p) and composition a value for the minimum fluidization voidage (ε_{mf}) can be obtained. The obvious drawback for this method is that it depends solely on the material chosen for the particles being one that has had previous experimentation accomplished.

The second method is used with those beds for which particle ε_{mf} data is not available. It requires that the bed be subjected to the fluidizing gas until particle motion initializes, at which time the bed height (L_{mf}) is recorded. The minimum fluidization voidage (ε_{mf}) can then be calculated from the equation

$$\varepsilon_{mf} = 1 - \frac{V_p \gamma_f}{L_{mf} A_c (\rho_s - \rho_f)} . \qquad (3.2)$$

The accuracy of this estimate will depend on the mass characteristics of the bed particles, i.e. sphericity, whether solid or hollow, degree of particle porosity, etc. Particles of high porosity are usually unsuitable for fluidized bed use as they have a tendency to break up with increased fluid flow.

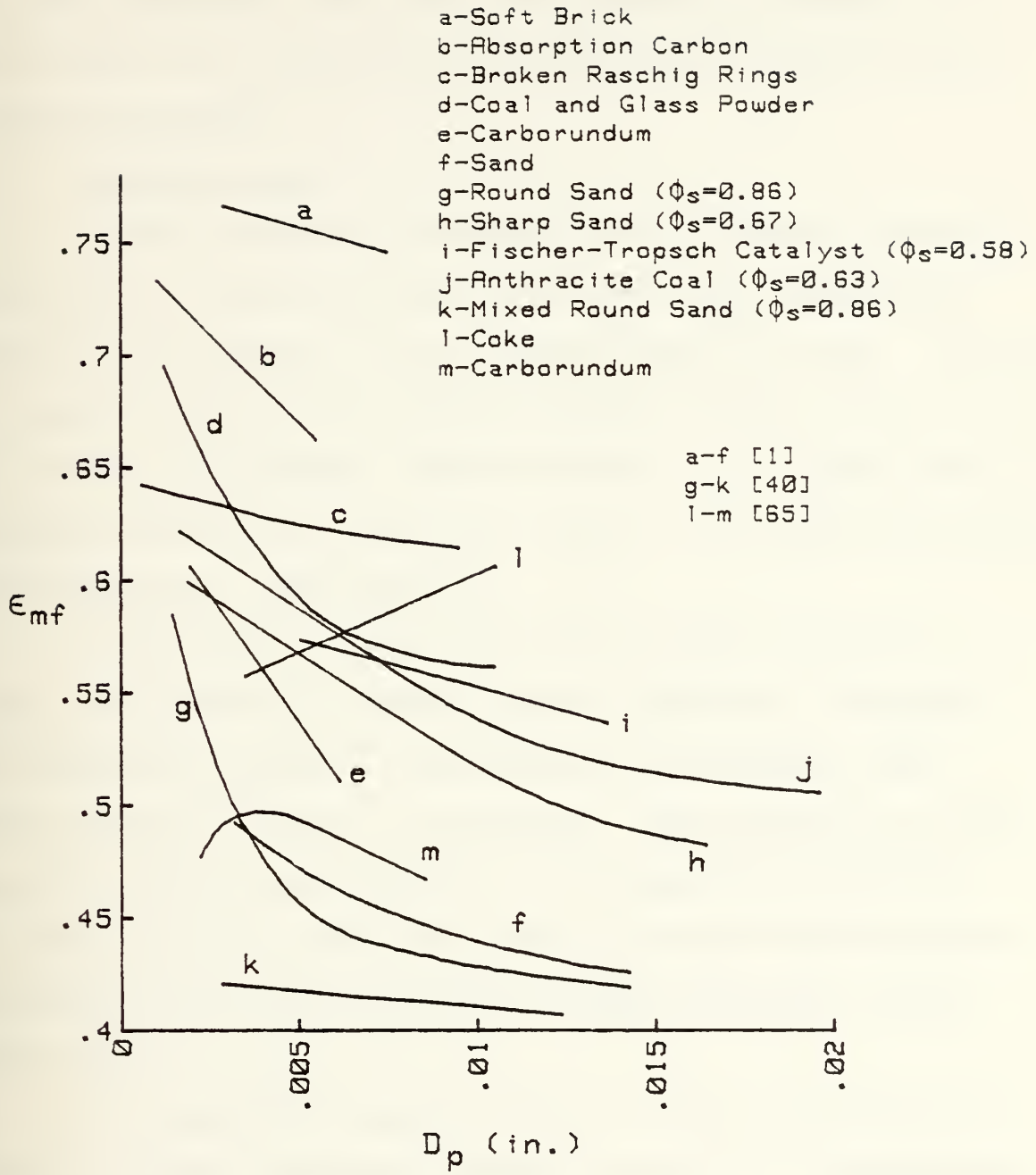

Figure 3. Values of ϵ_{mf} vs. particle diameter.

Once a value for the minimum fluidization voidage has been estimated, additional bed behavior characteristics can be predicted and the bed's suitability for the intended process determined.

3. Pressure Drop

Another excellent indication of fluidization behavior of the particle material may be obtained from the pressure drop-flow relationship of the expanded bed [36,40,64]. Ideally, the pressure drop across the bed should increase linearly until the voidage has reached a maximum value (ε_e) at which time the pressure differential would level off for the remaining phases of fluidization. See Figure 4.

Unfortunately, the idealization never occurs as a result of three major factors; namely channeling, slugging and distributor design. With channeling a pressure drop occurs (Figure 5) when ε_e is reached. The magnitude of this drop will depend on the extent of the channeling phenomenon but eventually a minimum drop point is reached and the pressure differential then increases to some new lower steady state value.

The channeling can be either "through channeling" in which it extends completely through the bed or "intermittent channeling" where it extends through part of the bed. Fortunately, as the gas flow rate is increased the tendency for the bed to have channeling decreases. Some factors [38] which tend to promote channeling are poor distributor design,

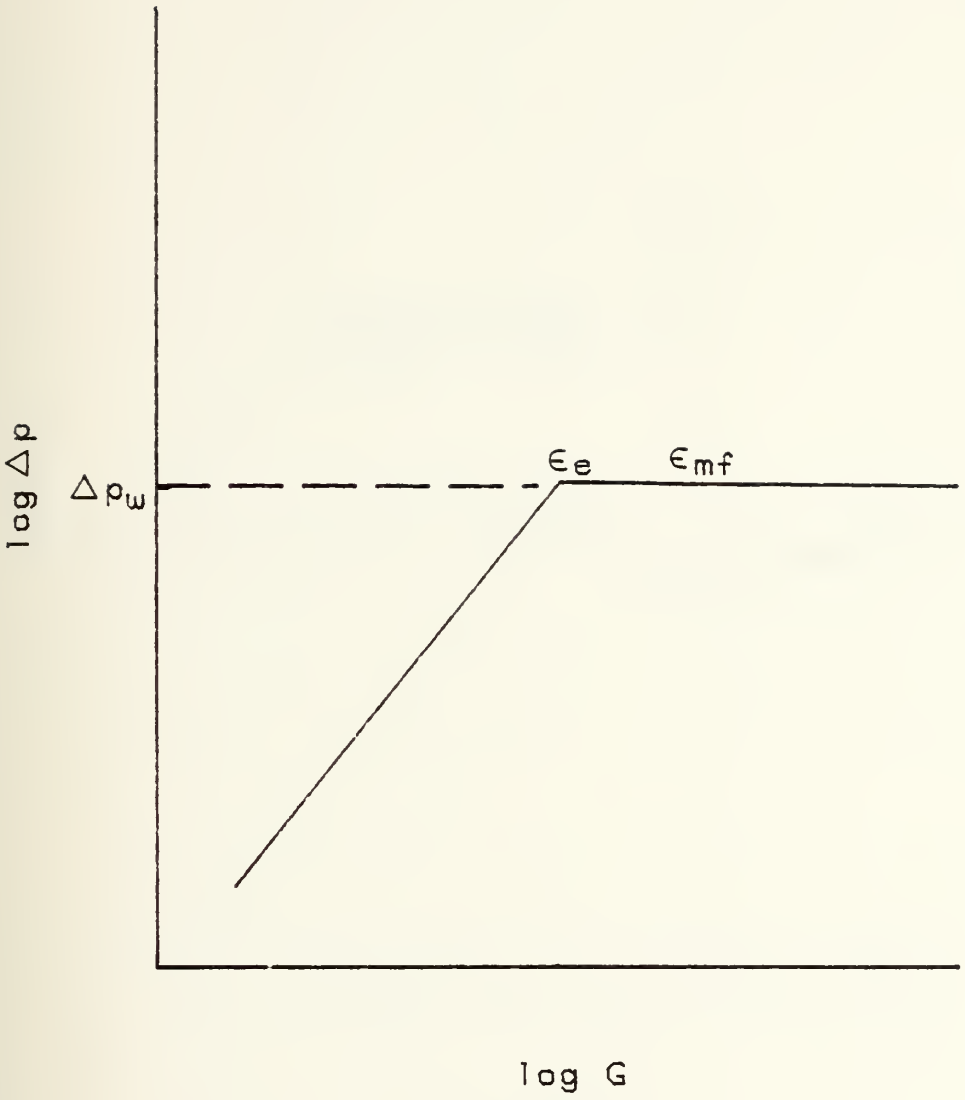

Figure 4. Ideal pressure-drop-flow diagram.

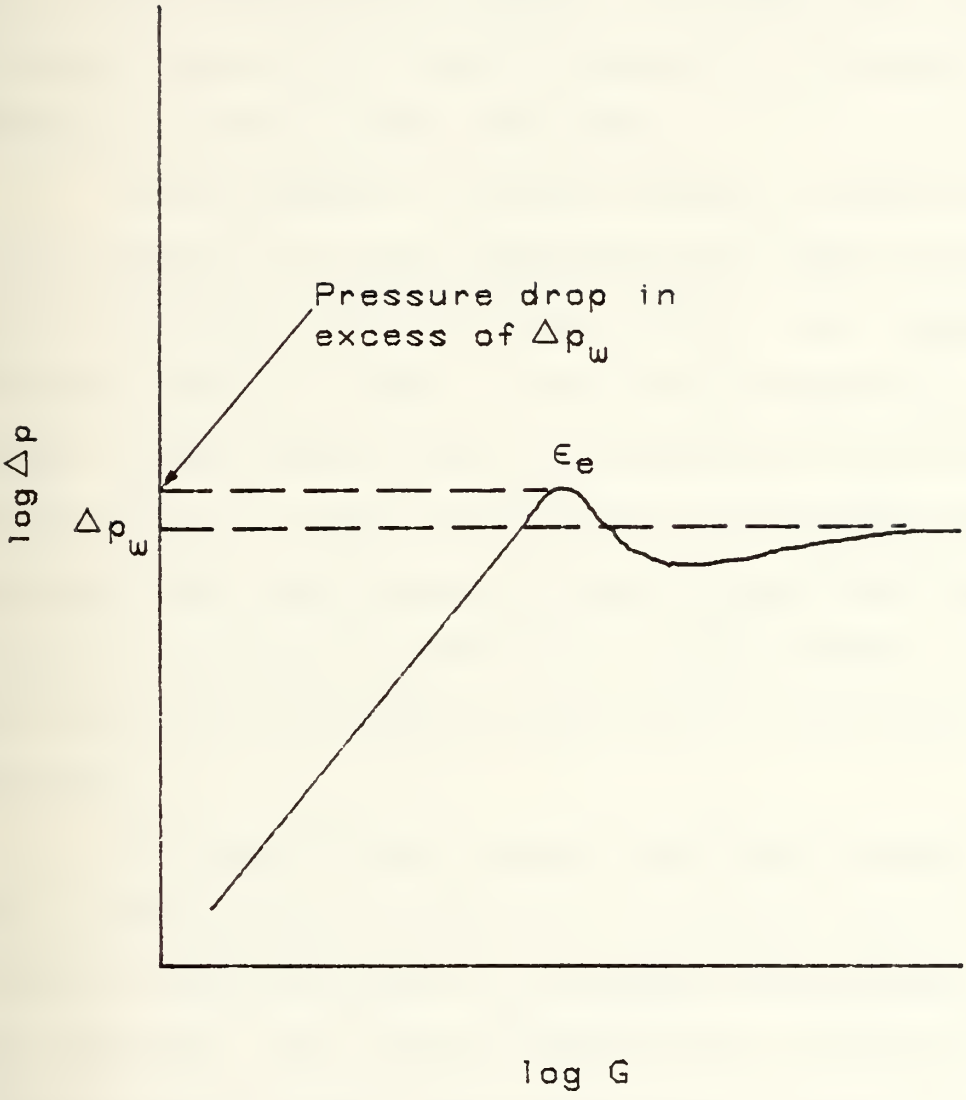

Figure 5. Pressure-drop-flow diagram for channeling.

the shape of the bed particles (less sphericity the greater the channeling), moisture in the bed and the rate of fluid flow through beds of small particles. If the bed is moist, the particles will tend to clump together, and the gas flow will channel between the clumps. At higher flow rates the increased agitation of the bed apparently destroys the channels as soon as they are formed.

With slugging a condition exists in which the bubbles of gas combine to a size approaching the order of magnitude of the diameter of the confining vessel. As a result, the particle layers or slugs of granular particles will move upward through the bed like a piston until they disintegrate at the bed top. When this happens, the pressure drop will increase above the predicted steady state value (Δp_e), see Figure 6. If the flow rate is increased further, the pressure drop rise continues and the bed will slug even more severely.

The third factor, namely distributor design, was well investigated by Grohse [27] who stated that for the multiorifice plate the point of incipient fluidization is not well defined. The gradual pressure-drop increase up to the theoretically demanded suggests that the bottom portion of the bed is not fluidized to the same extent as the upper region. With the screen distributor, a certain amount of channeling probably occurred. There is the possibility that the holes in the screen were locally blocked; this could

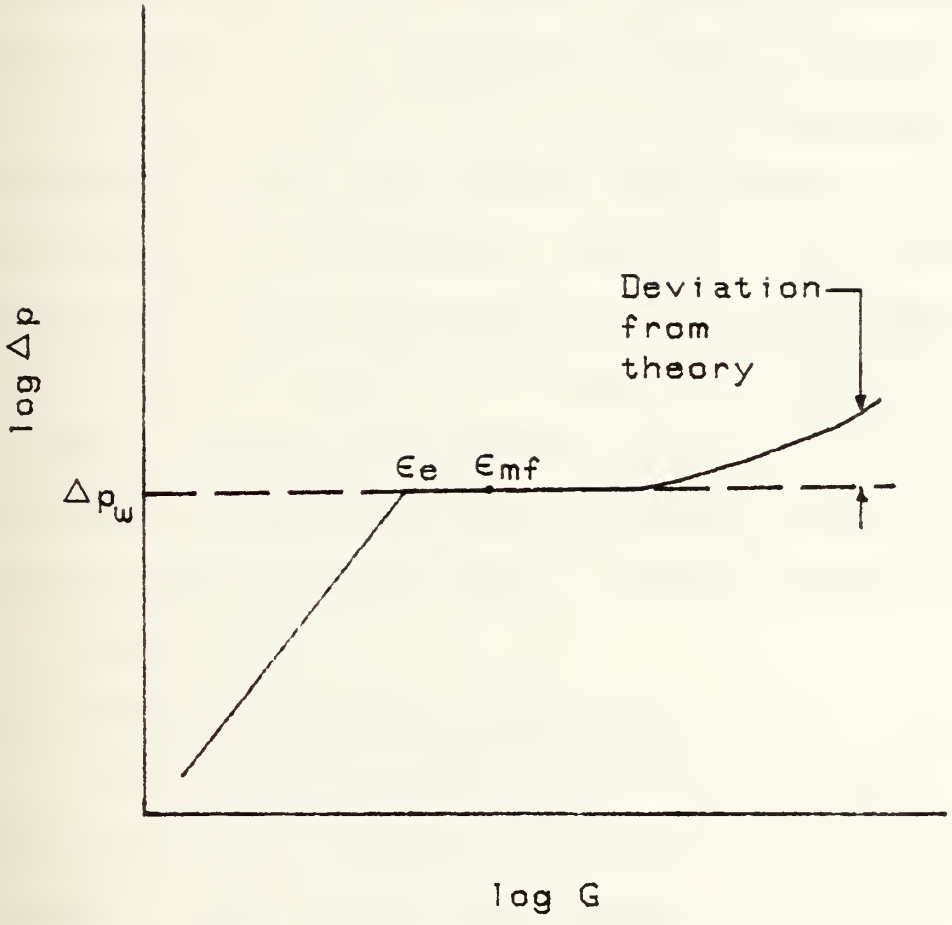

Figure 6. Pressure-drop-flow diagram for slugging.

create a condition favorable for channeling. With the porous plate the point of incipient fluidization is well defined and there is no tendency for channeling. See Figure 7.

Since the point of minimum fluidization is the key starting point on fluidization studies, it seems extremely important to be able to predict that point both theoretically and through experimental results. Therefore, the distributor design's effect on the pressure drop at u_{mf} becomes a very important factor. According to Kunii and Levenspiel [34], distributors should have a sufficient pressure drop to achieve equal flow through all openings. As a result, the pressure drop across the distributor plate by direct measurement should be at least 10% of the pressure drop of the bed to ensure effective fluidization. Theoretically the pressure drop at the minimum fluidization velocity (Δp_{mf}) can be found by substituting L_{mf} and ε_{mf} for the values of L_e and ε_e in equation (3.1).

4. Minimum Fluidization Velocity

The ability to predict the point of initial fluidization reliably is of basic importance in virtually all fluidized-process studies and designs. By operating at mass velocities which are slightly higher than the minimum fluidization mass velocity (G_{mf}) attrition and elutriation (stratification) losses will be minimized. The by-product of the low flow rates is then a low particle velocity in the bed and correspondingly a relatively low bed wall heat transfer coefficient (h_w).

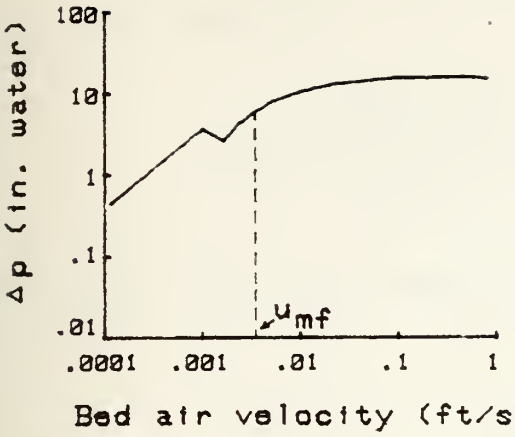

Multi-orifice

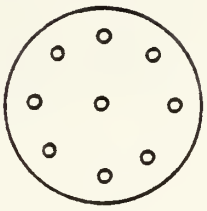

0.0625in. sheet metal with a 0.052in. hole per square inch of area.

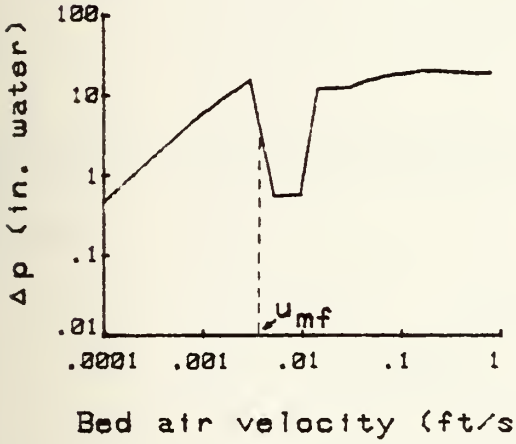

Screen

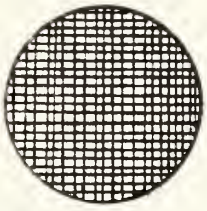

300-mesh screen on 0.017in. thick plate, with twenty-four 0.021in. holes on triangular diamond pitch.

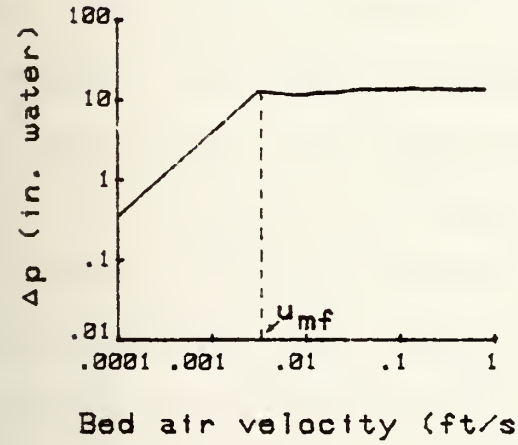

Porous plate

0.125in. sintered-metal plate of 0.0008in. mean pore opening.

Figure 7. Gas distributor effect on fluidization onset.

The general equation [36] for the minimum fluidization mass flow rate is

$$G_{mf} = \frac{688\ \bar{D}_p^{1.82}\ \{\ \rho_f\ (\ \rho_s - \rho_f\ )\ \}^{0.94}}{\mu^{0.88}}\ , \qquad (3.3)$$

with $\bar{D}_p$, the average particle size,

$$\bar{D}_p = \frac{1}{\Sigma\ \frac{x_i}{D_i}}\ . \qquad (3.4)$$

Equation (3.3) can only be used, however, when the Reynolds number

$$Re_{mf} = \frac{0.03445\ \bar{D}_p\ G_{mf}}{\mu} \qquad (3.5)$$

is less than ten. Should the value of Re_{mf} be greater than ten, then the alternative is to use the nomograph [72] of Figure 8, with the calculated value of $\bar{D}_p$, μ and $\rho_f(\rho_s - \rho_f)$ to recalculate the value of G_{mf}. If, however, the value of $\bar{D}_p$, μ or $\rho_f(\rho_s - \rho_f)$ does not appear on the nomograph, then go to Figure 9 [72] and with the calculated value of Re_{mf}, from equation (3.5), determine the correction factor to be applied to the value of G_{mf} calculated from equation (3.3). The new value of G_{mf} is then calculated from the equation

$$(\ G_{mf}\ )_{new} = (\ G_{mf}\ )_{correction}\ (\ G_{mf}\ )_{calculated}\cdot \qquad (3.6)$$

NOTE-Left (or right) scale of $(\rho_s - \rho_f)\rho_f$ corresponds to left (or right) scale of G_{mf}

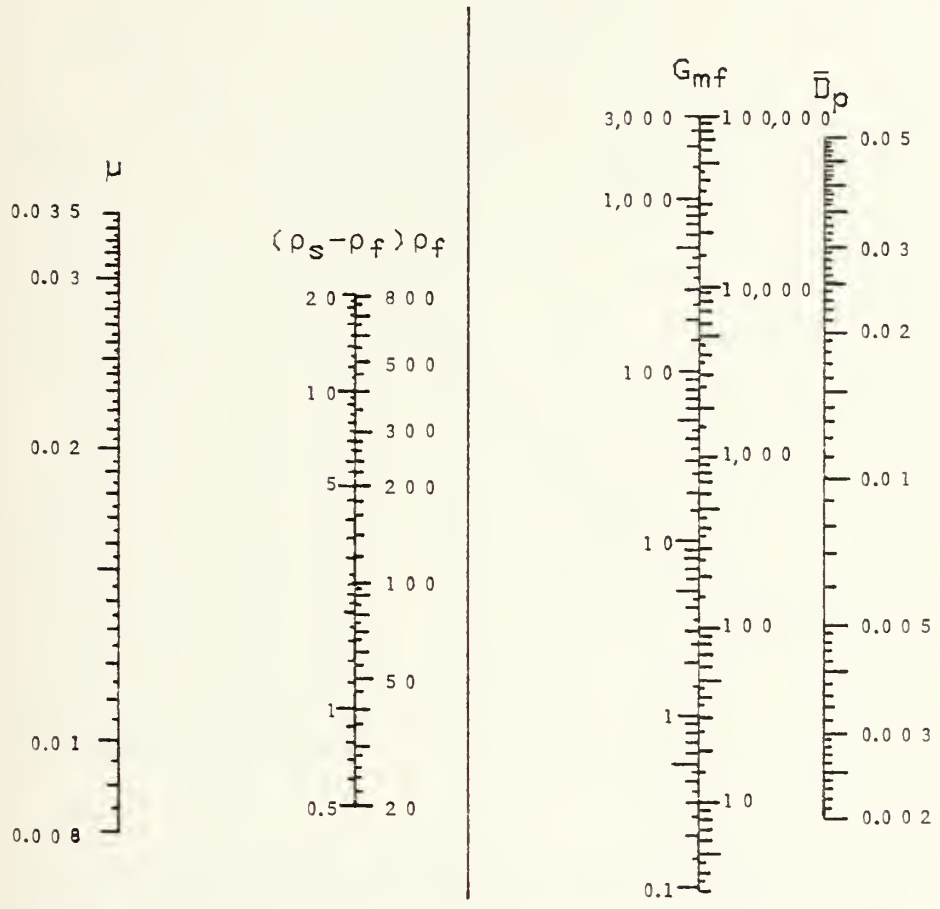

Figure 8. Nomograph to calculate G_{mf}.

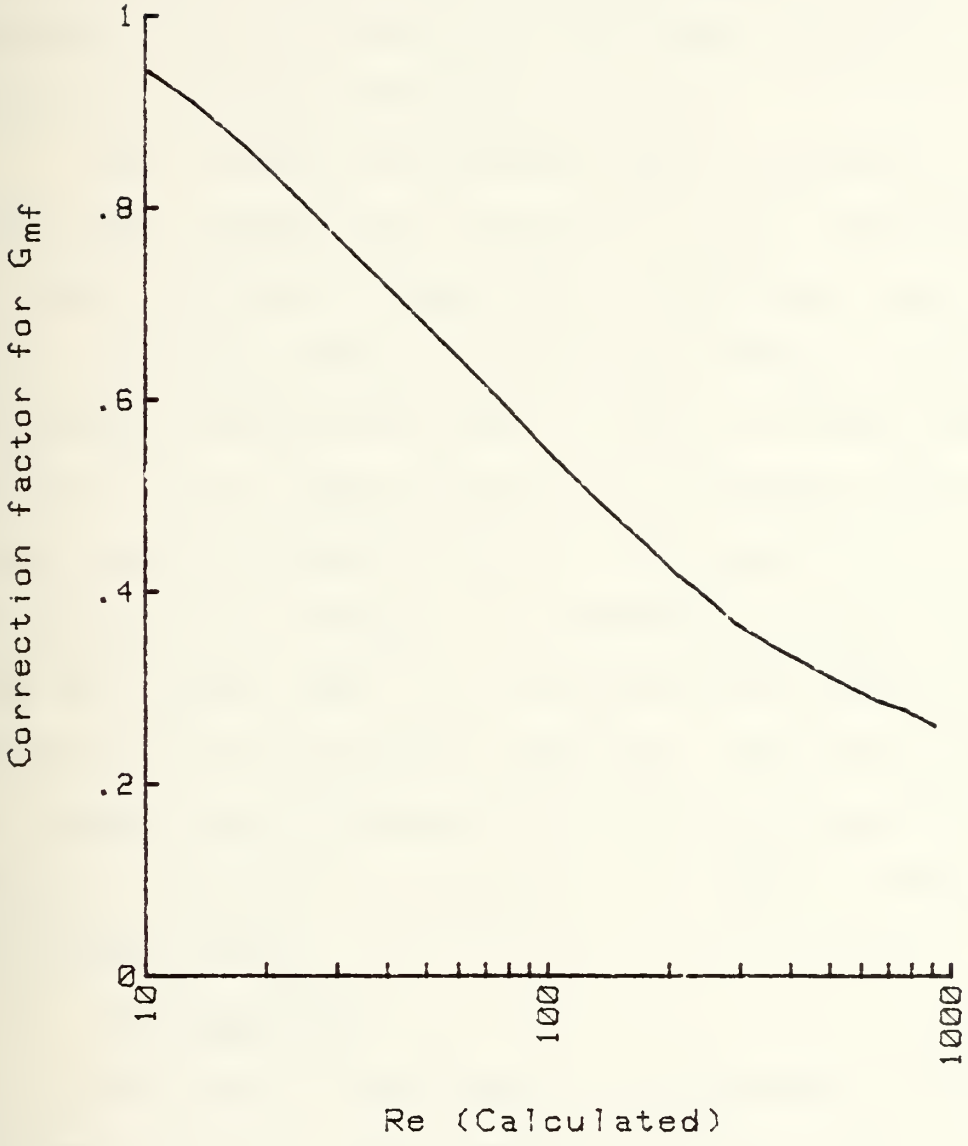

Figure 9. Correction Factor for Re>10.

It should be mentioned that there are numerous correlations proposed for the minimum fluidization mass velocity (G_{mf}) that are applicable to the experimental results of various researchers. These predictions are not in very close agreement and are a function of different apparatus constructions, fluids used, particles used, etc.

One variation considered worthy of note is a result of the work accomplished by Wen and Yu [73]. They demonstrated that when particles of more than two different sizes are fluidized, they either separate completely, forming distinct layers or intermix forming one layer of rather uniformly distributed particles. For a bed containing two different particle sizes, if the particle diameter ratio is less than 1.3, the particles were observed to intermix. If, however, the particle size ratio was greater than 1.3, the smaller particles fluidized separately above the larger particles. When this occurs, the voidage must be obtained for each layer and special procedures, delineated in Reference [73], used to compute the fluid mass velocity.

5. Bed Expansion

This area of bed behavior is important in that it resolves the minimum bed chamber height that must be designed to enable fluidization to occur. Unfortunately, although gas-fluidization processes are more prevalent than liquid-fluidization processes, the mechanics of the gas-fluidization process is not as well understood in comparison to the liquid

process. It has been found that the liquid systems will expand smoothly almost to a voidage of 1.0. With a gas system, however, somewhere along the course of the expansion, a point of mechanical instability is reached which degrades the expansion process. The location of this trip point or the reasoning as to why it occurs has so far eluded researchers. There is some speculation, however, that it may be caused by the formation of aggregates of particles in the bed and that it is somehow related to the fluid velocity.

Based on analytic and experimental data, Leva et al. [36,40] formulated a simple relationship between the fluid mass velocity and bed particle voidage that enabled the generation of a prediction model for bed expansion. Some examples of this gas-solid expansion data can be found in Figure 10. What is shown is that at higher flow regions the data will align along curves rather than linear lines and at intermediate flow regions the reverse is true. Note that as the voidage increases, $(1 - \varepsilon)/\varepsilon^3$ will decrease. Also, at elevated flow rates, the slopes (m) become less negative indicating that aggregation becomes more prevalent while the linear lines indicate little or no aggregation (intermediate flow region). It is also noted that small-particle beds may be expanded over substantially wider flow ranges than larger-particle beds before aggregation conditions will set in. This is indicated by the fact that, with smaller particles, departure from the straight line occurs at higher values of the reduced mass velocity than with larger particles.

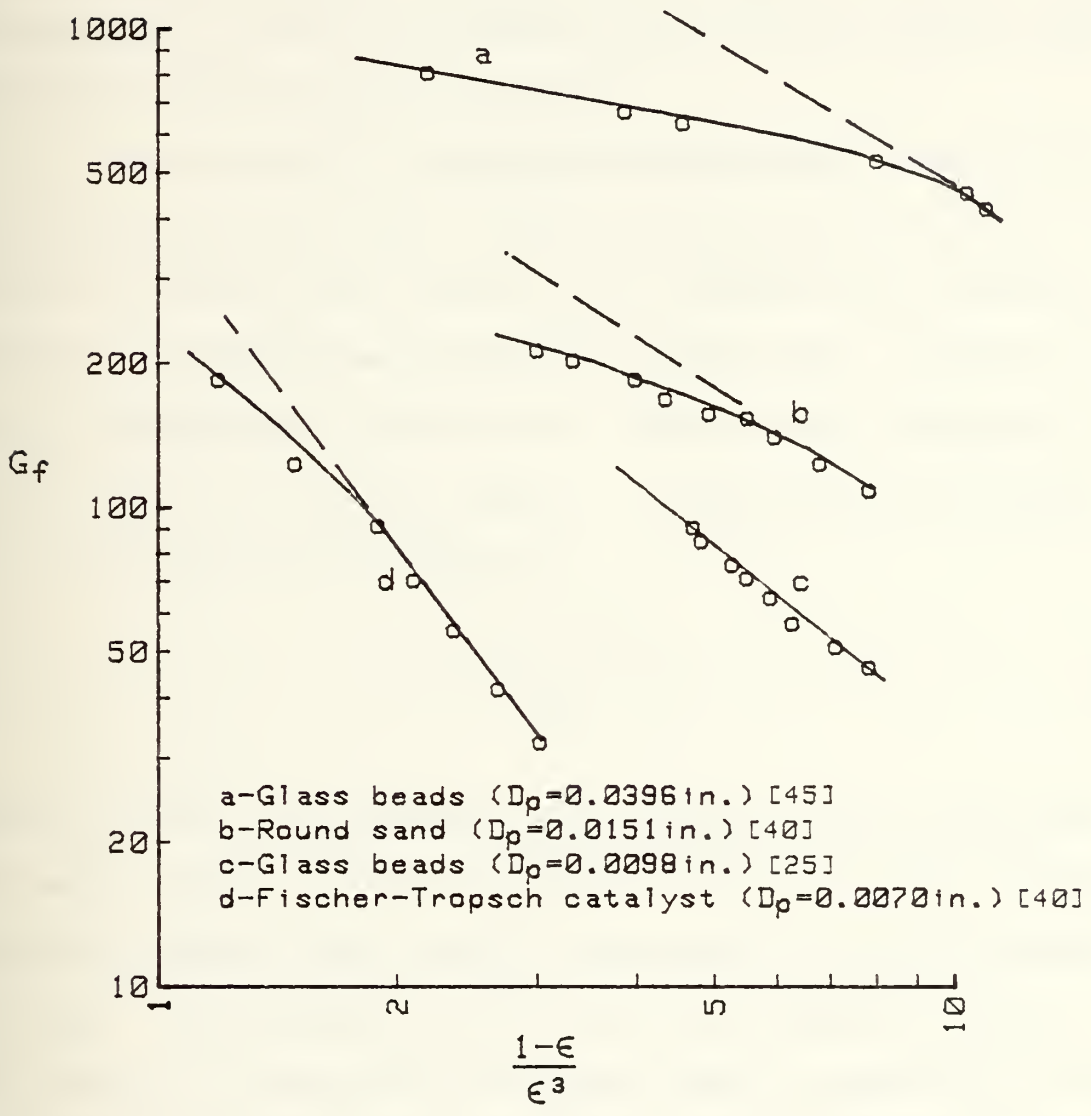

Figure 10. Gas-particle expansion data.

As far as practical methods of correlation are concerned, the data is most cases may be represented by straight lines. This will produce the relationship between slopes (m) and particle size (D_p) indicated in Figure 11 [36,40]. This correlation is based on virtually all of the available bed-expansion literature data to date.

To calculate a predicted expanded-bed height of the gas-fluidized particles, two basic methods may be used. The choice of method will depend on the bed-particle diameter. However, a maximum mean particle diameter ($\bar{D}_p$) of about 0.015 in is recommended, otherwise the fluidization efficiency will be so low as to promote slugging. Fluidization efficiency (η) is defined by the equation

$$\eta = \frac{G_f - G_e}{G_f} , \qquad (3.7)$$

where G_f and G_e are respectively defined as the fluidizing gas mass velocity flowing through a bed at a given instant in time and the gas mass velocity required to initially expand the bed. Once slugging sets in the bed expansion height will begin to fluctuate as the gas bubbles expand and collapse. When this observed condition occurs no correlation to date has been found to give a predictable bed height.

a. Method One

(1) With $\bar{D}_p$ known, m may be found from Figure 11.

(2) Determine ε_{mf} from Figure 3 or equation (3.2).

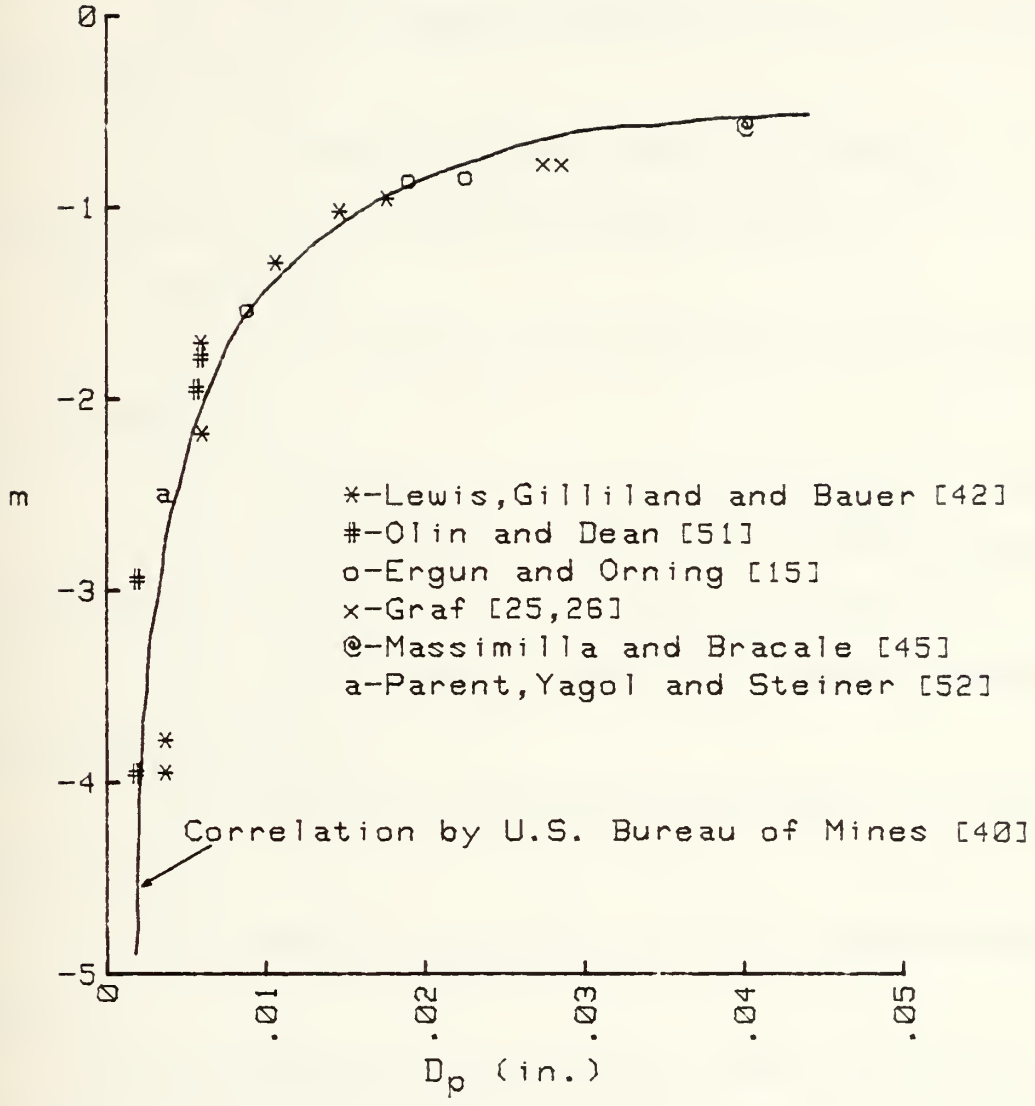

Figure 11. Gas-fluidized slope values vs. particle diameter.

(3) Calculate G_{mf} using equations (3.3) and/or (3.6) or Figure 8.

(4) Draw fluidization line on log-log paper with slope m, see Figure 12 [40].

(5) For the chosen value of G_f, find the corresponding value of ε_f.

(6) Solve the voidage equation, equation (3.2), for L_f by substituting L_f and ε_f for L_{mf} and ε_{mf}.

b. Method Two

(1) Calculate G_{mf} using equations (3.3) and/or (3.6) or Figure 8.

(2) Calculate the reduced mass velocity, G_f/G_{mf}.

(3) Go to Figure 13 [36] with the reduced mass velocity and $\bar{D}_p$ to find the fluidization efficiency (η).

(4) Go to Figure 14 [36] with η and $\bar{D}_p$ to evaluate the bed expansion ratio, R.

(5) Calculate the static bed height L_{mf} from equation (3.2).

(6) Multiply L_{mf} by R to get the expanded bed height, L_f.

Once the expanded bed height has been calculated there still remains one check to be performed on its validity. This is a check on the extent of height fluctuations that may occur for the flow rate chosen. It has been found that under conditions of high gas flow rates that an oscillation of the expanded bed height can occur. This concept has been termed

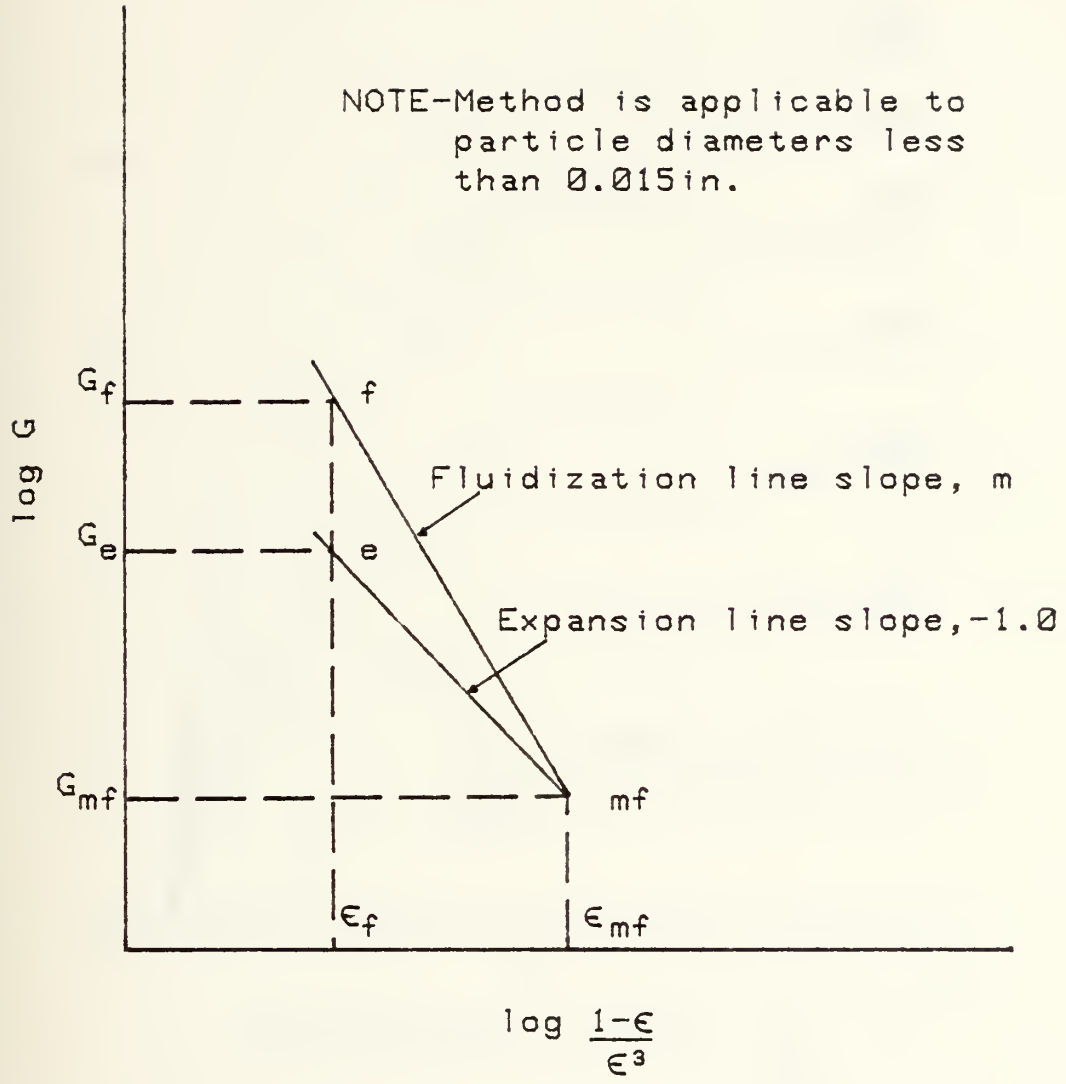

Figure 12. Gas fluidization and expansion lines.

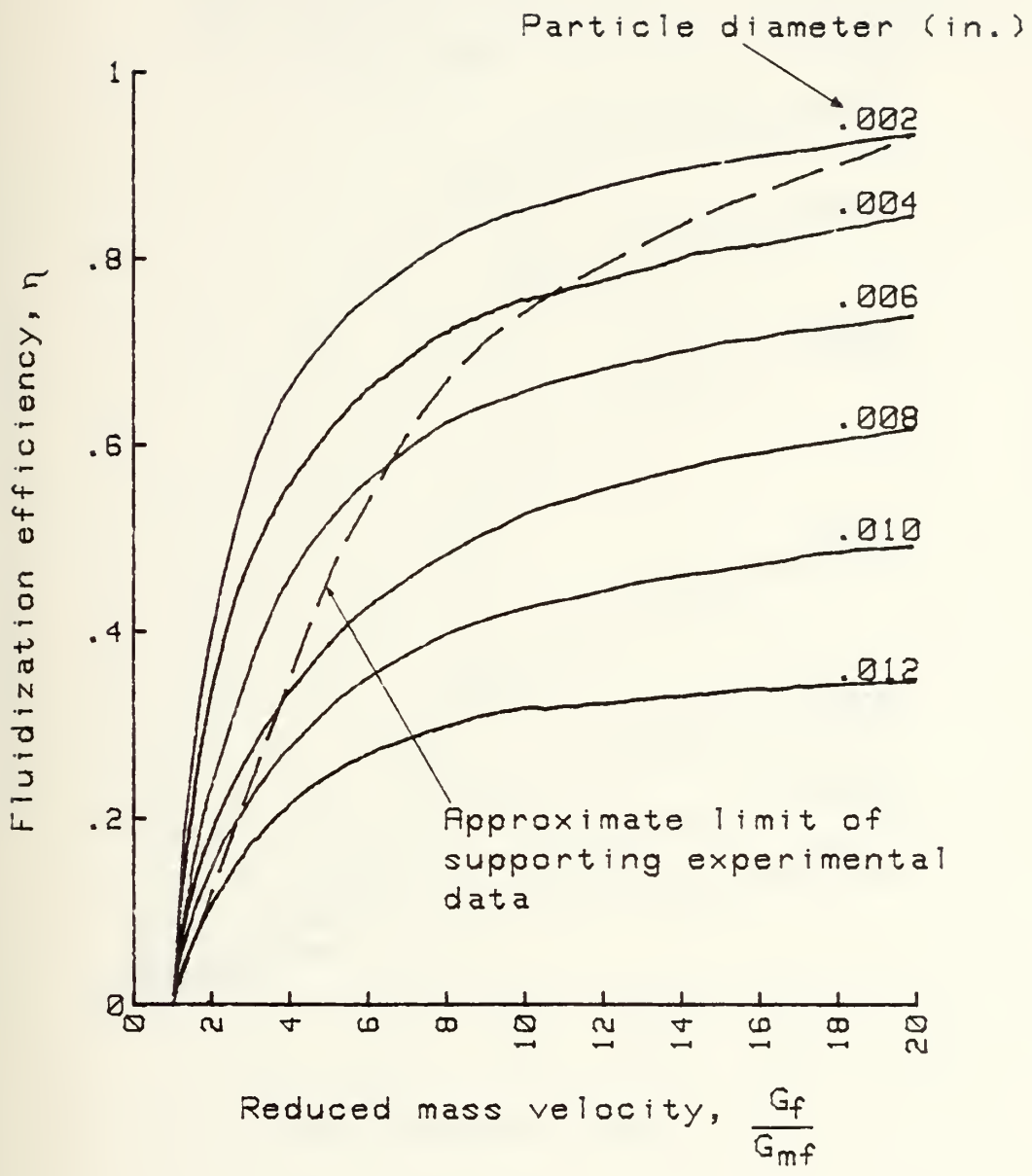

Figure 13. Fluidization efficiency vs. reduced mass velocity.

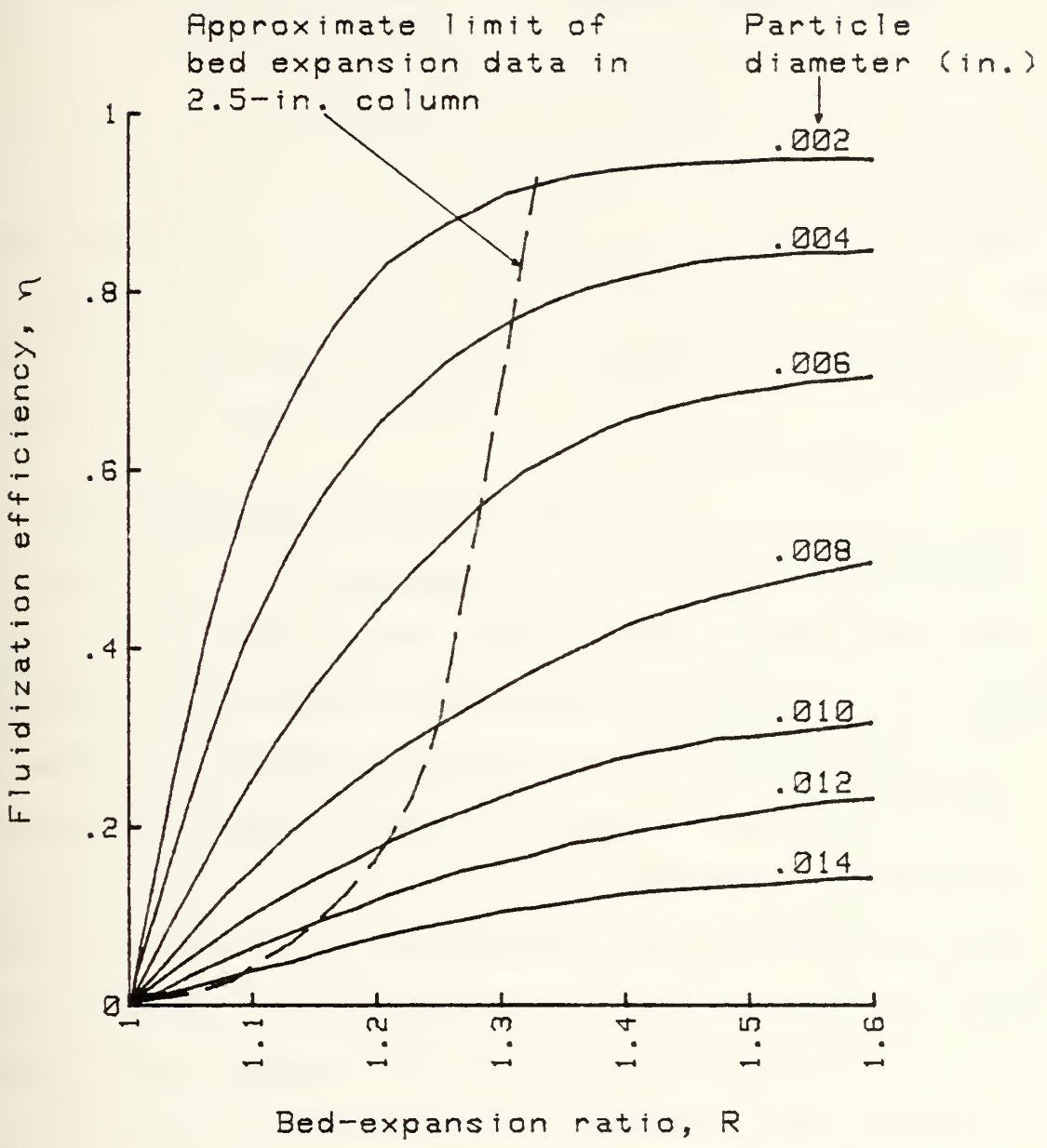

Figure 14. Fluidization efficiency vs. expansion ratio.

the fluctuation ratio, r, the ratio of the highest to lowest levels which the bed top occupies for a particular gas flow rate. The value of r can be determined from the equation

$$r = \exp \frac{m' (G_f - G_{mf})}{G_{mf}} \qquad (3.8)$$

where slope m´ is related to the particle diameter as shown in Figure 15 and is based on data of Lewis et al. [42]. The closer the fluctuation ratio to 1.0 the more accurate the expanded bed height estimate.

B. HEAT TRANSFER PHENOMENON MODELS

There is little agreement in the reported experimental values of the heat transfer coefficients in the literature. The reasons can best be summarized as follows: 1) a variety of contacting patterns between particles and the fluid resulted in different models from which to base the average heat transfer coefficient; 2) the temperature measurements taken in the beds by thermocouples were interpreted differently (usually the readings were related to the gas temperature in some manner); or 3) that direct measurement of solid particle temperatures are unreliable with present state-of-the-art methods, especially for the smaller size particles (less than 100 microns).

As a result, due to the generally low accuracy of in-bed temperature measurements and the oversimplifications in the

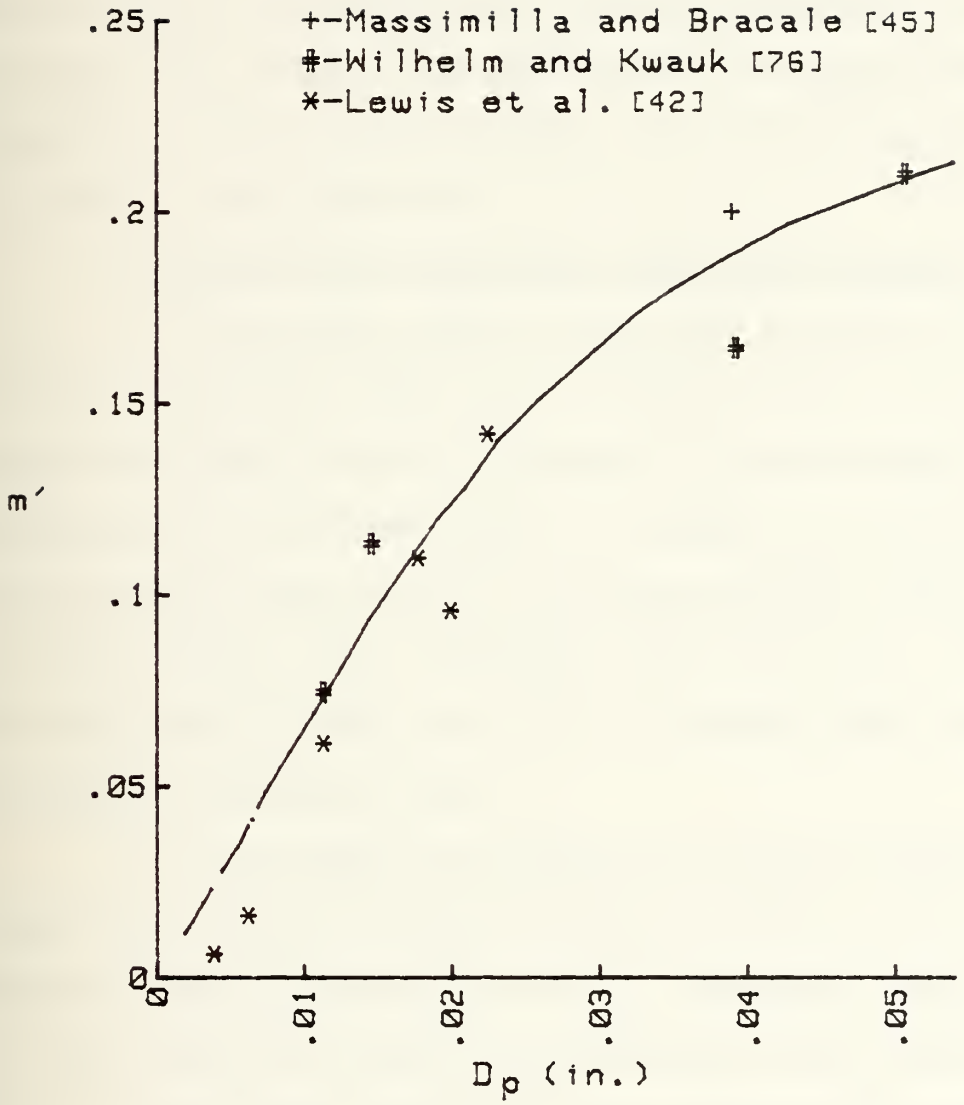

Figure 15. Slope m′ in relation to particle diameter.

flow models, heat transfer coefficients so far reported have varied widely. Although there is no complete theory that can predict the heat transfer data for fluidized beds, there are several theories that correlate the published data. Each resulting heat transfer model has some experimental or design situation for which it is appropriate. What follows is an overview of these various models all of which are based on cylindrical bed geometries.

1. Steady State Conduction Across the Gas Film

In this model heat is conducted through the gas boundary layer near the heat exchange surface. In order to explain the high values of the heat transfer rates obtained experimentally, the gas layer is assumed to be scoured by solids moving along the heat exchange surface, thus decreasing the boundary layer thickness near the wall. This model was developed by Leva et al. [37], Dow and Jakob [13], and Levenspiel and Walton [41].

Dow and Jakob [13] studied the gas-fluidization mixtures and classified them as either a dense or lean phase mixture based on the gas velocity. The dense phase occurred at gas velocities close to u_{mf} while the lean phase was close to u_t. Their model applied to the mechanically smooth dense phase fluidization although they did observe bubble formation and slugging in the dense phase region of fluidization.

The model's motion, Figure 16, is primarily upward at the center of the bed and downward along the wall.

Temperature measurements showed the entire bed was at a constant temperature except for a small region at the bottom and a narrow layer near the wall. Heat is tranferred radially through a thin air film to the particles and air moving downward outside this film. The particles carry the heat to the bottom of the bed where thermal equilibrium is attained almost instantaneously with the incoming cold air. The bombardment of small particles prevents the formation of a laminar boundary layer, and leaves a very thin laminar sublayer and a thicker turbulent outer layer.

The heat transfer rate from the surface to the fluidized bed was found to be independent of the thermal conductivity of the solid particles, and the large isothermal region of the fluidized bed could be destroyed if the downward flow of the small particles was short-circuited into the main flow before they reached the bottom, i.e. under slugging conditions.

Levenspiel and Walton [41] presented a similar model where the resistance to the heat flow is due to the laminar gas layer which is destroyed by solid particles passing through it. Thus the average thickness of the laminar layer is much less than in an empty tube. They assumed that the particles are of uniform diameter (d_p), stationary, and arranged in equally spaced horizontal layers. The boundary layer formation at the wall is similar to that of a flat

plate, see Figure 17. At points of contact with the stationary particles, the boundary layer is destroyed and starts once again.

Unfortunately, the two models do not take into account the influence of the solid particles on the heat transferred, so they must be considered of limited application.

2. Unsteady Heat Conduction by Single Particles in Direct Contact with the Heat Exchange Surface

With the advent of photographic studies of the boundary wall during fluidization, it was shown that the particles tended to associate in groups which moved slowly along the wall or remained in contact with the wall a certain length of time. Those observations led Botterill et al. [6] to propose that heat was transferred from the vertical surface to the adjacent layer of particles arriving together at the wall. If the residence time of the particle near the wall was long, heat would penetrate further into the bulk of the particles and if the residence time was short, heat exchange calculations would be limited to only one particle, the nearest to the surface. They confined their theoretical considerations to an isolated particle lying in contact with the wall.

After much experimentation this model was extended to cover different particle sizes and materials and a wide range of residence times for the particles at the surface. The results showed the validity of the model for short residence times with the observed effect that the heat transfer

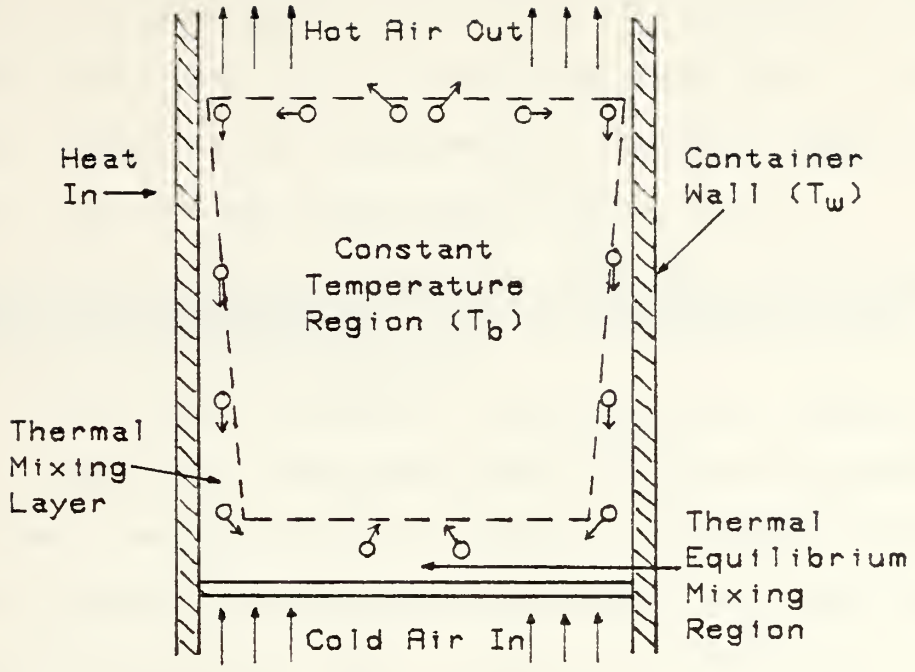

Figure 16. Heat transfer mechanism and particle motion.

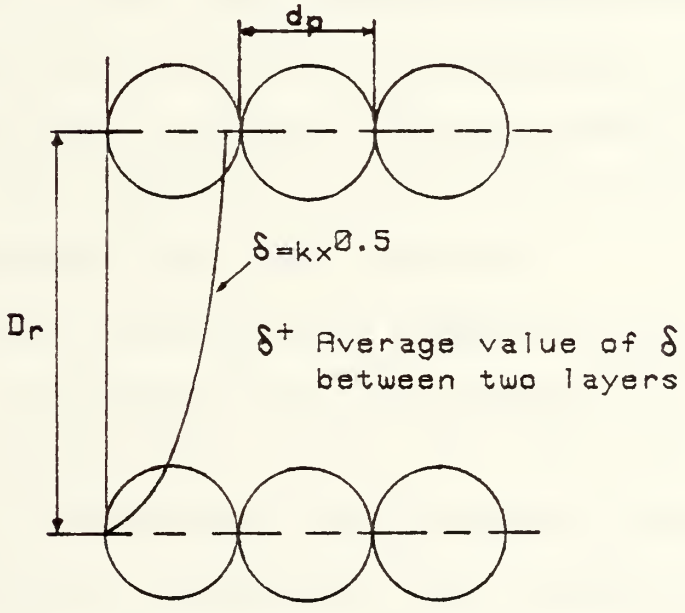

Figure 17. Laminar boundary layer thickness between two layers.

coefficient is a decreasing function of the residence time. Again, this model can only be applied to mechanically smooth dense phase fluidization as the model's validity breaks down in the lean phase or when bubbling/slugging occurs.

3. Unsteady Transfer of Heat to "Packets" of Particles Which are Renewed by Violent Disturbances in the Core of the Fluidized Bed

In an attempt to present a mechanism for the heat transfer in bubbling, dense phase beds, Mickley and Fairbanks [47] proposed a model of a small group of particles moving as individual packets. They based their model on the fact that the voidage of the dense phase bubbling beds was found to be close to the voidage of quiescent beds.

In the dense phase fluidized bed, each particle was expected to be in contact with several neighbors most of the time. The packets are not considered permanent; they have a finite life expectancy; and their voidage, density, heat conductivity, and heat capacity are assumed to be the same as those of the quiescent bed. See Figure 18.

This model assumes that as a packet at bed temperature T_b comes into contact with a flat surface at a temperature T_w that unsteady heat transfer will start upon contact. Further, if A_m is the contact area between the packet and the wall, and the packet is homogenous, then the heat transferred after some time t will be given by the equation

$$q_{wi} = h_{wiL} A_m (T_w - T_b) , \qquad (3.9)$$

where the local instantaneous heat transfer coefficient is given by the equation

$$h_{wiL} = \left[\frac{k_m \rho_m c_m}{\pi t}\right]^{0.5} . \qquad (3.10)$$

Mickley and Fairbanks [47] also presented two deviations from their original model which covered the phenomenons of slug flow and side mixing. The first, on slug flow, was for fluidized beds with very low gas flow rates and no turbulent mixing. In this model, Figure 19, the particles were to move downward along the outside wall of the bed. The flow is not smooth but is spasmodic owing to the intermittent passage of ascending gas bubbles near by in the core of the bed. However, assuming that the particles moved downward at a constant velocity (u_s), the age of all the packets at a distance ℓ from the bed top was $t = \ell/u_s$ and the resulting average heat transfer coefficient for a heater of length L_H could be found from the equation

$$h_w = 2\left[\frac{k_m \rho_m c_m u_s}{\pi L_H}\right]^{0.5} . \qquad (3.11)$$

The second model deviation, on side mixing, was for beds with large heat transfer surfaces that were highly turbulent. To represent this case, Figure 20, they assumed that as the particle packet is moving downward some of it is exchanged with some other packet at temperature T_b, brought

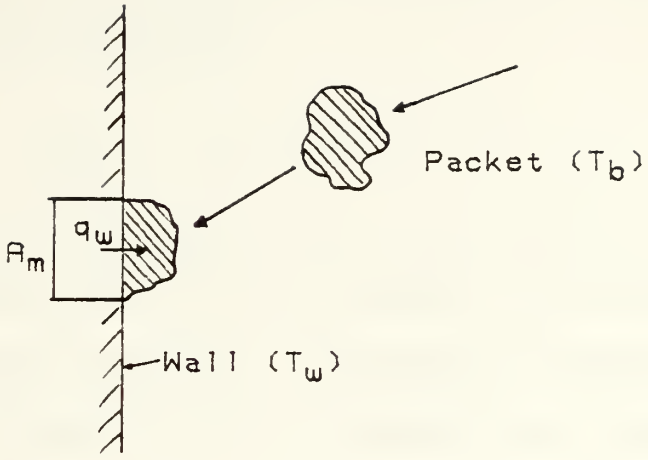

Figure 18. Transfer of packet to wall.

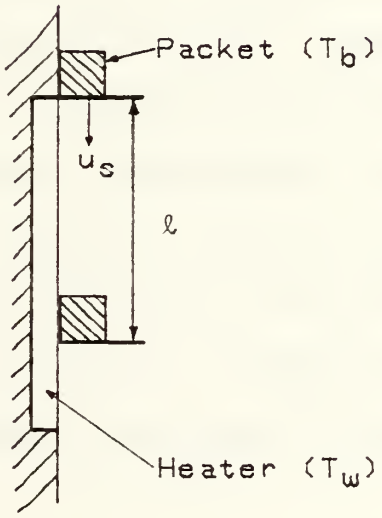

Figure 19. Slug flow of particles over a surface.

in sideways from the core of the bed. The average number of replacement packets at the wall per unit time resulting from side mixing was then defined as s, resulting in the local heat transfer coefficient equation

$$h_{wL} = (k_m \rho_m c_m s)^{0.5} . \qquad (3.12)$$

It should be noted that for these penetration type models the residence time of the particle is of fundamental importance and has generated a considerable amount of research both in its determination and its effect on the various models of this section.

Patel [53], in a further spin-off of Mickley and Fairbank's original models presented two surface renewal models that can be characterized as follows.

In model one, Figure 21, a packet initially at the bed temperature T_b arrives at the wall (temperature T_w) at time t = 0. The packet is assumed to have the same properties as the bed at minimum fluidization. It receives heat from the wall through a contact resistance and returns to the bed after some length of time. During that residence time, heat penetrates a distance x; beyond this distance the temperature is constant and equal to the bed temperature T_b.

In model two, Figure 22, the fluidized particles are assumed to be spherical and of the same diameter (d_p). A particle at the bed temperature T_b arrives at the heating

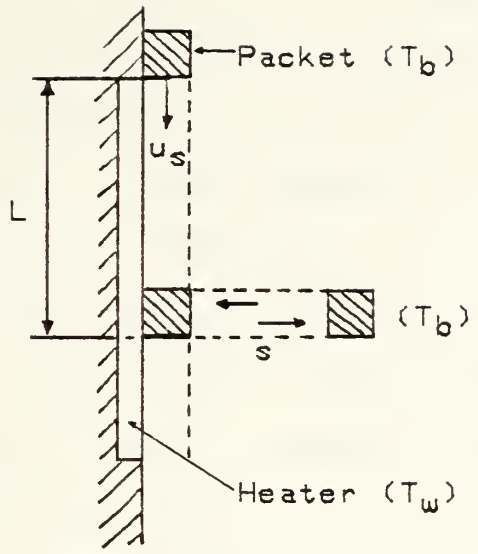

Figure 20. Downflow of particles with side mixing.

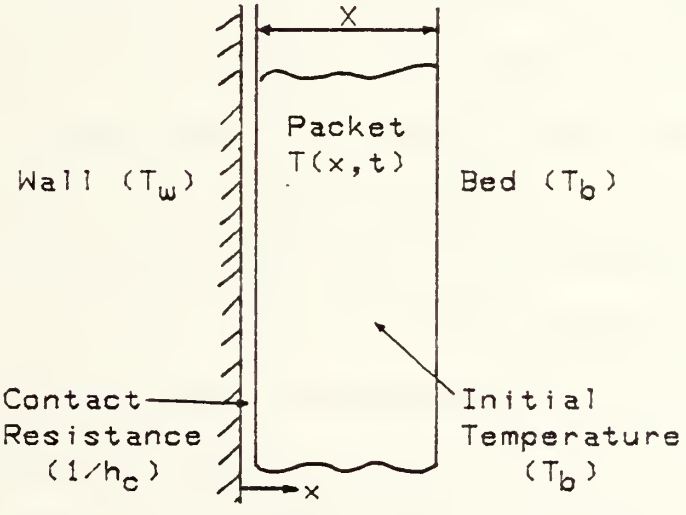

Figure 21. Patel Model I.

surface (temperature T_w) and receives heat from the fluid adjacent to the wall. This fluid is assumed to be stagnant and at wall temperature T_w. While the particle is at the surface it also loses heat by conduction to a packet of particles of thickness x situated between the wall particle and the bulk of the bed. The packet is assumed to have the same properties as the bed at minimum fluidization conditions.

Patel by no means had the only variation on Mickley and Fairbank's packet theory. Numerous other variations exist with different h_w values being correlated by each researcher. Appendices A through C give some of the resulting correlations.

4. Steady Convection Through the Emulsion Layer

van Heerden et al. [66] observed that the heat capacity of the particles per unit volume is of an order of magnitude of thousands times greater than that of the gas and that the mean particle velocity is much lower than the gas velocity. Therefore, the largest portion of the heat will be transferred by the moving particles. They assumed that the gas temperature was that of the particles and as a result that the gas only provided a suspension for the particles.

They observed negligible radial motion of the bed particles and therefore concluded that the radial heat transfer was a function of the thermal conductivity of the suspension. Experimentally, they verified that the heat transfer coefficient is large for short heat exchange surfaces and vice versa.

Wicke and Fetting [75] furthered van Heerden's work and proposed a model, Figure 23, for those observations. In their model, heat (q_w) from an exchange surface was first transferred by conduction through a gas layer whose thickness was δ_G. This heat was then divided into two components: namely heat (q_z) taken by the particles flowing parallel to the surface in a second zone of emulsion of thickness δ_e, and heat (q_r) transferred into the core portion of the bed by interchange of the particles. In their calculations, however, they neglected the term q_r.

The last model to be presented is actually a combination of several heat transfer mechanisms proposed in earlier models.

5. Kunii and Levenspiel Model [34]

In this model, Figure 24, four mechanisms operate together.

a. A film of gas coats the surface. Its thickness (δ_G) is large or small depending on whether a bubble of air is near the surface or the emulsion is uniform and close to the surface.

b. Some solid particles are in direct contact with the heat exchange surface.

c. There is a layer of emulsion with thickness δ_e which flows along the wall.

d. Part of the emulsion layer is replaced occasionally by fresh emulsion coming from the core of the bed or by bubbles rising along the wall.

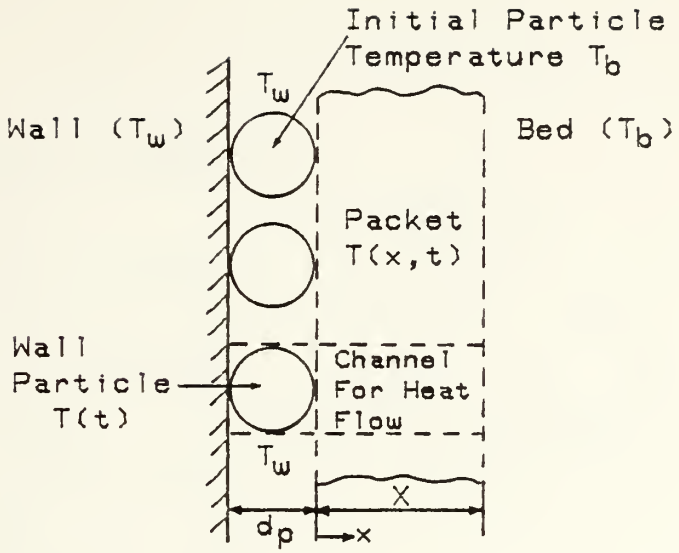

Figure 22. Patel Model II.

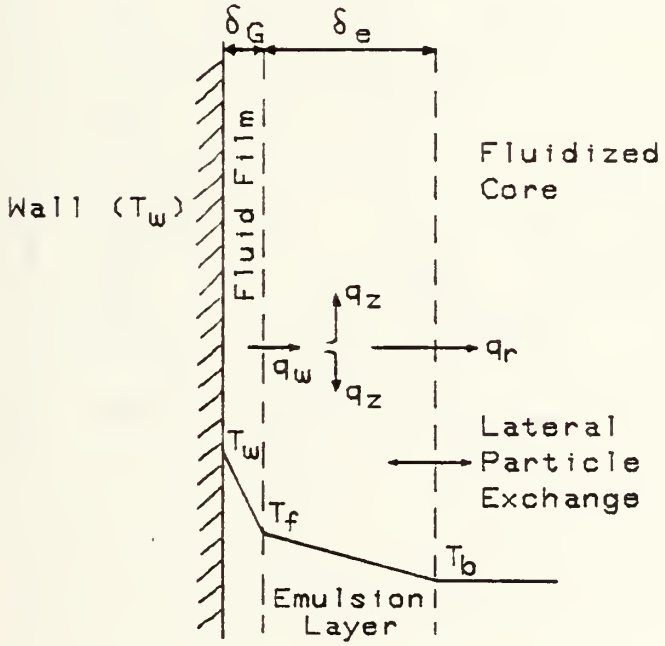

Figure 23. Wicke and Fetting Model.

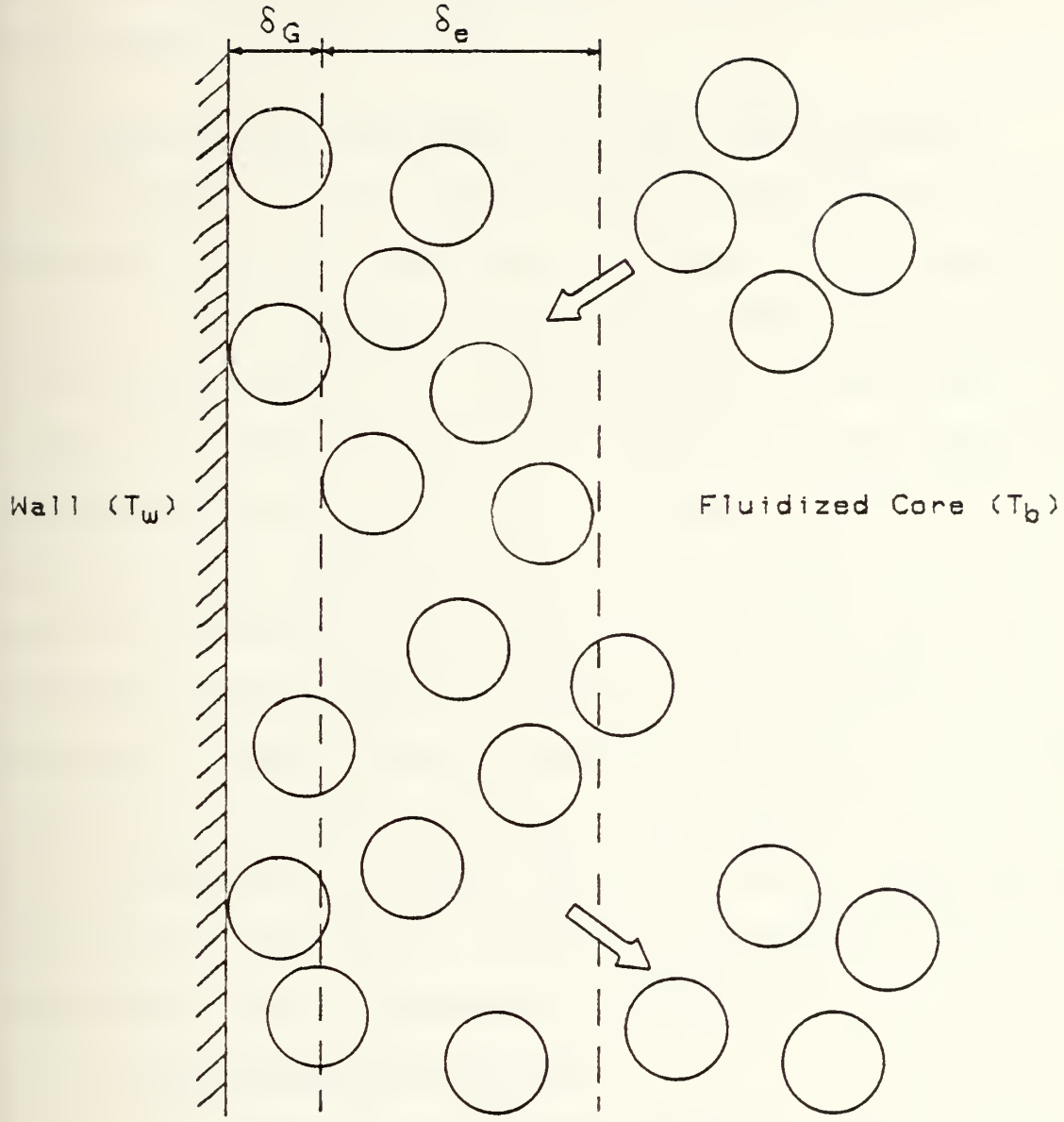

Figure 24. Kunii and Levenspiel Model.

Depending upon the fluidization conditions and the position of the heat exchange surface in the bed, emphasis can be placed upon any combination of the above four mechanisms.

C. FLUIDIZED BED VARIABLES THAT AFFECT HEAT TRANSFER

In addition to the large number of models that have been proposed by various researchers to explain their experimental results in heat transfer, there are a number of variables which have been found to affect the heat transfer rate. In general, the factors which will control the heat transfer characteristics of the bed will be those variables which determine the fluidizing properties of the bed. In this section an attempt will be made to list some of the more important factors and their effect on heat transfer. An excellent indepth review of general fluidized bed characteristics was researched by Gutfinger and Abauf [28]. Additionally, Appendices A through C present a list of nondimensional correlations reported by different investigators while trying to correlate their experimental findings.

1. Properties of the Fluid

a. Density (ρ_f) and Specific Heat (c_{pf}) of the Fluid

The dependence of the heat transfer coefficient on the specific heat of the gas has not been clearly determined as the existing data shows no common trend. However, Gelperin and Einstein [18] have predicted that there would

be an increase in the heat transfer rate with an increase in c_{pf} or the product $\rho_f c_{pf}$ when the fluid was at high pressures and velocities.

b. Gas Viscosity (μ)

The majority of researchers agree that with an increase in the gas viscosity the wall heat transfer coefficient will decrease.

c. Thermal Conductivity of the Gas (k_f)

This is the fluid property that has the most pronounced effect on the heat transfer coefficient. Depending on which researcher is consulted the value of h_w will increase proportional to k_f to the power of 0.5 - 0.67.

2. Properties of the Bed Particles

a. Diameter (D_p) and Shape of the Particle (ϕ_s)

A significant number of researchers [37,47] have concluded that the heat transfer coefficient decreases when large diameter particles are used. However, the results of Sarkit et al. [60] as reported by Gelperin and Einstein [18] show that for the laminar flow region the heat transfer coefficient varies inversely with particle diameter and for the turbulent flow region it has a direct variation.

The values for the heat transfer coefficient tend to increase as the sphericity (ϕ_s) increases (rounder and smoother particles).

b. Density of the Particle (ρ_s)

Experimentation has shown that the wall heat transfer coefficient increases with the increasing density

of the solid particles. However, this increase slows in its magnitude as the fluid flow becomes more turbulent.

c. Specific Heat of the Particle (c_{ps})

The heat transfer coefficient increases with an increase in the specific heat of the particle.

d. Thermal Conductivity of the Particle (k_s)

Based on measured experimental results over a wide range of particle thermal conductivities it has been determined that the effect of the thermal conductivity of the particle on the heat transfer coefficient is slight, so much so that it is usually neglected as a factor of concern.

3. Fluidization Conditions

a. Gas Mass Velocity (G)

The increase in the heat transfer coefficient is proportional to G^n where n will vary according to the experiment being conducted. Its range has been shown to be quite large. About the only facts that have been agreed upon by researchers for this variable is that of the general shape of the gas mass velocity versus heat transfer coefficient curve [72], Figure 25, and that there is some maximum value for h_w which exists at some gas mass velocity G_{opt}. Tables listing the nondimensional correlations for both the rising and falling sides of the curve, for the maximum heat transfer coefficients, and for the special gas flow rates when the h_{wmax} is attained are presented by Einstein and Gelperin [14].

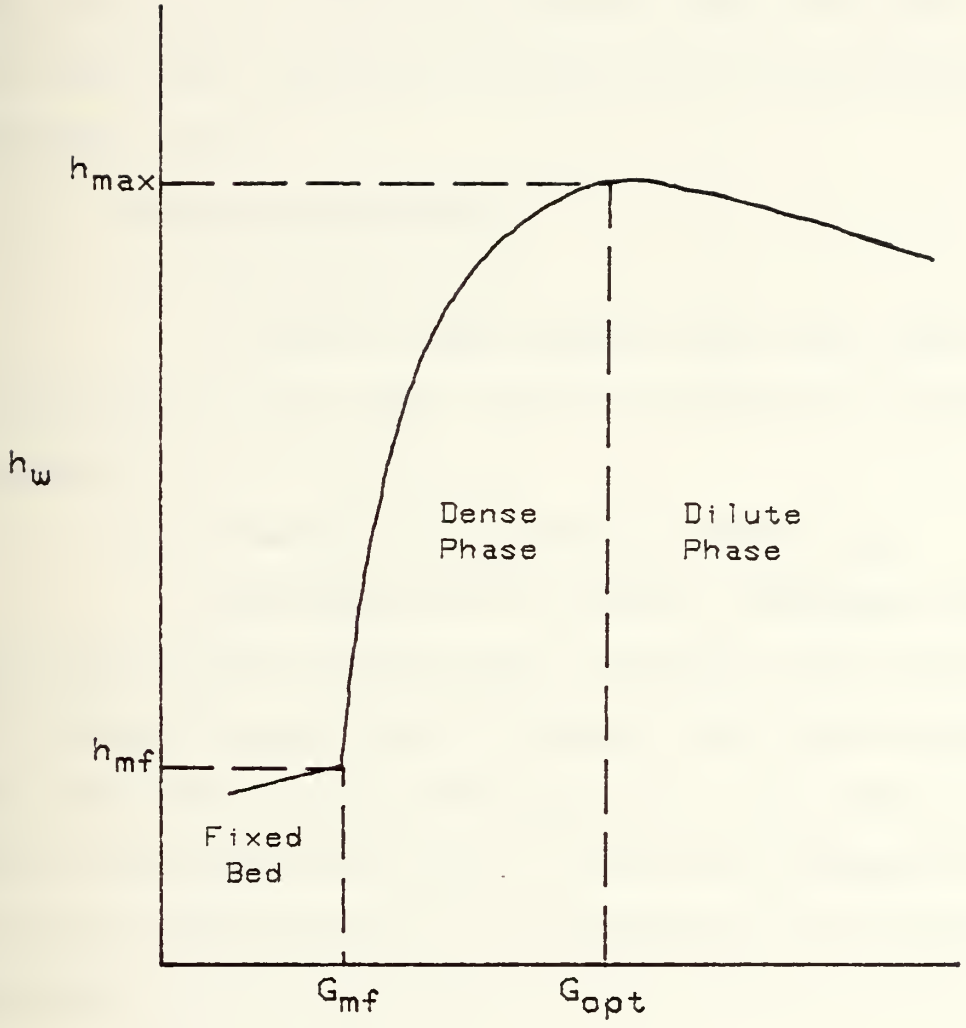

Figure 25. Heat transfer coefficient vs. mass velocity.

b. Bed Porosity or Voidage (ε)

Based on film theory the heat transfer coefficient will vary inversely with some function of the bed porosity. That is, as the particle aggregate at the wall decreases so will the heat transfer rate. However, there has been some experimental data which has demonstrated the opposite effect.

4. Geometric Variables

a. Bed Diameter (D)

It has not been demonstrated that there exists a dependency of the heat transfer coefficient on the bed diameter.

b. Diameter of an Immersed Heater (D_H)

Researchers are in general agreement that the wall heat transfer coefficient increases with a decrease in the immersed heater (tube) diameter, and that the heat transfer rate diminishes as the diameter of the heater is increased. These effects are valid up to a particle diameter of 10 mm (0.39 in) after which h_w is independent of the heater diameter.

c. Fluidized Bed Height (L)

There has been no dependence shown between the heat transfer coefficient and the fluidized bed height.

d. Length of Heat Exchange Surface (L_H)

This is a variable that has had several different results on its effect on the heat transfer coefficient

all of which have been substantiated by additional research. Basically, one research group has found that the heat transfer coefficient decreases with an increase in the length of the heat exchange surface. Another research group concluded that if L_H/D was greater than 7 for an external heat transfer surface, then the heat transfer coefficient was independent of heater length and that internal heat exchange surfaces had no observed effect on the heat transfer coefficient. And yet a third research group found that if the heat exchange surface was located above the active section of the bed (mixing region), then the heat transfer coefficient would be independent of the heater's length.

e. Heat Exchange Surface Roughness

It has been determined [31,68] that the heat transfer coefficient is sensitive not only to the type and orientation of the roughness but also to the size of the particles relative to the size of the roughness. When the particles are of a large size relative to the roughness, the gas conduction paths will be longer and the heat transfer will be lower as compared to a smooth tube or surface. See Figure 26a and 26b.

When particle and roughness sizes are similar, the multiple contact should reduce the mean gas conduction paths and gives rise to a considerable increase in the heat transfer, Figure 26c. However, possibly due to particle capture and the consequent increase in particle residence

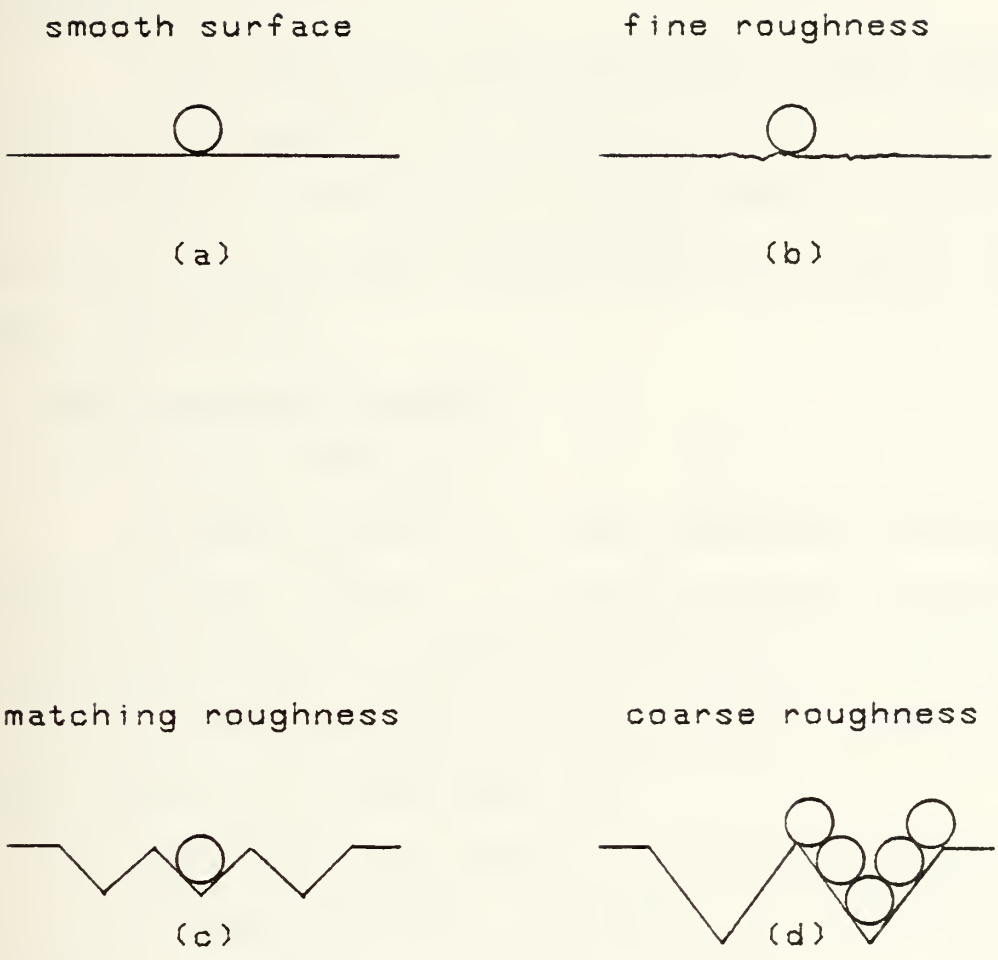

Figure 26. Contact geometry of surface-particle.

times, the increase in the maximum heat transfer coefficient for vertical grooves, is of the order of 50% for the smaller particles and 18% for the larger particles. The particle capture and inability of the bubbles to replenish particles in the case of horizontal grooves undoubtedly contributes to this difference.

Where the size of the particles is much smaller relative to the roughness size, particle capture is not a serious problem, but there is some improvement in particle-surface contact as well as a larger effective area for heat transfer, Figure 26d.

5. Miscellaneous Variables

a. Entrance Effects

Entrance effects in a flow situation cannot be ignored or avoided. Control or limiting entrance effects can only be accomplished by careful design of the gas distributor, which in turn, will influence the configuration of the active (mixing) region of the fluidized bed.

b. Temperature and Pressure of the Fluidized Bed

The heat transfer coefficient is independent of the pressure of the fluidized bed or fluidizing fluid. The temperature of the fluid, however, is another matter. In general it can be assumed that the heat transfer coefficient is independent of the temperature of the bed or fluid. Studies by Zabrodsky [79] and Yoshida et al. [77], however, indicate that the radiation component of the overall heat

transfer coefficient must be taken into account when the bed temperature exceeds 900-1300 K. In turn, the magnitude of the radiation component effect will be dependent on the bed container geometry.

D. IMMERSED BODIES

Experimental work conducted in fluidized beds can be subdivided into two distinct categories. The first deals with all experimental work that uses an external heat transfer surface, i.e. the wall of the fluidized bed container itself is used as the heat exchange surface. The second category uses an internal heat transfer surface. In this case, bodies of different shapes (sphere, cylinder, plate, coil, etc.) which are immersed in the bulk of the fluidized bed become the heat transfer surface.

While the previously discussed variables and characteristic bed behavior are equally germane to either category, the use of immersed heating surfaces will have additional factors that will need to be taken into account during a design process. The location of the heat source with respect to the gas distributor plate and its plane of orientation will have a significant effect on the heat transfer coefficient. The results of the variations are sometimes contradictory and depend strongly on the local hydrodynamic conditions in each case.

Limited experimentation has been conducted in the use of spheres, flat plates and small cylinders with the data

obtained being sketchy at best. The bulk of the immersed body experimentation has been with tubes for which additional variations in heat transfer tube design (size, shape, spacing, gap, pitch and material) will complicate the general heat transfer mechanism. An excellent indepth coverage of this topic was conducted by Saxena et al. [61] and is summarized as follows.

1. Horizontal Tubes

The total heat transfer coefficient (h_w) for single cylindrical tubes increases with factors that increase the gas thermal conductivity near the tube wall (i.e. temperature at the tube surface) and reduces the particle residence time (i.e. decrease in tube diameter and increase in fluidization velocity). However, at higher gas velocities the decrease in bed density reduces the heat absorption capacity of the fluidized particles, resulting in a decrease in the heat transfer coefficient (h_w). The heat transfer coefficient also increases with decreasing particle diameter (d_p).

The heat transfer coefficient is highest for tubes with a lenticular cross section for dense moving packed beds. Gas pockets are not created in the flow wake (downstream side) of a lenticular tube, and the particles are not stagnant on the upstream side of the tube.

The presence of surrounding tubes in an array affects the total heat transfer coefficient for an individual tube by resisting particle movement and by altering the particle

temperature from that of the bed bulk, which reduces the temperature driving force. This is at least one of the reasons why the heat transfer coefficients for the lower tubes are greater than for the upper tubes, and a close spacing of the tubes results in a decrease of the heat transfer coefficient.

Fins will increase the rate of heat transfer to the tubes. However, their effectiveness increases, reaches a maximum, and then decreases with decreasing spacing distance and increasing fin length [54].

An increase in tube-to-tube spacing in a bundle of short-finned tubes, which reduces the resistance to particle movement between the tubes, increases the total heat transfer coefficient. However, an increase in tube-to-tube spacing for a bundle of long-finned tubes does not noticeably increase the heat transfer rate, implying that the resistance to particle movement between fins predominates.

2. Slanted Tubes

There does not appear to be any particular advantage in slanting the heat transfer tubes. Minimum heat transfer coefficients have been observed at 45^0 for bare tubes and at 60^0 for finned tubes with respect to the horizontal bed axis. The heat transfer coefficient values obtained were in comparison to the values obtained for tubes of the same configuration but in a horizontal and vertical position [23].

3. Vertical Tubes

The total heat transfer coefficient for a single vertical tube generally increases with a decrease in tube length

and diameter, a decrease in the fluidized particle size (sizes less than about 1 mm (0.039 in) at atmospheric pressure), and an increase in fluidization gas velocity up to u_t.

The heat transfer coefficient for a tube within a bundle increases with an increase in the tube spacing and is greater for tubes located nearer to the center of the bundle, at least for small bundles.

The heat transfer coefficient for a finned tube generally increases with the fin height and a decrease in the frequency of fins along the tube length (in the range of 21-10 fins/in). Heat transfer also improves with roughened and grooved tubes.

IV. EXPERIMENTAL APPARATUS AND PROCEDURES

This section will describe the details and procedures as related to the experimental apparatus. The methodology and experimental procedures will also be discussed.

A. DESCRIPTION OF THE FLUIDIZATION APPARATUS

The fluidization container for the experimental investigation was constructed of one half inch thick clear plexiglas (Grade GM). The inside dimensions of the rectangular enclosure were variable as one wall was capable of movement within the boundaries of the container. This movement allowed the variation of the inside dimensions from six inches wide by six inches deep by eighteen inches high to twenty four inches wide by six inches deep by eighteen inches high above the distributor plate. All joints were glued together and wood screws added in mounting the distributor plate for additional weight carrying support. Mounted within each of the two side walls is a five inche wide by ten inch high strip heater that has the heating surface on the same plane as the inside plexiglas wall. Backing the strip heaters are two layers of insulation (silicone rubber sponge and plexiglas) which provide both rigidity and a mounting platform for the strip heater. Static pressure taps and bed thermocouple taps were installed at evenly spaced intervals as shown in Figure 27.

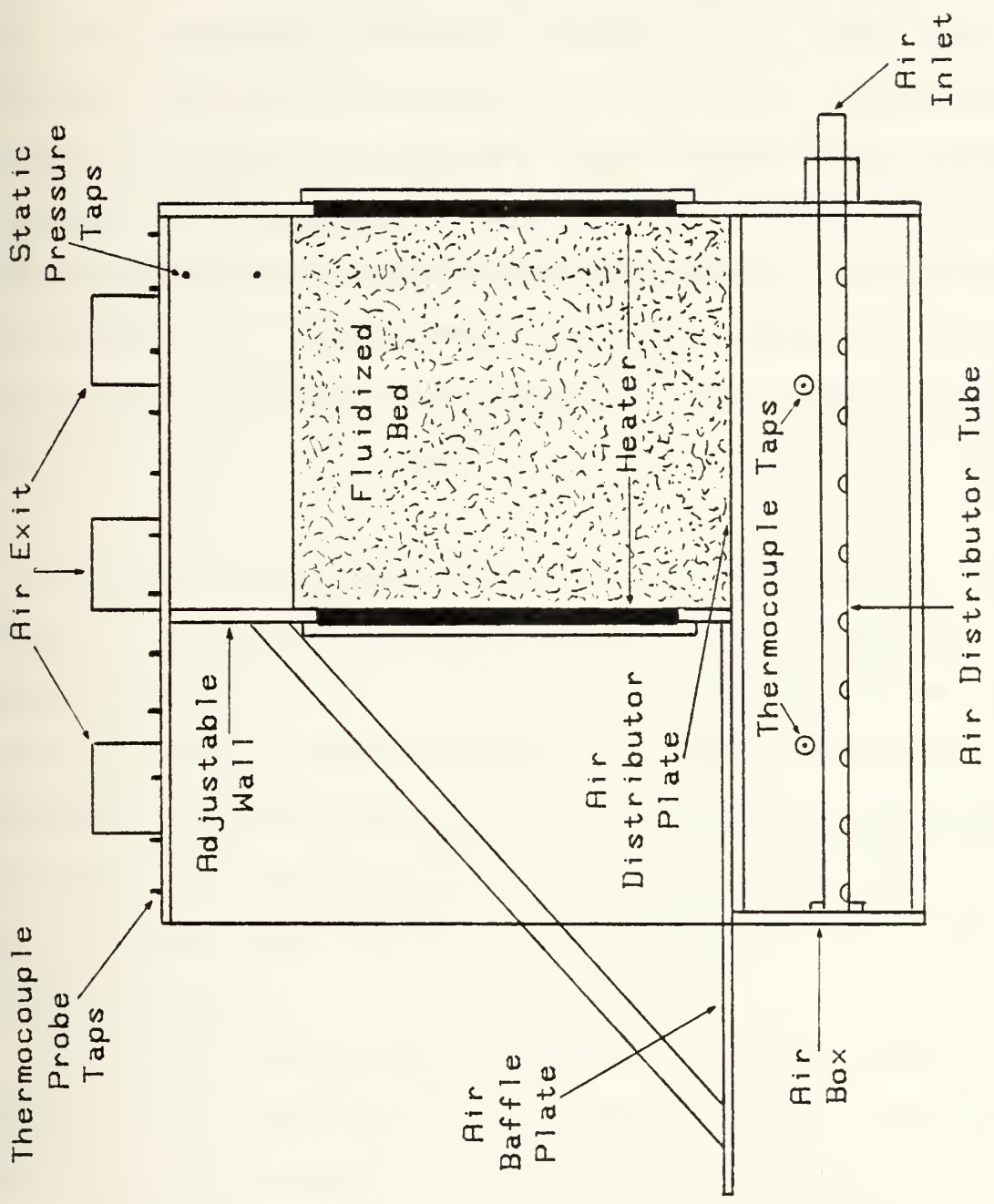

Figure 27. Fluidization apparatus.

Pressure drops were measured using the static pressure taps with the output going to a Meriam Type W Model A324 sixty inch water manometer or a Model 33KA35 thirty inch water manometer via a pressure manifold. Air and bed temperatures within the experimental apparatus are measured with copper-constantan thermocouples as described in the EXPERIMENTAL HEAT TRANSFER PROCEDURE AND APPARATUS section of this thesis and recorded on a Newport Model 267B-TF2, Multipoint (12 Channel) Digital Temperature Recorder. The complete equipment listing for this experimental study is given in Appendix E.

The distributor plate utilized in the fluidization container was constructed of one half inch thick plexiglas (Grade GM) with a grid of 0.125 in diameter holes bored at 0.25 in center to center spacing. To cause the required pressure drop which aids the air distribution and to prevent the particles from falling into the air box, one layer of 140 mesh stainless steel wire cloth was mounted on top of the distributor plate.

The air was supplied by a Clements Cadillac Blower/ Suction Cleaner Model G12 with a nominal output of about 20 scfm of air at a nominal line pressure of 1.5 psig. The flow output data is based on experimental testing of the blower since blower characteristic curves are not available. The air inlets to a two and one half inch inside diameter plexiglas tube that has one half inch circular air ports spaced

at one inch center to center intervals along its length. The air ports are located at the underside of the tube allowing the air to exhaust downward into the air box. The plexiglas tube runs the length of the air box which has inside dimensions of twenty four inches wide by six inches deep by six inches high. The air is unfiltered and prevented from exiting outside of the variable bed inlet area by an air baffle mounted to the movable wall above the distributor plate. The schematic line diagram of the air supply system is shown in Figure 28.

The air flow rate was measured with a Fischer and Porter Company Model 10A3565A Flowmeter (rated at 11.1 scfm) which was corrected for local barometric pressure. Photographs showing two views of the overall experimental apparatus can be found in Figure 29 and 30.

B. EXPERIMENTAL HEAT TRANSFER PROCEDURE AND APPARATUS

Four different rectangular bed configurations using a standard static bed height were investigated. For each bed configuration both an unheated and heated run were conducted with various pressure, temperature and visual data taken on each run.

Once the bed size was adjusted, the bed of particles was initially fluidized at a point above minimum fluidization. When steady state conditions had been reached, the bed and air (inlet and outlet) temperatures were recorded and a

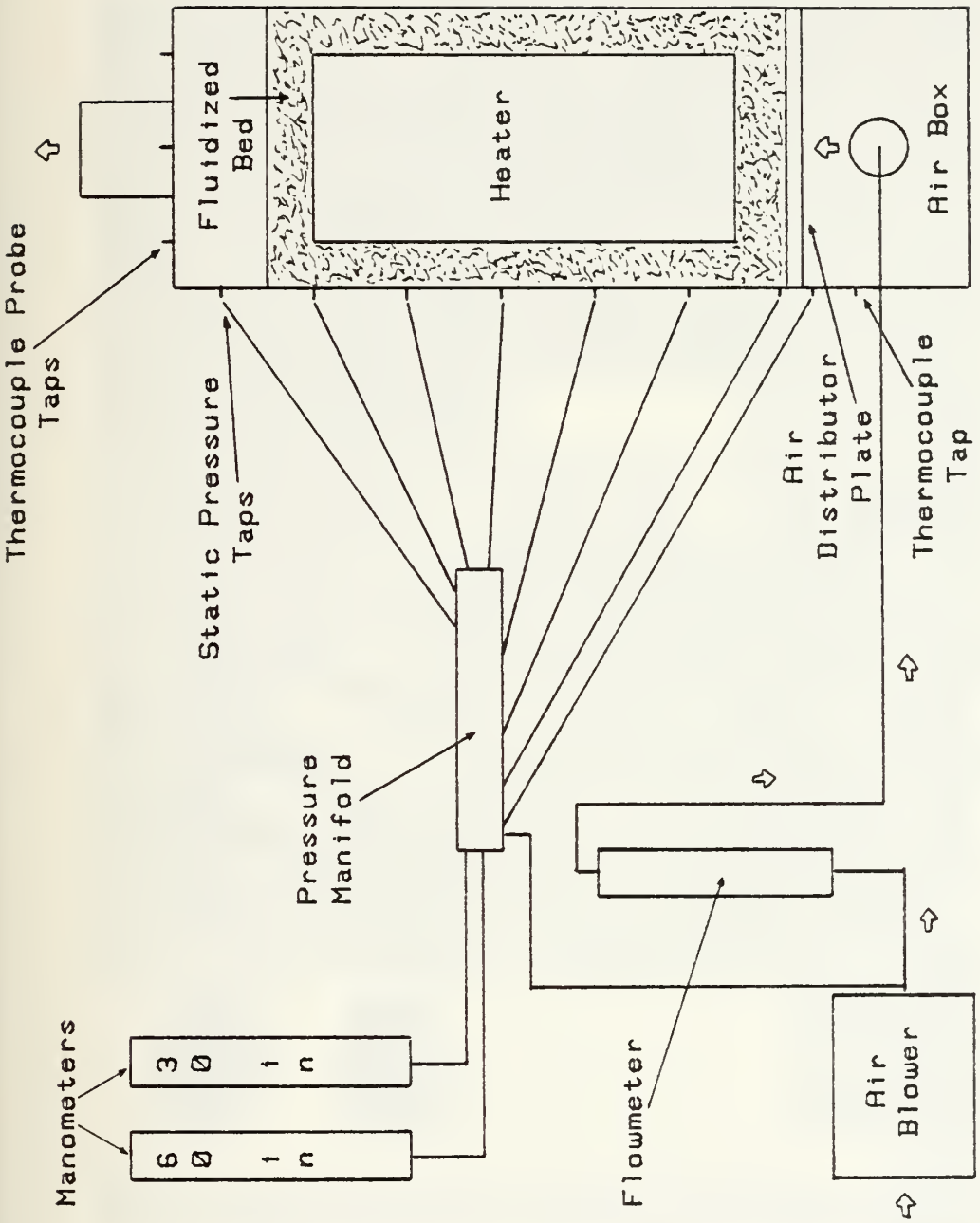

Figure 28. Diagram of fluidization system.

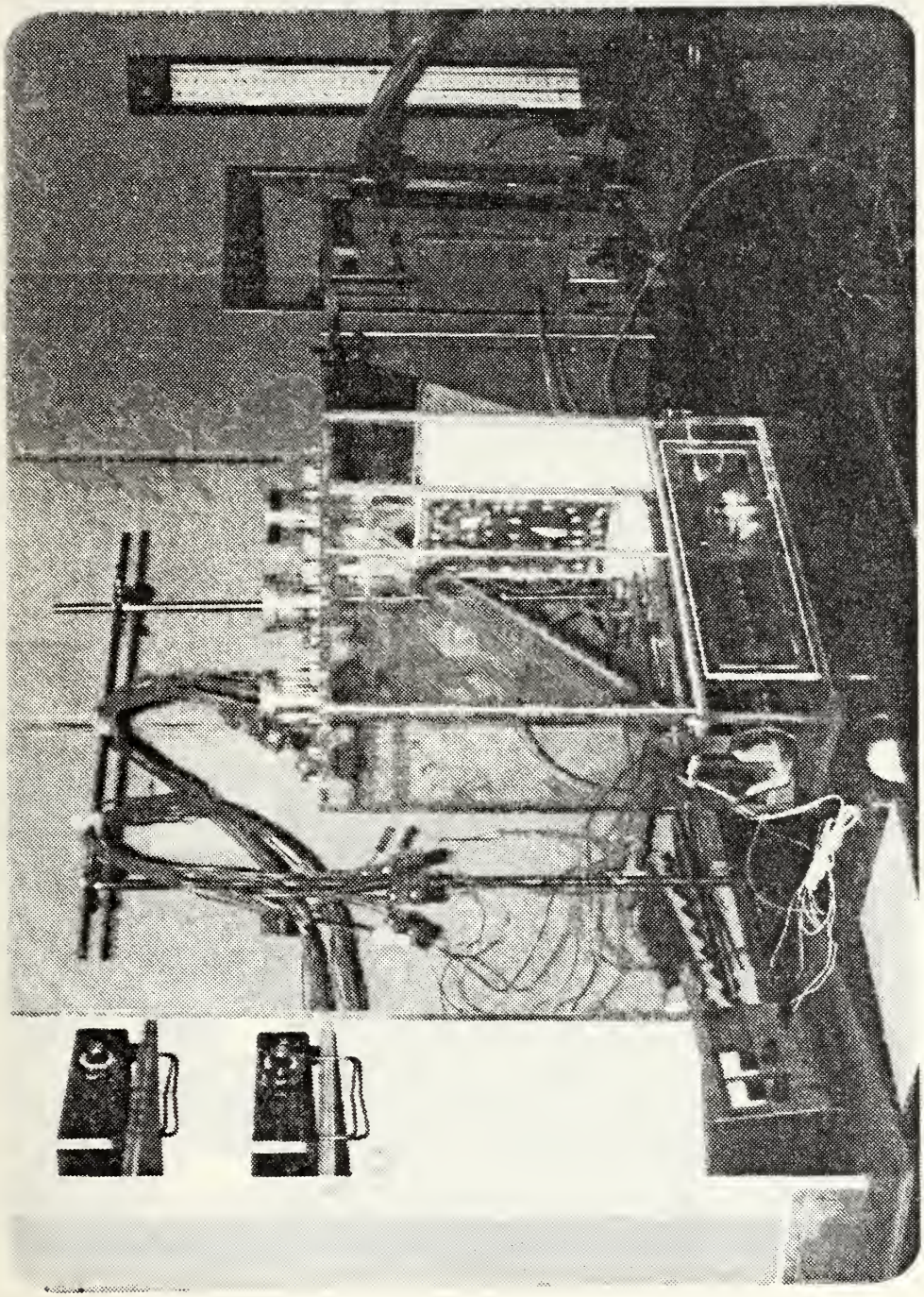

Figure 29. Photograph of experimental apparatus.

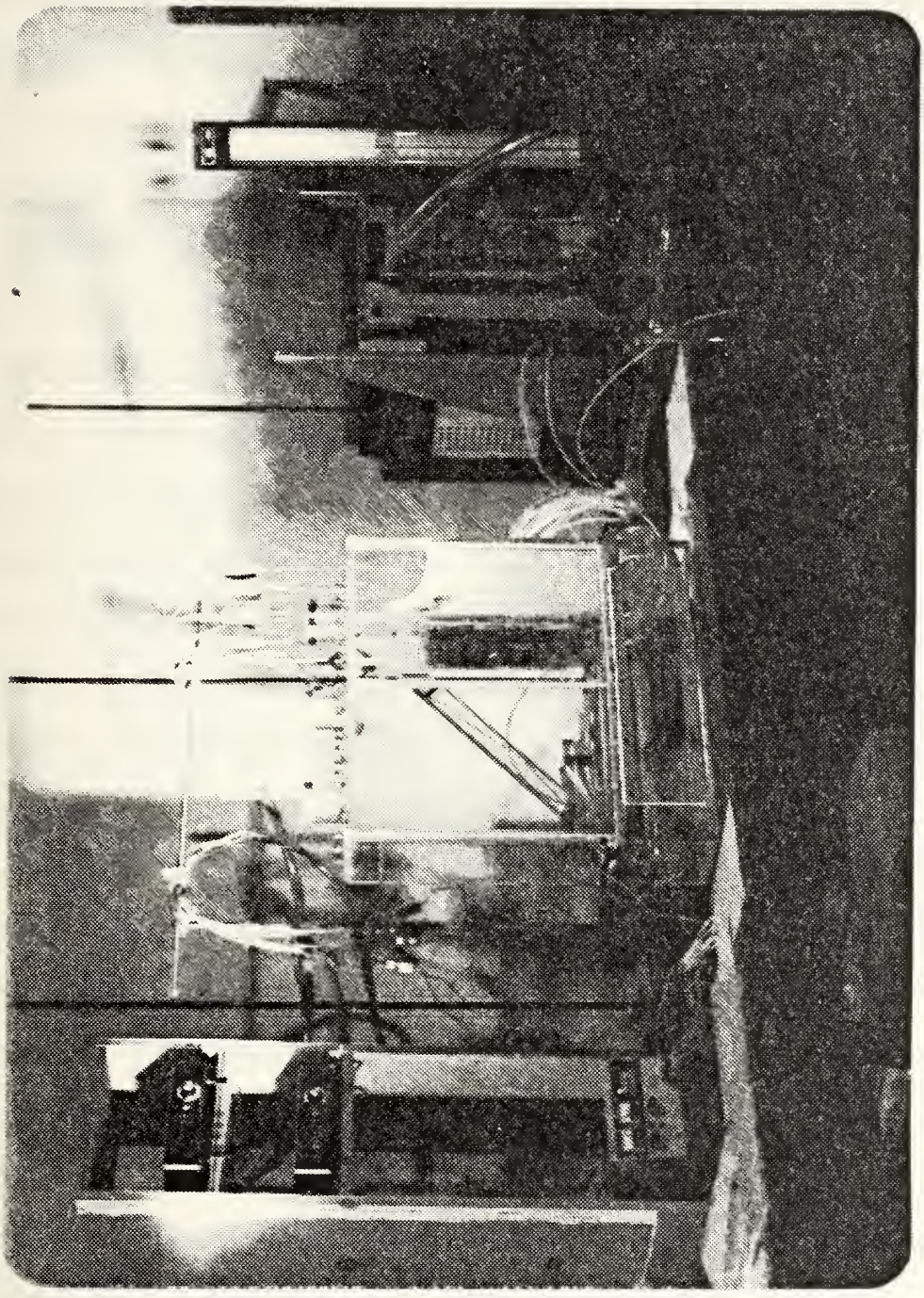

Figure 30. Photograph of experimental apparatus.

comment recorded describing the visual condition of the external boundaries of the bed. This was the starting point for the run.

As a separate study, bed pressure drop was recorded as a function of several flow rates. This information was used to determine the point of minimum fluidization for the particular bed configuration and to serve as an indicator for the presence of slugging or channeling conditions within the bed.

After the base data run was recorded, power was applied to the two Watlow Silicone Rubber strip heaters by way of a Lamba Regulated Power Supply, Model LK345A. The power supplied to the heaters was computed by measuring the voltage and amperage. Energy losses by conduction were accounted for in the heater configuration and an energy balance computed for each run.

Since the purpose of this experiment did not include a need to determine a heat transfer coefficient, provisions were not made to determine heater wall temperatures or the temperature gradients close to the heater wall. On all runs the expanded bed height covered the strip heaters ensuring that all heat transfer was either to the bed or losses through the insulation. Radiation losses were neglected since bed/wall temperatures were considerably less than 1000 K.

At various heater power levels a series of temperature readings were recorded until flow characteristics were

determined for each bed configuration. The above experimental procedures were continued until all bed geometry configurations had been studied.

The details of the heater configuration and mounting method are shown in Figure 31. Insulating end blocks were used for both mounting and end heat loss reduction for the two heaters. Heater insulation consisted of 0.5 in of silicone rubber sponge with a mounting block of 0.5 in of clear (Grade GM) plexiglas. Two insulated copper-constantan thermocouples were applied to the outside of the plexiglas mounting blocks to measure their outer surface temperature. These temperatures were used to estimate the heat loss through the back of the heater by conduction for use in the heat balance of the model.

The strip heater resistance element is constructed of a fine nicket alloy wire wrapped around a glass cord. The element wires are arranged in a parallel rectangular configuration thus confining any failure to a single element rather than the entire unit. Each heater is rated at 250 watts, 115 volts with a temperature range of 0-200^{0}F. A considerably higher temperature range is possible by cementing the heater to various metal plates, but is limited in this application due to the melting temperature of the plexiglas.

To measure the bed temperatures a grid pattern of thirty retractable Omega Engineering ANSI T (Copper-constantan) twenty-four inch stainless steel sheathed exposed junction

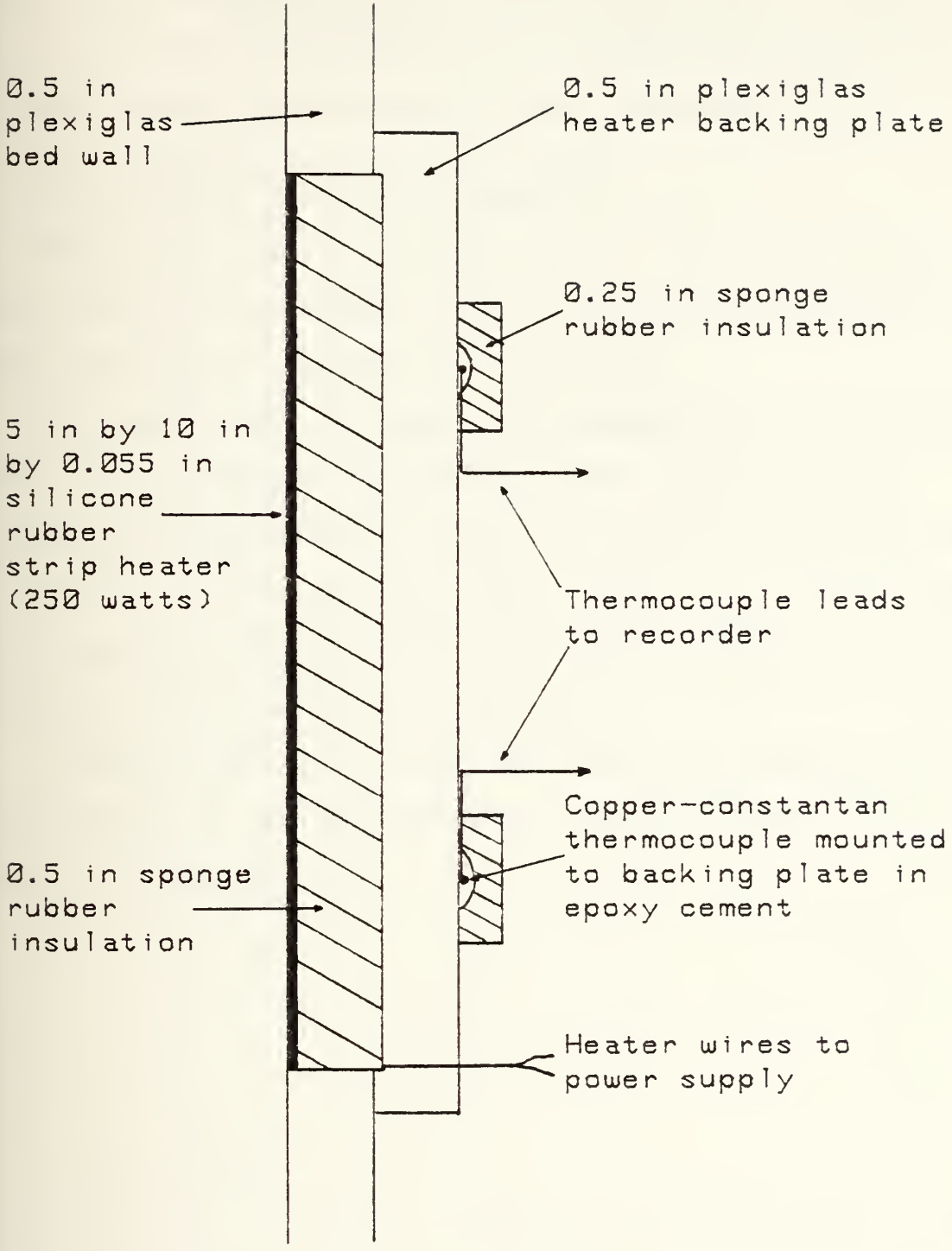

Figure 31. Heater Assembly.

thermocouple probes was used. By varying the depth of the individual thermocouples the boundary positions of the particle and fluid flow cells could be determined and changes to the original pattern noted during the various runs.

C. EXPERIMENTAL APPARATUS CALIBRATION

Manometers used for static pressure drop and differential pressure measurements were continuously rechecked for zero readings and readjusted as required.

The temperature recorder and thermocouples were calibrated with a Rosemount Commutating Bridge Model 920A and Rosemount Calibration Bath Model 913A using liquid nitrogen and water. A least squares linear curve fit was applied to the resulting data for each thermocouple to obtain suitable constants for temperature correction.

Technical data on the bed particles and experimental verification of the manufacturer's specifications can be found in Appendix F.

V. PRESENTATION AND DISCUSSION OF RESULTS

Based on bed observations during the fluidizing process a very definite electrostatic charge built up within the bed container, see Figure 22. This phenomenon was characterized by the bed particles adhering to the walls of the bed after the air had been turned off and to the thermocouple probes during fluidization. Based on evidence provided by Miller and Logwinuk [49] this phenomenon will to some extent contribute to erratic results in the heat transfer and data measurements. Some of the factors which are thought to affect the magnitude of the electrostatic charge effects are (1) the dielectric constant of the bed material used, (2) the contact potential difference, (3) the ratio of fluidized bed particles to gas, (4) the properties of the gas, (5) the temperature of the solid-fluid system, and (6) the nature of the surface of the bed particles. For the purpose of this thesis, the electrostatic charge existance will be acknowledged but no data correction will be considered warranted. Further study on this area is, however, considered worthwhile.

A. FLOW PATTERNS

The particle movement along the wall at any level is influenced by the movement within the fluidized bed at that level, as it is the movement of the inner particles which

drag the outer particles along the wall. Therefore the wall velocity profile should represent approximately the average particle velocity at the various levels within the bed. Had the motion been smooth with all particles starting at the top of the bed and flowing straight down to the bottom of the bed then the ideal, Figure 2, flow pattern would have occurred and the velocity of the particles could be assumed to be constant at the wall with a positive linear gradient into the axis of symmetry for the bed. In actuality this was neither observed nor anticipated within the rectangular bed under study due to the geometry involved.

In the initial geometric configuration, that of a square column (6x6x12.5 in), the particle motion appeared to conform to the particle circulation pattern of Figure 33. The fluidization somewhat resembled waves in that there were intermittent fronts moving smoothly up through the bed which terminated in a percolating (rupture) action at the top of the bed. The domed bulge, Figure 34, of particles was observed roughly in the center of the column and after rupturing, the bed particles would be thrown to the sides where they would start down the bed walls.

It was not possible to observe any distinct points of emergence into the bed of the particles in the downward transit but a definite entry point was visible at the bottom of the bed. The characteristic shape of the non-movement area was elliptical along the bed bottom and curving up at the corners, see Figure 35.

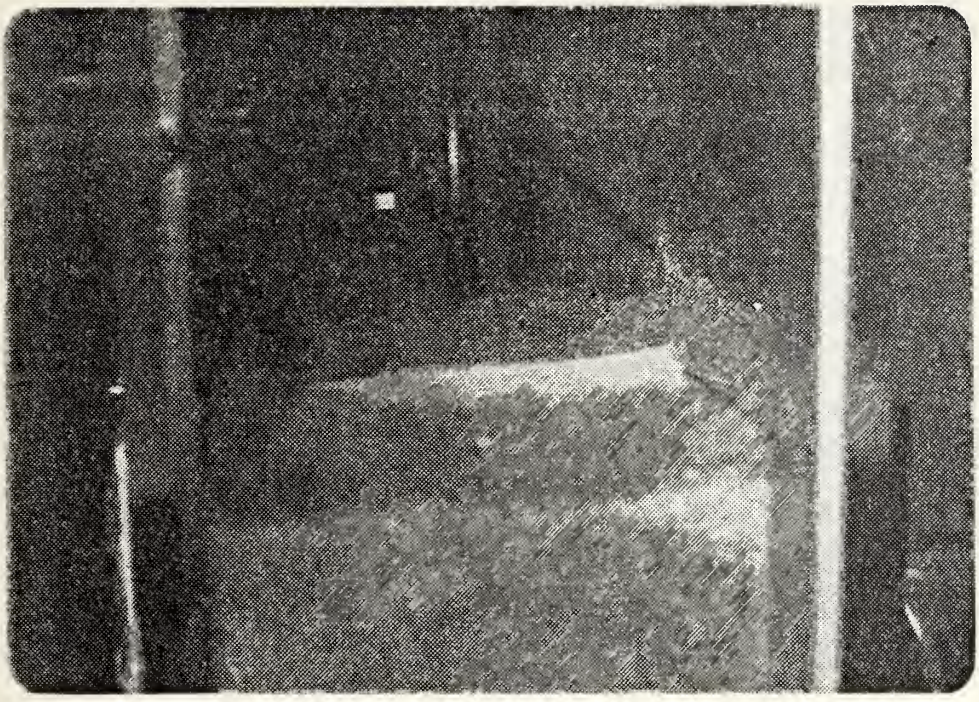

Figure 32. Electrostatic charge.

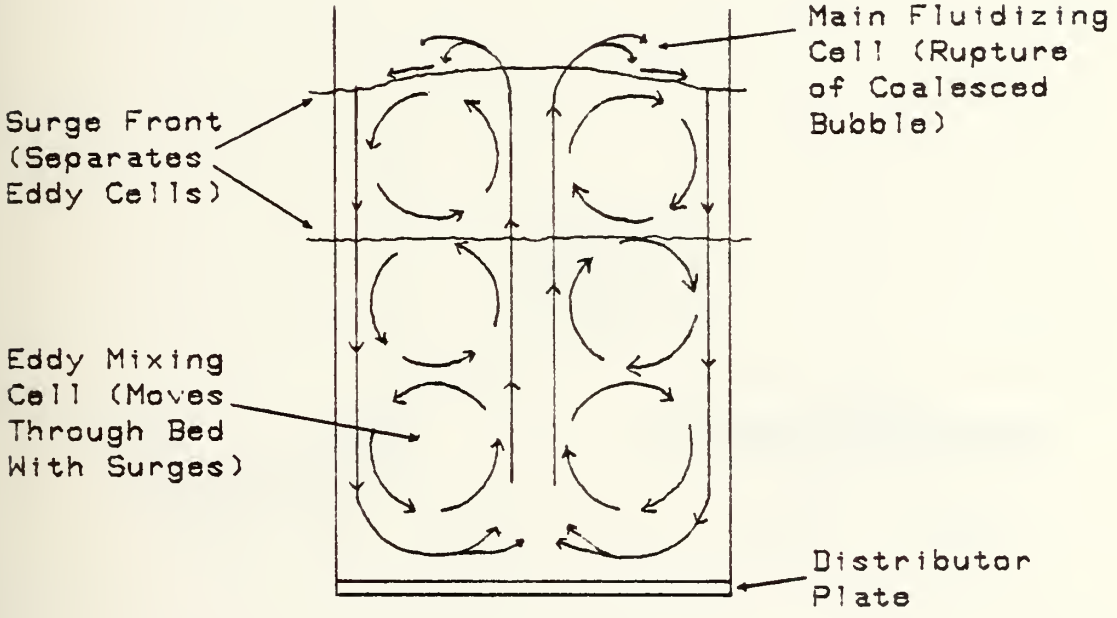

Figure 33. Proposed particle cell circulation.

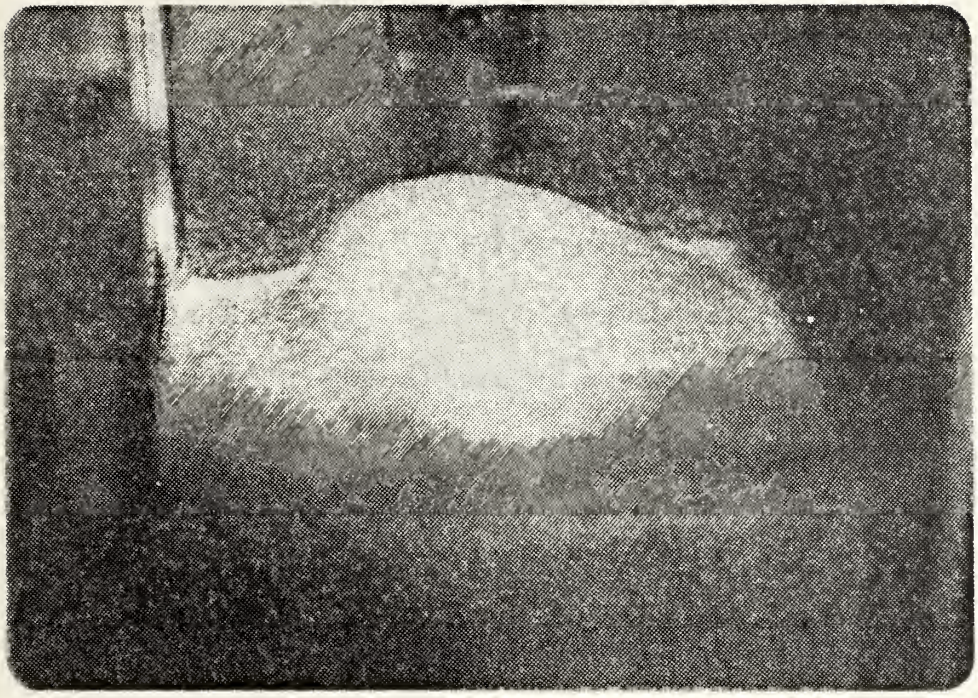

Figure 34. Square fluidized column - top.

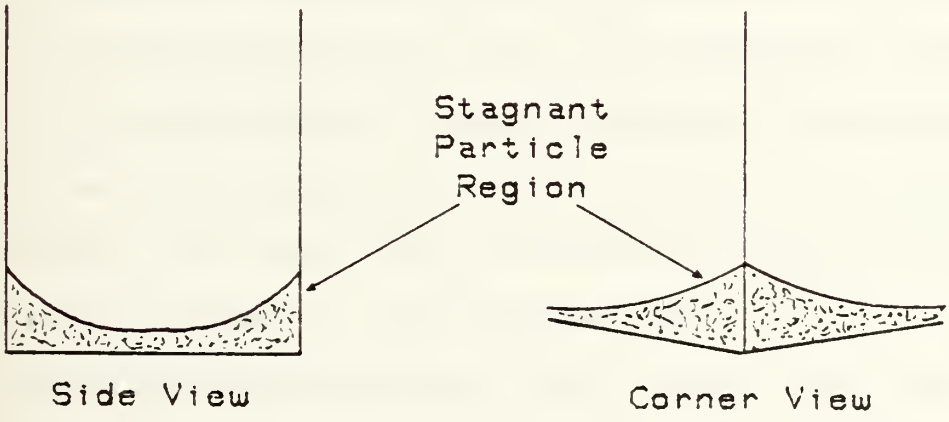

Figure 35. Fluidized column - bottom.

Initially, the shape of the non-movement area was not elliptical. If the side of the apparatus as shown in Figure 27 is considered to be the front face then bubbles were initializing in the front left corner of the bed along the movable wall. This shift in symmetry of the fluidizing cell generation was resulting in a shallower non-movement area at the left front corner and a larger build up at the right front corner. The cause of the problem turned out to be that the distributor plate was not at a right angle to the air flow. Downward motion was observed at all four walls and the non-movement zone was located within one inch of the bottom of the bed.

It was readily observable that the velocity of the particles emerging at the center of the bed was higher than that transiting down the face of the wall. This differential while not empirically measured during this study was attributed to frictional drag at the wall both mechanical and as a result of the electrostatic charge present at the bed wall. There is some justification provided by Toomey and Johnstone [62]. Marsheck [43] also gives an excellent treatise on the velocity profile across a gas-fluidized bed.

The height of the domed bulge would pulse during the fluidization more so as the air velocity was increased. If the air blower was fully energized with the initial bed configuration then the entire top of the bed would rise up as a mass and then collapse on itself. This was an example of

slug flow where the rising bubbles had coalesced into one large bubble stretching from one wall to another. Slug flow was not achieved or expected in any of the other configurations as the bed was not deep enough nor was the air velocity high enough to provide the right conditions for the bed cross-sectional areas present.

For the air flow that just permitted particle circulation the bed height fluctuations were negligible although the particles at the wall still moved downward in an irregular slightly surging movement. It is felt that at some point in the bed for this minimum fluidization velocity that the flow pattern internally is such that the flow pattern distributes the particle velocities more evenly throughout the column. In other words, the circulating motion caused by the higher velocity in the center and slower velocity along the wall gives way to a more random or eddying motion that evenly distributes the small air bubbles within the two velocity boundaries thus preventing rapid bubble coalescence. These eddy cells once formed in the mixing region of the bed will be moved up through the bed by the surges resulting from the cell rupture at the bed top. Between each surge line it is theorized that only one eddy cell will exist and that it will grow as it progresses through the bed until it coalesces with the gas in the central cell core at the bed top prior to cell rupture.

It was also noted that as the thermocouple probes were lowered into the bed that a flattening of the bed top would occur. This effect became more pronounced as the probe penetration increased and is felt to be as a result of the probe providing a grounding channel for bubble/particle flow. In effect the probes acted as a calming agent in the agitation of the bed without changing the overall bed flow cell configuration.

When the movable wall was positioned for a 6.25 inch width (A_c = 37.5 in^2) and also for an 8 inch width (A_c = 48 in^2) the bed expansion observed at the minimum fluidizing air velocity was 0.125-0.375 in. When the bed width was then increased to 10 inches (A_c = 60 in^2) and subsequently 12 inches (A_c = 72 in^2) the bed expansion observed did not exceed 0.25 in. This measurement does not take into account the height increase of the cell dome prior to rupture. There was no general horizontal movement of the particles near the wall except at the top of the fluidized bed and in a rather turbulent mixing region near the bottom of the fluidizing bed.

As the movable wall was repositioned thus increasing the bed air inlet area the bed became an aggregative fluidized bed. This resulted in multiple cell formations within the bed vice the single cell observed in the initial bed configuration. Unfortunately, there was no observable pattern to the cell formations as their overall positioning was

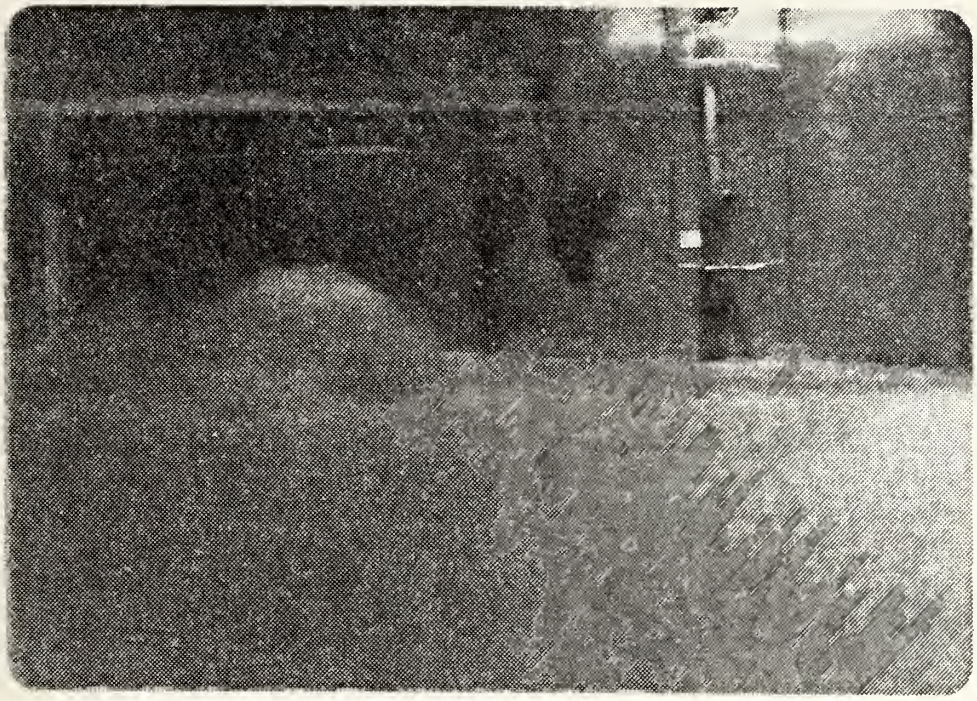

Figure 36. Bubbling bed photograph (A_c = 60 in^2).

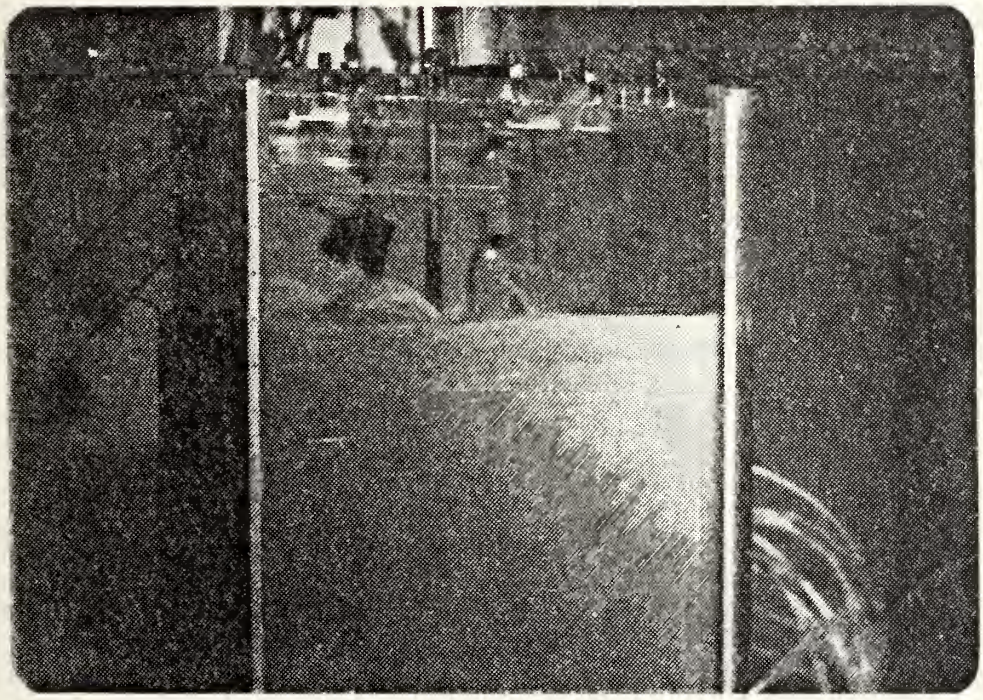

Figure 37. Bubbling bed photograph (A_c = 72 in^2).

random in nature, see Figures 36 and 37. Only one cell was observed to break the surface of the bed at any given instant. Occasionally, small bubbles were noticed breaking the surface of the bed between the larger bubble cells. This was thought to be caused by channeling between the larger bubble cell boundaries.

There was no noticeable change in the outward appearance of the particle cell flow patterns in any of the bed configurations when the external heaters were energized during fluidization.

B. PRESSURE DISTRIBUTION

Static pressure readings were taken at various intervals along the height of the fluidized bed on all experimental runs. In order to determine the gas mass flow rates for minimum fluidization, measurements of the pressure drop across the bed were also made at various flow rates. All data obtained during the various runs can be found in Appendix H. The mass flow rate at the maximum pressure drop was then taken as the point of minimum fluidization in each case. The maximum pressure drop was used because it is the most sharply defined point on the plots, see Figure 38.

The results of plotting the pressure drop versus gas mass velocity profiles produced very similar patterns which are in general agreement with the expected curve for the distributor design used. As can be seen from Figure 38, when the air inlet bed cross-sectional area was increased the curve would shift

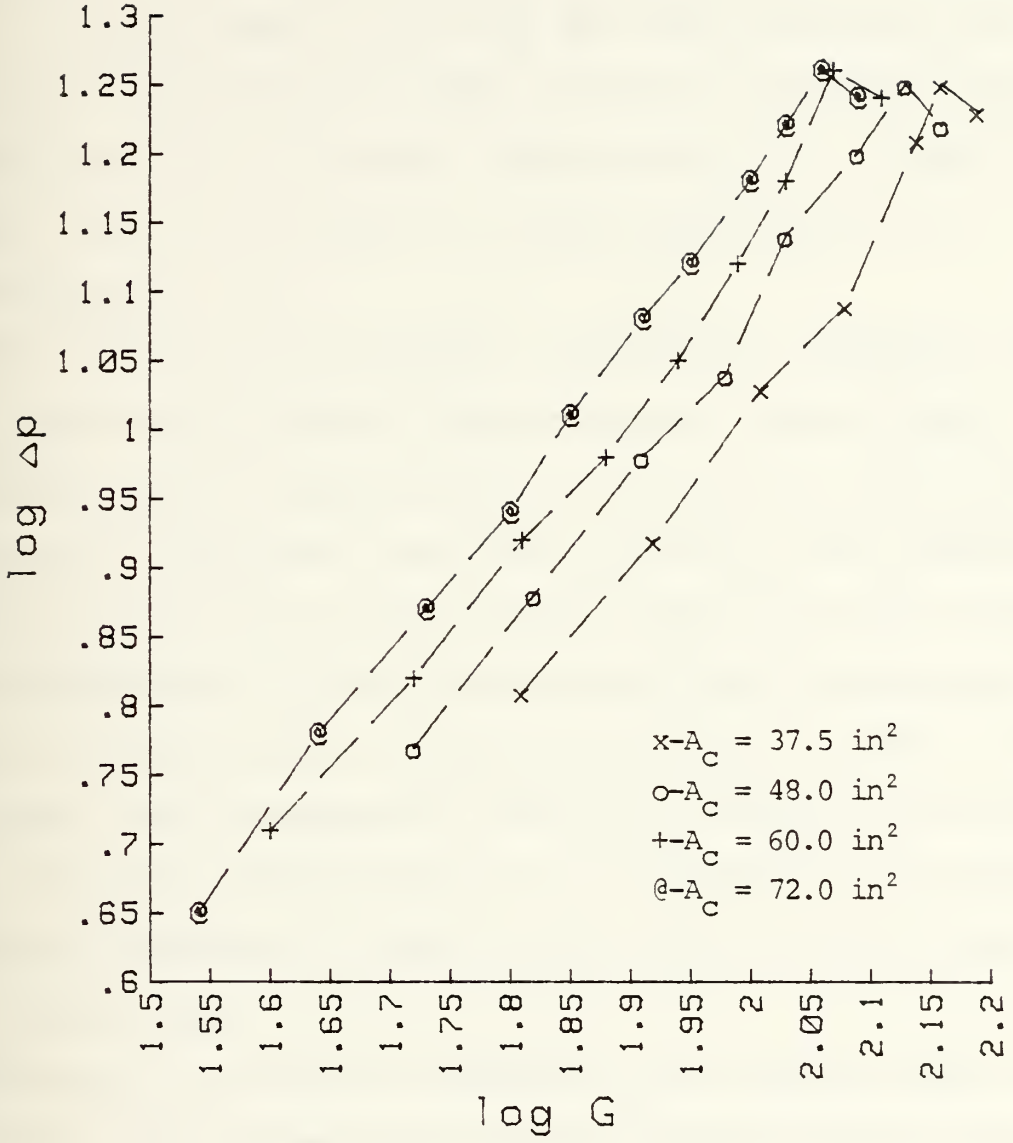

Figure 38. Bed pressure drop vs. gas mass velocity.

to the left. This displacement may have been as a result of the lessening in the contribution of the mechanical wall friction drag to the total overall drag experienced by the bed with the increased air flow for fluidization. Nevertheless, it would appear as the bed air inlet cross-sectional area was increased the gas mass velocity required for fluidization would also increase. Additionally, in all cases observed, the log Δp value for minimum fluidization was approximately 1.25.

The results of the pressure measurements seemed to indicate that mechanically smooth fluidization was taking place. Channeling and/or slugging was not occurring at the minimum fluidization operating conditions although it was possible to demonstrate both channeling and slugging for the initial bed configuration. It was noted that during fluidization small fluctuations were visible in the liquid levels in the manometer that was measuring the static pressure in the bed. This operating characteristic is in agreement with similar conditions observed by Parent et al. [52] in their study of gas fluidization.

The chain of events in measuring the pressure drop is as follows. Once the bed was initially settled the air flow was initialized to the bed. As the air flowed through the bed, a corresponding pressure drop occurred. This pressure drop increased linearly with the gas flow until at some point the bed began to expand. At this point the pressure drop

became nonlinear yet still increased to some maximum value. This maximum value was picked as the minimum fluidization point as previously stated. The pressure drop would then decrease until the bed started to circulate or fluidize at which time the pressure drop would stabilize at some point lower than the maximum value recorded earlier. The pressure drop remained steady as the air velocity was increased further but soon started to rise again. This new rise in the pressure drop across the bed was an indication that slugging was starting to set in and was especially prevalent in the initial bed geometry. It was also noted that this secondary pressure drop increase was less prevalent as the bed cross-sectional area was increased.

C. TEMPERATURE DISTRIBUTION

Air entered the air box at temperatures between 70^0 and 120^0F and in every case left the bed at a temperature within 1^0F of that of the top of the bed, as measured at a point in the axial center of the bed. Only two data runs were made with the bed instrumented to record the temperature distribution. The first run (A_c = 37.5 in^2) had an average air inlet temperature of 108^0F $\pm 2.5^0$F and attained a constant air outlet temperature of 125^0F $\pm 0.4^0$F, see Figure 39. The second temperature instrumented data run (A_c = 72 in^2) had an average air inlet temperature of 116^0F $\pm 2^0$F and attained a constant air outlet temperature of 129.5^0F $\pm 0.7^0$F, see Figures 40A and 40B.

In the graphics of Figures 39 through 40B it was necessary to plot the profiles for each thermocouple probe as there were too many variables to produce a true three dimensional temperature profile. The x-axis of each graph is the height of the probe tip in inches above the bed distributor plate. The y-axis of each graph is the temperature in ^{0}F. A probe grid is provide for each bed configuration with the probe number for reference. In all cases the temperature recorded by each probe above the 1.5 inch height was within the constant air outlet temperature range specified above for each data run. All temperature data recorded can be found in Appendix H.

As can be readily observed, the bed quickly attains a constant temperature except for a very small region at the bottom of the bed and a narrow layer near the container walls. The area near the walls is by assumption as the experimental apparatus was not instrumented to read that area.

It appears that the particles were heated by the heater as they transited the heater surface. Then, when they reached the bottom of the bed, thermal equilibrium with the incoming cold air was attained almost instantaneously. Except for the layer along the walls of the bed and in the small turbulent mixing region at the bottom of the bed, thermal equilibrium between the particles and the gas very nearly exists throughout the fluidized bed.

Since the inside walls of the bed container were not instrumented with thermocouples it was not possible to

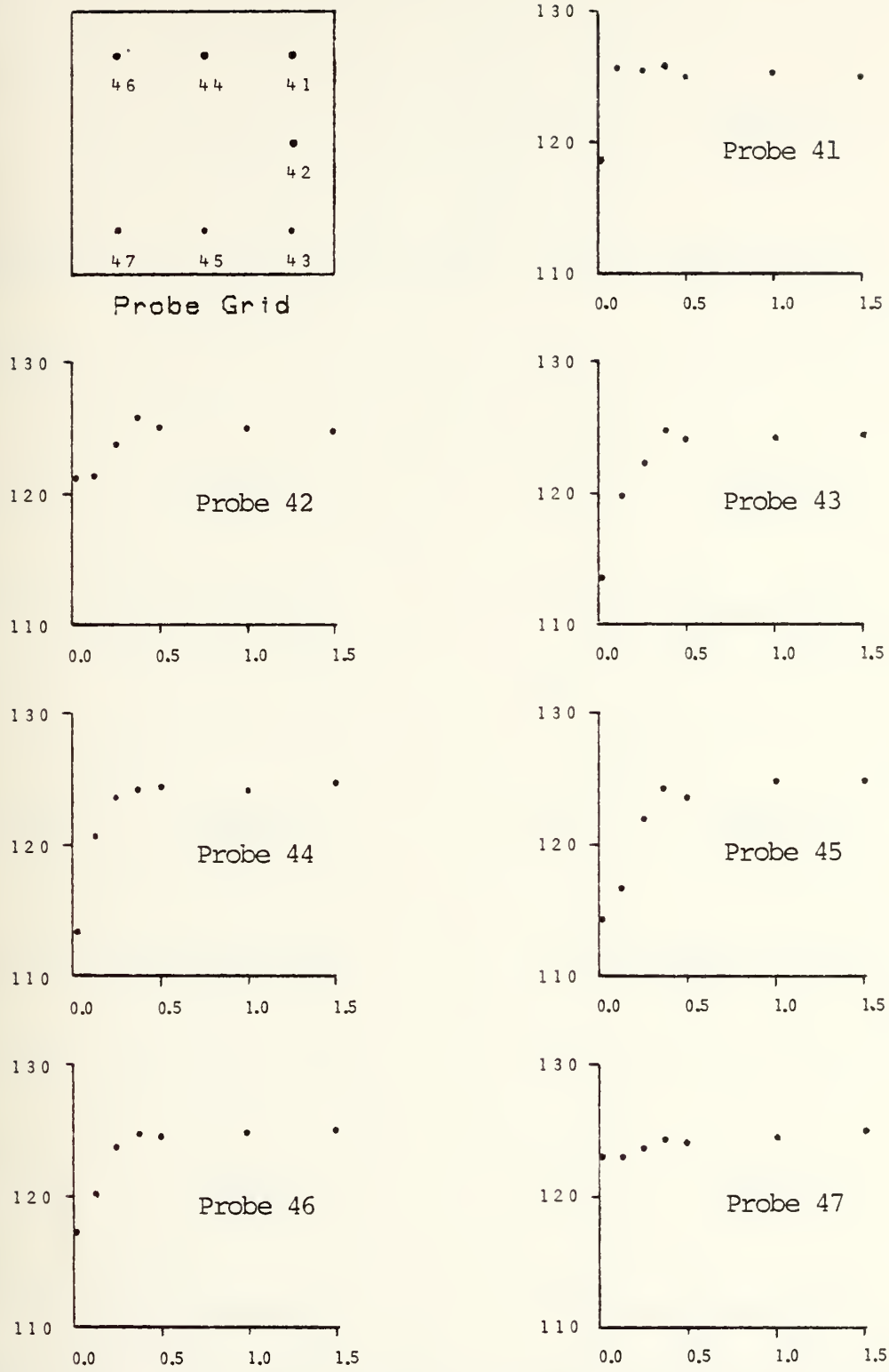

Figure 39. Bed temperature vs. bed height (A_c = 37.5 in^2).

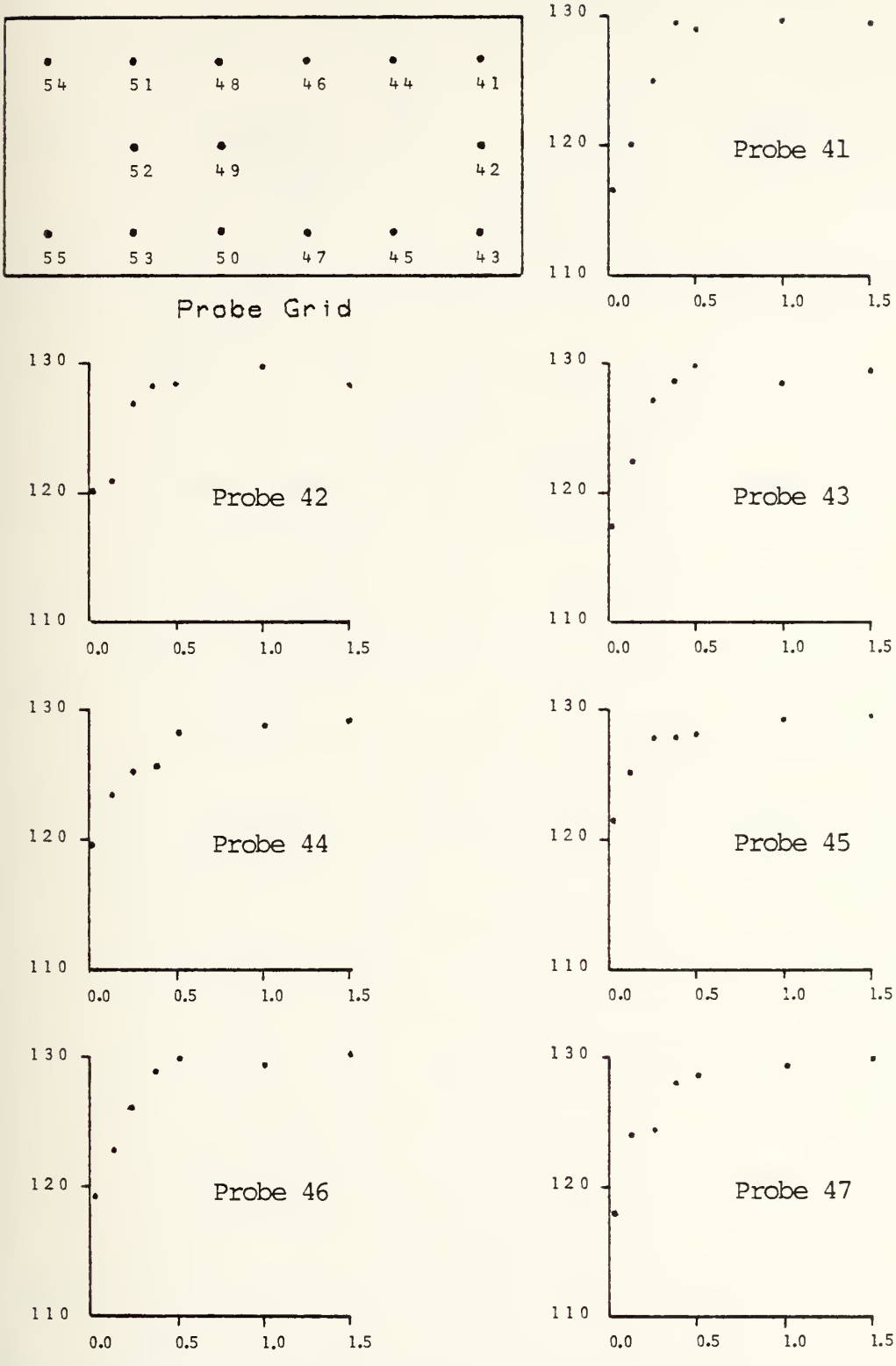

Figure 40A. Bed temperature vs. bed height (A_c = 72 in^2).

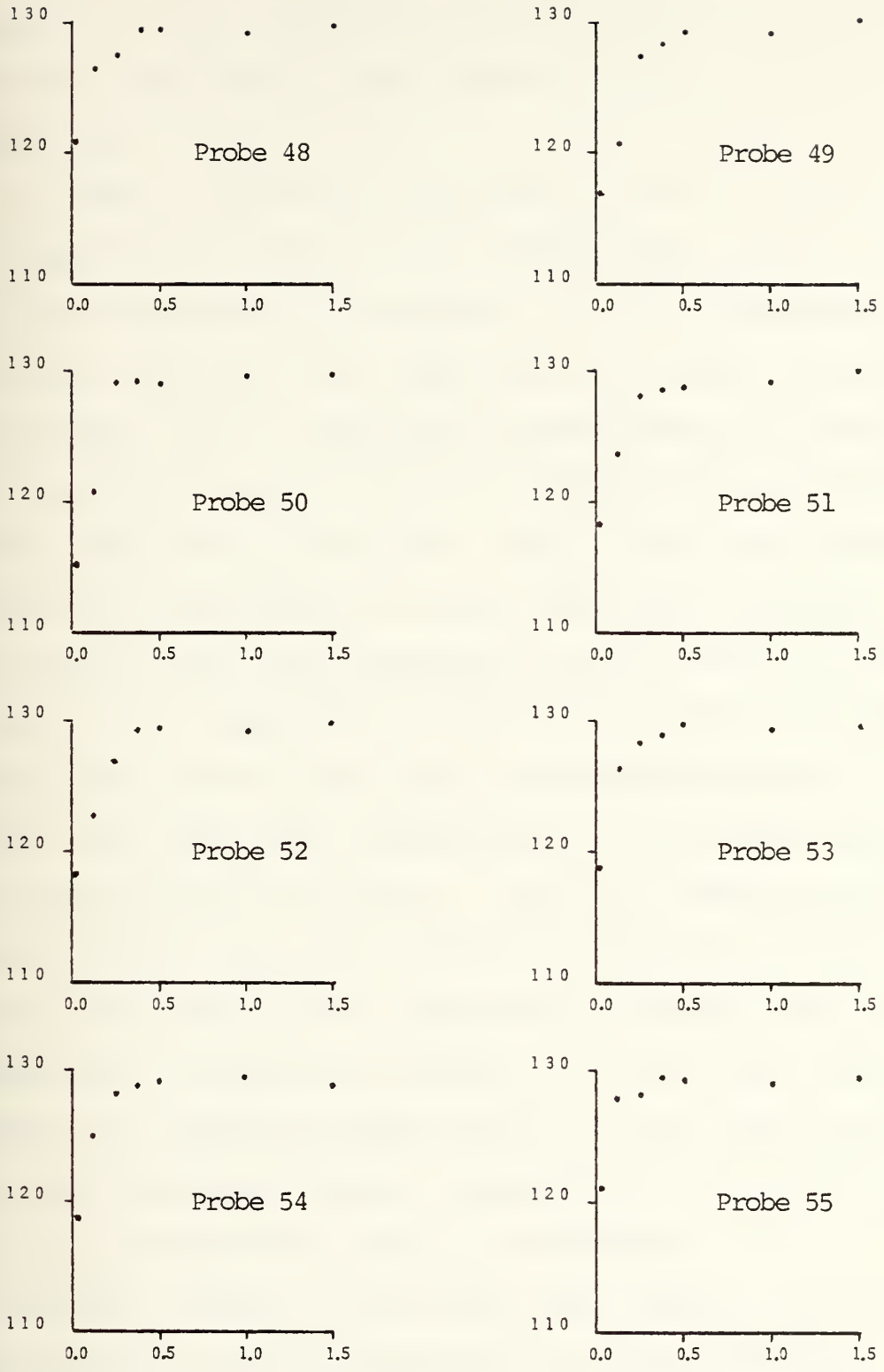

Figure 40B. Bed temperature vs. bed height (A_c = 72 in^2).

determine if there existed a temperature differential between the walls which did not have heaters and the bed bulk temperature.

In order to determine the effect of the air velocity on the temperature readings of the thermocouple probes several runs where conducted at different air inlet velocities with the probe tip placed six inches above the top of the distributor plate. Small temperature fluctuations of at most 1^0F were observed while the bed was fluidized and being heated under steady state conditions. The air flow was then terminated while monitoring the bed temperature readings. It was observed that the thermocouple reading would initially stabilize at a temperature within the range of the previous fluctuations and did not change for several seconds. A gradual rise then would commence due to the heat conduction from the heaters in the walls. Since the temperature rise did not exceed 1^0F at the end of four minutes it would seem to indicate that the bed thermocouple readings were basically independent of the fluid velocity. It would also tend to support the assumption made earlier in this thesis that the particle temperature and gas temperature at any point in the bed can be considered to be at equilibrium.

The only change in the mixing cell pattern within the fluidizing particle cell appeared to be the production of the temperature gradient at the bottom of the bed and an

increased bulk bed temperature. This was in comparison to a steady state bulk bed temperature equal to the air inlet temperature prior to energizing the plate heaters.

VI. CONCLUSIONS AND RECOMMENDATIONS

A. CONCLUSIONS

The following conclusions may be made from the results of this investigation:

1. Upon fluidization of the bed an electrostatic charge will build up within the bed. Although no data correlation error is used in this thesis, there most probably is some effect on data results.

2. With a square column bed the particle flow cell formed is basically as shown in Figure 33. Only one major cell is formed with its axis of ascent roughly located at the center of the bed.

3. With an expanded rectangular bed several particle flow cells form in a random fashion. There is no pattern to the overall cell coverage and the bed can be termed a bubbling bed.

4. That since the bulk bed temperature remains constant throughout the bed that there must exist eddy cells within the bed that continually mix the bed particles as they move up through the bed. Otherwise, a gradient would form between the heater walls and the center of the bed.

5. That the velocity in the center of any cell was greater than the velocity of the particles being forced down the walls. In the expanded bed the particles moving down the walls were a mixture of the various ruptured cells.

6. That mechanically smooth fluidization was not taking place at all times. Occasional instances of channeling were present and could be distinguished by small pertubations to the bed surface that did not change position - a simmering appearance.

7. That the distributor plate used did provide enough of a bed pressure drop to allow fluidization to occur but that the tendency for channeling or slug flow was high if the air velocity was increased much past the minimum fluidization velocity.

8. That a temperature equilibrium between the incoming fluidizing air and the bed particles was reached almost instantaneously in a small mixing region of the bed located at the bottom of the column.

9. That the only temperature gradient that existed in the bed was located at the bottom of the bed where the mixing region was located. The remainder of the fluidized bed stayed at a constant bulk bed temperature irregardless of the number of flow cells present.

10. That the air velocity did not affect the bulk bed temperature readings. It does, however, affect the depth of the mixing region at the bottom of the bed.

11. That energizing the plate heaters did not visibly alter the particle cell flow pattern but that it did produce a gradient in the temperature profile of the bed interior.

12. That the rectangular bed configuration under study would trip into fluidization when the log Δp across the bed approached 1.25.

B. RECOMMENDATIONS FOR FURTHER STUDIES

Based on the results of the experimentation to date, research conducted in preparing this thesis and the problems experienced in trying to get the fluidization apparatus to work the following areas of study are recommended for future thesis study:

1. A determination of what effect the electrostatic charge which builds up during the fluidization process has on the heat transfer or flow cell formation.

2. A study of the resulting changes in the cell formation patterns when bed particles of sizes larger than 1 mm are used. Particles in this size range are of much more practical use in the metallurgical industry.

3. A study of the flow cell patterns with beads smaller than 300 microns which should give enhanced mechanical fluidization.

4. A study of the effect of particle stratification (elutriation) when particles of different sizes are combined in the bed. The combination can be of varying sizes/roughness/sphericity or any other physical property of the bed particles which would promote the separation of the particles into distinct layers during fluidization.

5. A review of the cell pattern formation when using particles from various manufacturers (same or different bead materials) while maintaining a constant particle size.

6. Conduct a pressure study on the bed with different distributor configurations. This would include such designs as porous plates, baffles, calming chambers, filter screens or various combinations of the aforementioned designs.

7. Study the effect of changing the location of the heat source from opposite wall external heaters to other configurational combinations such as all four walls, adjacent walls, single wall, submerged heater, etc.

8. Conduct a velocity profile study similar to that conducted in Reference [43]. That study used a modified thermistor anemometer probe to determine the flow pattern within a circular column bed.

Additionally, prior to conducting future research the following apparatus modifications are suggested:

1. Replace the left side sponge rubber gasket on the movable wall with a new gasket.

2. Implant a pair of thermocouples in the unheated walls of the fluidized bed.

3. Mount a pair of thermocouples on the surface of each strip heater to enable the monitoring of the heater wall temperatures.

4. Manufacture a stand for the cabling to the thermocouple probes. The stand should be of sufficient height

to prevent the bending of a probe from the weight of its cable when the probe is retracted from the bed.

5. Change the mounting method of thermocouples 35 through 38 so that they are mounted in the backing plate vice on the backing plate.

6. Unless the area of study is to focus on the electrostatic charge built up during fluidization, provide some means to ground out this phenomenon.

7. Provide a leveling system for the fluidization apparatus that will ensure that the fluid flow direction out of the distributor plate is parallel to the bed container walls.

8. The probe taps on top of the fluidizing apparatus should be bored to 5/64 inch for ease in inserting the probes during data runs. Additional nylon bushings should also be ordered.

9. A second flowmeter of greater capacity than 11.1 scfm should be installed in the air supply line. This will be required to measure the higher air velocities needed to fluidize the bed with further expansion.

10. A cooler air source should be used in future runs to enhance the temperature differential at the bottom of the bed during fluidization with the wall heaters energized.

11. A new cap for the fill vent is requird to prevent the glass beads from getting between the cap and plexiglas thus jamming the cap.

C. CONCLUDING REMARKS

Particle motion is a complex function of the particle and gas properties, fluidization velocity, gas distributor and geometry of the bed. While a simple correlation can easily be made it must be tempered in its general application by the fact that it will most likely not give adequate allowances for the way in which the particles circulate and subsequently change with changes in the bed particle material, fluidizing conditions, scale and design of the fluidization apparatus.

The interpretations presented in this thesis are based on the premise of visible particle movement at a given bed height and must be qualified by the fact that they represent a very limited amount of data.

There is a general opinion among researchers that the bubbles of air passing through a fluidized bed grow in size by coalescence of smaller bubbles into larger bubbles. Eventually given a deep enough bed the bubbles should coalesce into one large bubble located in the center of the bed in order to maintain the uniformity of the bed [43]. While this opinion has been generated as a result of experimentation using circular beds it would appear that it can be equally applied to rectangular beds. No doubt had the expanded rectangular bed been deep enough, eventually it also would have conformed to the aforementioned opinion.

The determination of particle flow patterns in a fluidized bed would be of extreme value in the establishment of a kinetic

or mass transfer model of a fluidized bed. The fact that there are a multitude of interrelated variables involved, unfortunately, has made the modeling a theoretical tool vice the needed operational scale-up tool required for industry. More study will undoubtedly be required until a workable industrial model can be produced.

It has also been an observation that while the majority of the fluidization research was conducted by American researchers in the the late forties and early fifties, that the bulk of the recent research has been conducted by the Russians with some notable exceptions. This trend is neither understood nor considered warranted by the researcher considering the very pronounce heat transfer improvement demonstrated through the use of fluidization.

APPENDIX A: NONDIMENSIONAL CORRELATIONS FOR EXTERNAL WALLS

These correlations are but a sampling of the many fluidization correlations for external walls that have been theorized.

1. Investigator - Baerg et al. [3]

   Correlation -

$$h_w = h_{wmax} - 55 \exp \left(-0.012 \{ G - 0.71 \rho_{sb} \} \right)$$

   Remarks - See Appendix C for h_{wmax}.

2. Investigator - Bartholomew and Katz [5]

   Correlation -

$$\frac{h_w}{c_{pf} G} = \frac{1.56 + \ln \left(Re \, Ga^{-0.667} - 0.012 \right)}{-0.227 \, Pr^{0.667} \, Ga^{0.42}}$$

   Remarks - None.

3. Investigator - Brazelton [7]

   Correlation -

$$\frac{h_w}{c_{pf} G'} = 0.72 \left[\frac{D' G'}{\mu} \right]^{-0.87} \left(1 - \varepsilon \right)^{-1.3}$$

   Remarks - None.

4. Investigator - Das and Sarkar [11]

Correlation -

$$\frac{h_w D}{k_f} = 140\ r^{0.18}\ Re^{0.09} \left[\frac{d_p}{D}\right]^{0.24}$$

Remarks - None.

5. Investigator - Dow and Jakob [13]

Correlation -

$$\frac{h_w D}{k_f} = 0.55 \left[\frac{D}{L}\right]^{0.65} \left[\frac{D}{d_p}\right]^{0.17} \left[\frac{(1-\varepsilon)\ \rho_s\ c_{ps}}{\varepsilon\ \rho_f\ c_{pf}}\right]^{0.25} \left[\frac{D\ G}{\mu}\right]^{0.80}$$

Remarks - None.

6. Investigator - Gamson [17]

Correlation -

$$St\ Pr^{0.667} = 2.0\ Re_m^{-0.69}\ (1-\varepsilon)^{-0.30}$$

Remarks - None.

7. Investigator - Lemlich and Caldas [35]

Correlation -

$$Nu = 0.055\ Re$$

Remarks - Low velocity liquid-fluidization.

Correlation -

$$St\ Pr^{0.667} = 1.4 \left[\frac{D}{d_p}\right]^{0.79} \left[\frac{1}{Re_t\ \varepsilon}\right]$$

Remarks - High velocity liquid-fluidization.

8. Investigator - Leva [36]

Correlation -

$$Nu = 0.5 \left[\frac{d_p \, G}{\mu} \right]$$

Remarks - None.

9. Investigator - Leva and Grummer [37]

Correlation -

$$h_w = 3000000 \, k_f \, \bar{D}_p \left[\frac{\bar{D}_p \, G_f \, \eta}{\mu \, R} \right]^{0.60}$$

Remarks - None.

10. Investigator - Levenspiel and Walton [41]

Correlation -

$$\frac{h_w \, D_r}{k_f} = \left[\frac{0.3}{\gamma} \right] \left[\frac{D_r \, G}{\mu} \right]^{0.50}$$

$$\frac{h_w \, D_r}{k_f} = 0.0018 \left[\frac{d_p \, G}{\mu} \right] \left[\frac{d_p}{D} \right]^{-1.16}$$

$$\frac{h_w}{c_{pf} \, G} = 10 \left[\frac{D_r \, G_e}{\mu} \right]^{0.65}$$

$$\frac{h_w}{c_{pf} \, G} = \frac{0.6 \, (d_p \, G)^{0.70}}{\mu}$$

10. Remarks -

$$D_r = \frac{\pi \, d_p}{6 \, (1 - \varepsilon)}$$

$$\gamma = (\{ 1 + \alpha^2 \}^{1.5} - \alpha^3)$$

$$\alpha = 0.041 \, (1 - \varepsilon) \left[\frac{D_r \, G}{\mu} \right]^{0.50}$$

$$G_e = \frac{G}{\varepsilon}$$

11. Investigator - Mickley and Trilling [48]

Correlation -

$$h_w = \frac{0.0118 \, \rho_m \, G^{0.263}}{\bar{D}_p^{\,3}}$$

Remarks - None.

12. Investigator - Rao and Kaparthi [56]

Correlation -

$$Nu = 0.014 \, Re^{1.1} \left[\frac{1 - \varepsilon}{\varepsilon} \right]^{0.40}$$

Remarks - Semi-fluidized bed.

13. Investigator - Richardson and Mitson [57]

Correlation -

$$Nu = 119\ Pr^{0.40} \left[\frac{c_{ps}}{c_{pf}}\right]^{0.28} \left[\frac{k_s}{k_f}\right]^{0.02} Re_f^{N} \left[\frac{D\ G}{\mu}\right]^{0.075}$$

Remarks - Liquid-fluidized system with

$$N = 0.02 \left[3.45 + \frac{\rho_s}{\rho_f}\right]$$

14. Investigator - Rukenshtein [58]

Correlation -

$$Nu = 0.326\ Re^{0.423}\ Pr^{0.33}\ Ga^{0.14}$$

Remarks - None.

15. Investigator - Toomey and Johnstone [62]

Correlation -

$$\log\left[\frac{h_w\ d_p}{k_f}\right] = 0.575 \log\left[\frac{d_p\ u_p\ \rho_f}{\mu}\right] + 0.130$$

$$Nu = 3.75 \left(\left[\frac{d_p\ u_{mf}\ \rho_f}{\mu}\right] \log\left[\frac{u_o}{u_{mf}}\right]\right)^{0.47}$$

Remarks - None.

16. Investigator - van Heerden et al. [66]

Correlation -

$$Nu = 0.58 \left[\frac{B\ d_p\ G}{\mu}\right]^{0.45} \left[\frac{\rho_{mf}\ c_{ps}}{\rho_f\ c_{pf}}\right]^{0.36} \left[\frac{\rho_f}{\rho_{mf}}\right]^{0.18} Pr^{0.50}$$

Remarks - None.

17. Investigator - Wen and Leva [72]

Correlation -

$$Nu = 0.16 \left[\frac{c_s\ \rho_s\ d_p^{1.5}\ g^{0.50}}{k_f}\right]^{0.40} \left[\frac{Re\ \eta}{R}\right]^{0.36}$$

Remarks - None.

APPENDIX B: NONDIMENSIONAL CORRELATIONS FOR IMMERSED BODIES

These correlations are but a sampling of the many fluidization correlations for immersed bodies that have been theorized.

1. Investigator - Andeen and Glickman [2]

   Correlation -

$$\frac{h_w D_T}{k_f} = 900 \left(1 - \varepsilon \right) \left[\frac{G D_T \mu}{\rho_f d_p^3 \rho_s g} \right]^{0.326} Pr^{0.3}$$

   Remarks - Sometimes called the modified Vreedenberg correlation.

2. Investigator - Gamson [17]

   Correlation -

$$St\ Pr^{0.667} = 2.52\ Re_m^{-0.80} \left(1 - \varepsilon \right)^{-0.30}$$

   Remarks - Vertical tubes.

3. Investigator - Gelperin and Einstein [18]

   Correlation -

$$Nu = 0.75\ Ga^{0.22} \left[1 - \frac{D_T}{P} \right]^{0.14}$$

   Remarks - Vertical tube bundle.

4. Investigator - Gelperin et al. [20]

Correlation -

$$Nu\left[\frac{\varepsilon}{6\ (\ 1-\varepsilon\ )}\right] = 0.73\ Re^{0.32}\left[\frac{1}{6\ (\ 1-\varepsilon\ )}\right]^{0.32}$$

Remarks - Horizontal tube.

5. Investigator - Glass and Harrison [24]

Correlation -

$$Nu = 57.4\left[\frac{d_p}{D_T}\right]^{0.91}\left[\frac{q}{u_{mf}^{\ 3}\ \rho_s}\right]^{0.1} N^{0.34}\left[\frac{P}{D_T}\right]^{0.08}$$

Remarks - Staggered tube bundle- $N = \frac{u_o}{u_{mf}}$.

6. Investigator - Huntsinger [29]

Correlation -

$$Nu = 1.4\ Re^{0.53}\ Pr^{-1.6}$$

Remarks - Coil.

7. Investigator - Kruglikov [33]

Correlation -

$$Nu = 0.66\ Re^{0.86}\ Pr^{0.29}$$

Remarks - Coil.

8. Investigator - Miller and Logwinuk [49]

Correlation -

$$h_w = 1.5 \frac{G^{0.5} k_s^{0.072} k_f^{2.4}}{d_p^{0.96} c_{pf}^{1.6} \mu^{0.8}}$$

Remarks - Vertical tube bundle.

9. Investigator - Petrie et al. [54]

Correlation -

$$\frac{h_w D_T}{k_f} = 14 \left[\frac{G}{G_{mf}}\right]^{0.33} Pr^{0.33} \left[\frac{D_T}{d_p}\right]^{0.667}$$

Remarks - Staggered and in-line tube bundles.

10. Investigator - Sarkits et al. [60]

Correlation -

$$Nu = 0.0133\ Re^{0.4}\ Ga^{0.27}\ Pr^{0.33} \left[\frac{c_s}{c_f}\right]^{0.45} \left[\frac{D}{d_p}\right]^{0.16} \left[\frac{H_o}{d_p}\right]$$

Remarks - Coil.

11. Investigator - Traber et al. [63]

Correlation -

$$Nu = 0.024\ Re^{0.65}\ Ga^{0.10}\ Pr^{0.33} \left[\frac{D}{d_p}\right]^{0.13} \left[\frac{H_o}{d_p}\right]^{0.16}$$

Remarks - Coil.

12. Investigator - Vreedenberg [69]

Correlation -

$$Nu = a \left[\frac{G_\nu}{G_{mf}\ \nu_{mf}} \right]^{0.35}$$

Remarks - Tube position varies.

13. Investigator - Vreedenberg [70]

Correlation -

$$Nu = 0.66 \left[\frac{G\ D\ \rho_s\ (\ 1 - \varepsilon\ )}{\rho_f\ \mu\ \varepsilon} \right]^{0.44} Pr^{0.30}$$

Remarks - Horizontal tube with- $\left[\frac{d_p\ G\ \rho_s}{\mu\ \rho_f} \right] < 2050.$

Correlation -

$$Nu = 420 \left[\frac{G\ D\ \mu}{\rho_f\ d_p^{\ 3}\ \rho_s\ g} \right]^{0.30} Pr^{0.30}$$

Remarks - Horizontal tube with- $\left[\frac{d_p\ G\ \rho_s}{\mu\ \rho_f} \right] > 2550.$

Remarks - When $\left[\frac{d_p\ G\ \rho_s}{\mu\ \rho_f} \right]$ is greater than 2050 but less than 2550 the value of Nu will be the average of the two Nu correlations above.

14. Investigator - Wender and Cooper [74]

Correlation -

$$Nu = 0.0119 \left(1 - \varepsilon \right) \left[\frac{\rho_f \, c_{pf}}{k_s} \right]^{0.43} \left[\frac{c_{ps}}{c_{pf}} \right]^{0.8} \left[\frac{\rho_s}{\rho_f} \right]^{0.66} Re^{0.23} \, C_R$$

Remarks - Vertical tube.

15. Investigator - Zenz and Othmer [80]

Correlation -

$$Nu = 14 \left[\frac{G}{G_{mf}} \right]^{0.33} Pr^{0.33} \left[\frac{D_T}{d_p} \right]^{0.67}$$

Remarks - Horizontal tube.

APPENDIX C: NONDIMENSIONAL CORRELATIONS FOR THE MAXIMUM HEAT TRANSFER COEFFICIENT

These correlations are but a sampling of the many fluidization correlations for maximum heat transfer coefficients that have been theorized.

1. Investigator - Baerg et al. [3]

   Correlation -

$$h_{wmax} = 49 \log \left[\frac{0.00037 \, \rho_{sb}}{d_p} \right]$$

   Remarks - None.

2. Investigator - Chechetkin [8]

   Correlation -

$$Nu_{max} = \frac{0.0017 \, Re_{opt}^{0.8} \, Pr^{0.4}}{d_p^{0.69}}$$

   Remarks - $Re_{opt} = 0.209 \, Ga^{0.52}$.

3. Investigator - Chekansky et al. [9]

   Correlation -

$$h_{wmax} = 28.2 \, \rho_s^{0.2} \, k_f^{0.6} \, d_p^{-0.36} \left[\frac{\Delta}{d_p} \right]^{0.04} \left[\frac{D_T}{D_{20}} \right]^{-0.12}$$

   Remarks - Staggered tube bundle.

4. Investigator - Gelperin et al. [19]

Correlation -

$$Nu_{max} = 0.74\ Ga^{0.22}\left[1 - \frac{D_T}{y}\left(1 + \frac{D_T}{z + D_T}\right)\right]^{0.25}$$

Remarks - Staggered horizontal tube bundle.

5. Investigator - Gelperin et al. [21]

Correlation -

$$Nu_{max} = 0.64\ Ga^{0.22}\left[\frac{P}{D_T}\right]^{0.09}$$

Remarks - Vertical tube bundle.

6. Investigator - Gelperin et al. [22]

Correlation -

$$Nu_{max} = 0.79\ Ga^{0.22}\left[1 - \frac{D_T}{y}\right]^{0.25}$$

Remarks - In-line horizontal tube bundle.

7. Investigator - Jacob and Osberg [30]

Correlation -

$$h_{wmax} = h_o\ (\ 1 - \varepsilon\ )\ (\ 1 - \exp\ \{\ -pk_f\ \}\ )$$

Remarks - h_o and p determined by experimentation.

8. Investigator - Maskayev and Baskakov [44]

Correlation -

$$Nu_{max} = 0.21\ Ga^{0.32}$$

Remarks - Vertical cylinder in coarse particle bed with $1.4 \times 10^5 < Ga < 3 \times 10^8$.

9. Investigator - Pillai [55]

Correlation -

$$Nu_{max} = 0.365\ \theta^{0.82}\ Ga^{0.22}$$

Remarks - Sphere with $Bi < 0.04$

10. Investigator - Ruckenstein [58]

Correlation -

$$Nu_{max} = Re_{opt}^{0.423}\ Ga^{0.14}\ Pr^{0.33}$$

Remarks - $Re_{opt} = 0.09\ Ga^{0.58}$.

11. Investigator - Sarkits [60]

Correlation -

$$Nu_{max} = 0.0087\ Ga^{0.42}\ Pr^{0.33} \left[\frac{c_{ps}}{c_{pf}}\right]^{0.45} \left[\frac{D}{d_p}\right]^{0.16} \left[\frac{H_o}{d_p}\right]^{0.45}$$

Remarks - $Re_{opt} = 0.2\ Ga^{0.5}$ (laminar region).

Correlation -

$$Nu_{max} = 0.019\ Ga^{0.5}\ Pr^{0.33} \left[\frac{c_{ps}}{c_{pf}}\right]^{0.1} \left[\frac{D}{d_p}\right]^{0.13} \left[\frac{H_o}{d_p}\right]^{0.16}$$

Remarks - $Re_{opt} = 0.66\ Ga^{0.5}$ (turbulent region).

12. Investigator - Traber et al. [63]

Correlation -

$$Nu_{max} = 0.021\ Ga^{0.4}\ Pr^{0.33} \left[\frac{D}{d_p}\right]^{0.13} \left[\frac{H_o}{d_p}\right]^{0.16}$$

Remarks - $Re_{opt} = 0.55\ Ga^{0.5}$.

13. Investigator - Varygin and Martyushin [67]

Correlation -

$$Nu_{max} = 0.86\ Ga^{0.2}$$

Remarks - $Re_{opt} = 0.118\ Ga^{0.5}$.

14. Investigator - Zabrodsky [78]

Correlation -

$$h_{wmax} = 33.7\ \rho_s^{0.2}\ k_f^{0.6}\ d_p^{-0.36}$$

Remarks - None.

APPENDIX D: GENERAL EQUATIONS AND UNITS

This appendix will be broken down into two sections. The first section will cover the general nondimensional heat transfer/fluids numbers used in this thesis. The second section will annotate the units to be used with each equation that is numbered within the main text. This requirement was necessitated by the use of different units (same variable nomenclature) among the various researchers cited in the thesis text.

A. GENERAL NONDIMENSIONAL HEAT TRANSFER/FLUIDS NUMBERS

1. Reynolds Number (Re)

$$Re = \frac{d_p \, u_o \, \rho_f}{\mu}$$

2. Galileo Number (Ga)

$$Ga = \frac{d_p^{\,3} \, \rho_f \, (\rho_s - \rho_f) \, g}{\mu^2}$$

3. Prandtl Number (Pr)

$$Pr = \frac{c_{pf} \, \mu}{k_f}$$

4. Nusselt Number (Nu)

$$Nu = \frac{h_w \, d_p}{k_f}$$

5. Stanton Number (St)

$$St = \frac{h_w}{c_{pf} \, \rho_f \, u_o}$$

6. Biot Number (Bi)

$$Bi = \frac{h_w \, r_{sp}}{k_{sp}}$$

B. EQUATION UNITS

1. Equation (3.1)

Δp_e - lb/ft^2

L_e - ft

ε_e - dimensionless

ρ_s - lbm/ft^3

ρ_f - lbm/ft^3

2. Equation (3.2)

ε_{mf} - dimensionless

V_p - ft^3

γ_f - lb/ft^3

L_{mf} - ft

A_c - ft^2

ρ_s - lbm/ft^3

ρ_f - lbm/ft^3

3. Equation (3.3)

G_{mf} - $lbm/(hr\text{-}ft^2)$

$\bar{D}_p$ - in

μ - centipoise

ρ_s - lbm/ft^3

ρ_f - lbm/ft^3

4. Equation (3.4)

$\bar{D}_p$ - in

D_i - in

x_i - dimensionless

5. Equation (3.5)

Re_{mf} - dimensionless

G_{mf} - $lbm/(hr\text{-}ft^2)$

$\bar{D}_p$ - in

μ - centipoise

6. Equation (3.6)

G_{mf} - $lbm/(hr\text{-}ft^2)$

7. Equation (3.7)

η - dimensionless

G_f - $lbm/(hr\text{-}ft^2)$

G_e - $lbm/(hr\text{-}ft^2)$

8. Equation (3.8)

r - dimensionless

m' - dimensionless

G_f - $lbm/(hr\text{-}ft^2)$

G_{mf} - lbm/(hr-ft^2)

9. Equation (3.9)

q_{wi} - BTU/hr

h_{wiL} - BTU/(hr-ft^2-^{0}F)

A_m - in^2

T_w - ^{0}F

T_b - ^{0}F

10. Equation (3.10)

h_{wiL} - BTU/(hr-ft^2-^{0}F)

k_m - BTU/(hr-ft-^{0}F)

ρ_m - lbm/ft^3

c_m - BTU/(lbm-^{0}F)

t - sec

11. Equation (3.11)

h_w - BTU/(hr-ft^2-^{0}F)

k_m - BTU/(hr-ft-^{0}F)

ρ_m - lbm/ft^3

c_m - BTU/(lbm-^{0}F)

u_s - ft/hr

L_H - ft

12. Equation (3.12)

h_{wL} - BTU/(hr-ft^2-^{0}F)

k_m - BTU/(hr-ft-^{0}F)

c_m - BTU/(lbm-^{0}F)

s - 1/sec

APPENDIX E: EQUIPMENT LISTING

Device	Manufacturer	Model #	Serial #
Temperature Recorder	Newport	267B-TF2	8500392
Temperature Recorder	Newport	267B-TF2	8500393
Thermocouple	Omega Engineering	ANSI T Type S Sheathed	---
Water Manometer (30 in)	Meriam Instrument	Type W 33KA35	A69513
Water Manometer (60 in)	Meriam Instrument	Type W A324	44F554
Flowmeter	Fischer and Porter	10A3565A	6908A2165A1
Variac	General Radio	Type V10	---
Air Blower	Clements National	G12	114986
Regulated Power Supply	Lambda Electronics	LK 345A FM	C 1821
Thermocouple Calibration	Rosemount Engineering	Bridge-920A Bath-913A	110 ---
Strip Heaters	Watlow Electric	250 Watts	8044
Weight Scale	Mettler Instrument	Type H15	119923
Optical Microscope	Bausch & Lomb Instrument	31-32-45	B-3539 RS

APPENDIX F: PARTICLE ANALYSIS

The particle specifications provided by the manufacturer, Potters Industries, are as follows:

1. Physical Properties

a. Size - Minimum 90% by weight in range on smaller U.S. Sieve, maximum of 10% by weight on larger U.S. Sieve. Tested in accordance with ASTM-D-1214-58 and MIL Spec. G-9954A.

b. Free Iron Content - Maximum of 0.1% by weight.

c. Chemical Content - Soda-lime silica glass. The solid glass spheres contain no free silica.

d. Specific Gravity - 2.45-2.55.

e. Hardness - DPH 100g load-515Kg/mm^2.

f. Color - Clear and colorless, free from surface films.

g. Roundness - Minimum percent round by roundometer is 90%. Determined in accordance with ASTM-D-1155-53 or MIL Spec. G-9954A.

h. Broken or Angular Particles - Maximum of 3% by count. Tested in accordance with MIL Spec. G-9954A.

i. Air Inclusions - Not more than 10% of the beads shall show air inclusions of more than 25% of their surface. Tested microscopically immersed in 1.5 refractive index fluid.

j. Average Settled Bed Density - 96 lbm/ft^3.

k. Average Particle Density - 156 lbm/ft^3.

l. Coefficient of Friction (Static) - 0.9-1.0.

2. Thermal Properties @ 70^0F

a. Specific Heat - 0.180 BTU/(lbm-^0F).

b. Thermal Conductivity - 0.515 BTU/(hr-ft-^{0}F).

3. Electrical Properties @ 77^{0}F

a. Dielectric Constant (1 Kc) - 7.6.

b. D.C. Volume Resistivity - $6.5X10^{12}$ Ohm-cm.

4. Size Analysis (Potters P-020 Designation)

a. Basic Sieve Analysis - U.S. Sieve 35 to 50.

b. Average Particle Diameter - $\bar{D}_p$ = 0.0122 inch (310 microns).

c. Maximum Percentage True Spheres - 90%.

Photographs of two groups of the particles are shown in Figures 41 and 42. Upon microscopic examination the beads appeared extremely spherical in nature with some air inclusions present in all beads. The inclusions appear as black areas on the photographs. There was little variation in particle diameters between the two sample groups. The diameter for each group was taken as the arithmetic mean of microscopic measurements on a representative sample of 50-60 beads in each group. Group I had an average particle diameter of 0.0111 in while Group II had an average particle diameter of 0.0110 in. For the purpose of calculations in this thesis an average particle diameter ($\bar{D}_p$) of 0.011 in was used.

A basic sieve analysis was performed on two samples of known volume and weight to verify the manufacturer's specifications. The sieves where U.S. Tyler Company standard screen mesh of 48 and 60 mesh size. Less than five

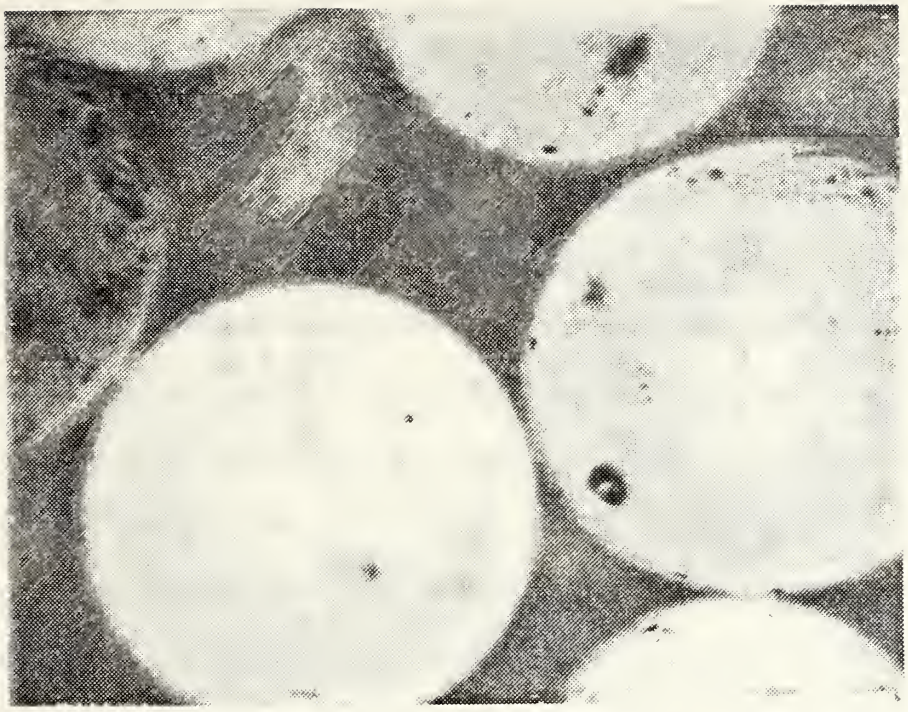

Figure 41. Microphotograph of beads-Group I.

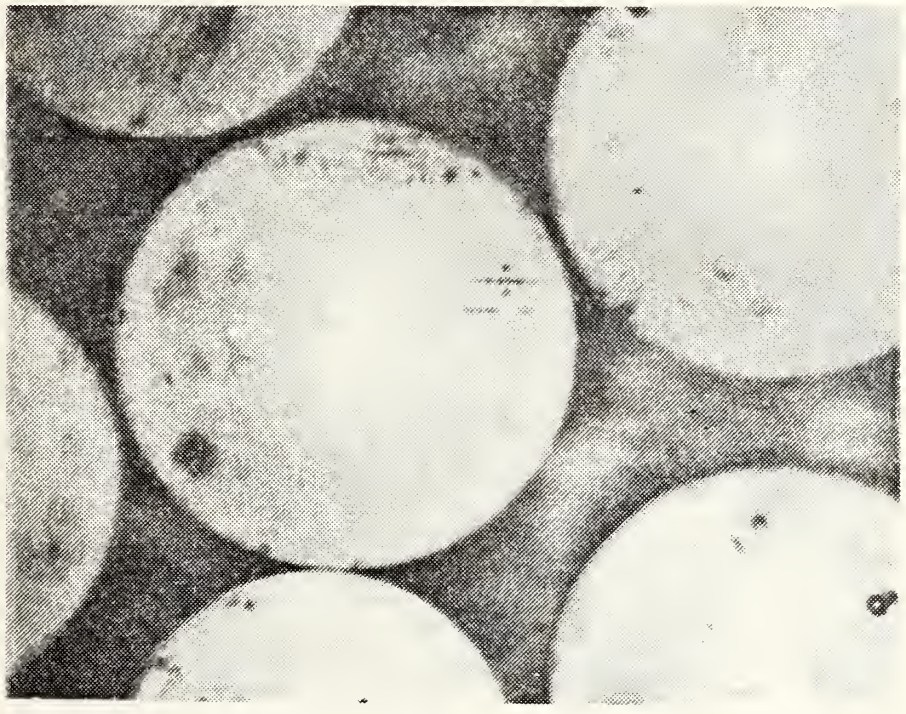

Figure 42. Microphotograph of beads-Group II.

percent by weight of the sample particles was larger than the 48 mesh screen and less than one percent by weight of the sample was smaller than 60 mesh. The Tyler screen scale of 48 (U.S. Sieve No. 50) has a sieve opening of approximately 0.0117 in and the Tyler screen scale of 60 (U.S. Sieve No. 60) has a sieve opening of approximately 0.0098 in.

Water displacement of a known weight of beads was used to determine the average particle density. The value obtained was 154.6 lbm/ft^3 which is considered to be within acceptable agreement of the manufacturer's specifications. Likewise, the average settled bed density was obtained by measuring the volume occupied by a packed bed of beads of known weight. The value obtained, 93.2 lbm/ft^3, is also within acceptable limits.

APPENDIX G: EXPERIMENTAL UNCERTAINTY ANALYSIS

The source of error in the results presented is considered to be due to instrument precision and accuracy, inaccuracies in geometrical measurements and inaccuracies in data recording. The following is a breakdown of the experimental uncertainties.

1. Distance Measurements

The tape attached to the side of the fluidizing apparatus has a minimum scale division of 0.25 in. Distance readings were made with this scale to the nearest 0.0625 in for both the bed height and width. While it was possible to get static readings with a precision of ±0.5%, the expanded bed heights were more on the order of ±2% with a worst case precision of ±4%.

The depth measurement of the thermocouple probes was based on measuring the removal distance of the probe from its tap at the top of the apparatus. The smallest scale division for this withdrawal measurement was 0.0625 in. However, since the probes were not rigid structures, the bending in the probe lengths resulted in precision estimates of ±2%.

2. Particle Diameter Measurements

The optical microscope used to measure bed particle diameters in the two samplings of beads has a minimum scale

division of 0.0001 in which allowed reliable measurements up to 0.00005 in at 100X magnification. The diameter precision based on scale readings is ±0.5%. However, operator error in reading the diameters places the precision estimate more realistically at ±1%. The standard deviation in particle diameter for the two bead groups was 0.00042 in and 0.00045 in.

3. Particle Density Measurements

The scale used to measure the particle bead weights has a minimum division of 1 mg which equates to a precision of ±0.6%. The minimum volume scale was 1 ml which equates to a precision of ±1%. Due to spillage in filling the measuring containers with water and beads in addition to the losses during the experimental runs it is estimated that the error in density measurements is closer to ±3% overall.

4. Temperature Measurements

Although the temperature recorder gives readouts in tenths of degrees, after taking into consideration the fluctuations experienced during fluidization and round off errors the overall error in temperature measurements is considered to be $\pm 1^0$ F.

5. Pressure Measurements

The minimum manometer scale division was 0.1 in H_2O with readings of 0.05 in H_2O possible for a full scale precision of ±0.2%. While this precision was possible during static bed conditions it was not possible to be as accurate

once fluidization occurred as the pressure level would fluctuate within the manometer column. For the worst case of the pressure measurement in the column, the pressure fluctuated ±0.3 in H_2O over the maximum pressure recorded for a recorded error accuracy of ±2%.

6. Flow Measurements

The minimum flowmeter division was 1% of 11.1 scfm or 0.111 scfm. This gives a scale precision of ±1.2% for the range measured. Precision in reading the float position especially with fluctuations during fluidization caused additional inaccuracies. As a result, the overall flow measurement was probably within ±5%.

7. Miscellaneous Measurements/Calculations

The following uncertainties were determined for various calculations/measurements required for data reduction by the method of Kline and McClintock.

a. A_c - ±1.5%.

b. G_f - ±5.7%.

c. ρ_f - ±2.4%.

d. Re - ±5.9%.

e. μ - ±1.0%.

APPENDIX H: EXPERIMENTAL DATA

The following temperature and pressure data was recorded during experimental runs of the fluidized bed apparatus.

1. Pressure Data - Run #1

   a. Static Bed Height - 12.5 inches.

   b. Static Bed Width - 6.25 inches.

   c. Air Inlet Cross-Sectional Area - 37.5 in^2.

   d. Bed Pressure/Gas Mass Flow Data - See Table 1.

   e. Comments -

      (1) Channeling observed to start at the edges of the bed at an air flow of 8.88 scfm.

      (2) Fluidization of the bed commenced at an air flow of 9.66 scfm.

      (3) Bed expansion during fluidization was 0.125-0.375 inch.

2. Pressure Data - Run #2

   a. Static Bed Height - 12.5 inches.

   b. Static Bed Width - 8.0 inches.

   c. Air Inlet Cross-Sectional Area - 48.0 in^2.

   d. Bed Pressure/Gas Mass Flow Data - See Table 2.

   e. Comments -

      (1) Channeling observed to start at the edges of the bed at an air flow of 9.44 scfm.

      (2) Fluidization of the bed commenced at an air

flow of 11.32 scfm.

(3) Bed expansion during fluidization was 0.125-0.375 inch.

3. Pressure Data - Run #3

a. Static Bed Height - 12.5 inches.

b. Static Bed Width - 10.0 inches.

c. Air Inlet Cross-Sectional Area - 60.0 in^2.

d. Bed Pressure/Gas Mass Flow Data - See Table 3.

e. Comments -

(1) Channeling observed at the corners of the bed at an air flow of 10.55 scfm.

(2) Channeling observed along the walls and occasionally in the bed at an air flow of 11.66 scfm.

(3) Fluidization of the bed commenced at an air flow of 12.77 scfm.

(4) Bed expansion during fluidization was 0.25 inch.

4. Pressure Data - Run #4

a. Static Bed Height - 12.5 inches.

b. Static Bed Width - 12.0 inches.

c. Air Inlet Cross-Sectional Area - 72.0 in^2.

d. Bed Pressure/Gas Mass Flow Data - See Table 4.

e. Comments -

(1) Channeling observed at the corners of the bed at an air flow of 11.66 scfm.

(2) Channeling commenced in the main part of

the bed at an air flow of 12.77 scfm.

(3) Fluidization of the bed commenced at an air flow of 15.00 scfm.

(4) Bed expansion during fluidization was 0.25 inch.

5. Temperature Data - Run #1

a. Static Bed Height - 12.5 inches.

b. Static Bed Width - 6.25 inches.

c. Air Inlet Cross-Sectional Area - 37.5 in^2.

d. Average Air Inlet Temperature - 108^0 F $\pm 2.5^0$ F.

e. Constant Air Outlet Air Temperature - 125^0 F $\pm 0.4^0$ F.

f. Temperature Distribution Data - See Table 5.

6. Temperature Data - Run #2

a. Static Bed Height - 12.5 inches.

b. Static Bed Width - 12.0 inches.

c. Air Inlet Cross-Sectional Area - 72.0 in^2.

d. Average Air Inlet Temperature - 116^0 F $\pm 2.0^0$ F.

e. Constant Air Outlet Air Temperature - 129.5^0 F $\pm 0.7^0$ F.

f. Temperature Distribution Data - See Table 6.

Pressure Below Distributor (in H_2O)	Pressure Above Distributor (in H_2O)	Air Flow (scfm)	Average Inlet Air Temp (^{0} F)	Air Δp (in H_2O)	log Δp	Gas Mass Velocity (lbm/hr-ft^2)	log G
6.48	5.98	3.77	73.8	6.48	0.81	64.79	1.81
8.38	7.75	4.88	77.6	8.38	0.92	83.20	1.92
10.60	9.80	5.99	81.5	10.60	1.03	101.31	2.01
12.25	11.45	7.22	89.1	12.25	1.09	120.43	2.08
16.35	15.20	8.33	96.0	16.35	1.21	137.41	2.14
17.80	16.30	8.88	100.9	17.80	1.25	145.27	2.16
17.10	16.10	9.66	106.4	17.10	1.23	156.46	2.19

Table 1. Bed Pressure/Gas Mass Flow Data (A_c = 37.5 in^2).

Pressure Below Distributor (in H_2O)	Pressure Above Distributor (in H_2O)	Air Flow (scfm)	Average Inlet Air Temp (^{0} F)	Air Δp (in H_2O)	log Δp	Gas Mass Velocity (lbm/hr-ft^2)	log G
5.90	5.50	3.89	75.2	5.90	0.77	52.05	1.72
7.55	7.00	5.00	78.8	7.55	0.88	66.38	1.82
9.55	8.95	6.11	82.0	9.55	0.98	80.65	1.91
10.90	10.05	7.22	86.2	10.90	1.04	94.62	1.98
13.80	12.75	8.33	91.0	13.80	1.14	108.27	2.03
15.80	14.90	9.44	93.1	15.80	1.20	122.25	2.09
17.75	16.70	10.55	95.9	17.75	1.25	135.97	2.13
16.60	15.50	11.32	101.5	16.60	1.22	144.46	2.16

Table 2. Bed Pressure/Gas Mass Flow Data (A_c = 48.0 in^2).

Pressure Below Distributor (in H_2O)	Pressure Above Distributor (in H_2O)	Air Flow (scfm)	Average Inlet Air Temp (^{0} F)	Air Δp (in H_2O)	log Δp	Gas Mass Velocity (lbm/hr-ft^2)	log G
5.15	4.78	3.77	78.1	5.15	0.71	40.10	1.60
6.60	6.15	5.00	80.1	6.60	0.82	52.95	1.72
8.35	7.70	6.11	82.4	8.35	0.92	64.48	1.81
9.55	8.75	7.22	87.1	9.55	0.98	75.58	1.88
11.20	10.45	8.33	92.0	11.20	1.05	86.47	1.94
13.20	12.35	9.44	97.2	13.20	1.12	97.11	1.99
15.30	14.25	10.55	99.1	15.30	1.18	108.17	2.03
18.20	16.85	11.66	103.4	18.20	1.26	118.64	2.07
17.35	16.40	12.77	109.7	17.35	1.24	128.49	2.11

Table 3. Bed Pressure/Gas Mass Flow Data ($A_c = 60.0$ in^2).

Pressure Below Distributor (in H_2O)	Pressure Above Distributor (in H_2O)	Air Flow (scfm)	Average Inlet Air Temp (^{0} F)	Air Δp (in H_2O)	log Δp	Gas Mass Velocity (lbm/hr-ft^2)	log G
4.50	4.20	3.89	80.1	4.50	0.65	34.33	1.54
6.05	5.60	5.00	81.2	6.05	0.78	44.06	1.64
7.45	6.90	6.11	82.7	7.45	0.87	53.71	1.73
8.80	8.10	7.22	85.9	8.80	0.94	63.11	1.80
10.25	9.40	8.21	90.9	10.25	1.01	71.16	1.85
12.05	11.10	9.44	96.1	12.05	1.08	81.08	1.91
13.25	12.75	10.55	99.5	13.25	1.12	90.08	1.95
15.25	14.20	11.66	103.0	15.25	1.18	98.93	2.00
16.60	15.40	12.77	108.0	16.60	1.22	107.39	2.03
18.00	16.85	13.88	113.1	18.00	1.26	115.68	2.06
17.55	16.55	15.00	117.8	17.55	1.24	123.96	2.09

Table 4. Bed Pressure/Gas Mass Flow Data (A_c = 72.0 in^2).

Probe Grid Number	Height Above Distributor Plate (in)												
	0.0	0.125	0.25	0.375	0.5	1.0	1.5	2.0	4.0	6.0	8.0	10.0	12.0
41	118.5	125.5	125.3	125.5	125.1	125.2	125.0	125.2	125.1	125.2	125.0	125.1	125.2
42	121.1	121.3	124.3	125.5	124.8	125.0	124.8	124.8	124.9	125.3	125.1	124.9	125.0
43	113.5	119.6	122.6	124.9	124.0	124.2	124.4	125.0	124.9	125.1	124.9	125.3	124.8
44	113.3	121.1	123.6	124.0	124.5	124.3	124.6	124.8	125.0	125.2	124.7	125.0	125.1
45	114.4	116.6	122.6	124.3	123.5	124.6	124.6	124.7	125.1	125.2	125.0	124.9	124.9
46	117.2	120.1	123.0	124.9	125.0	126.0	125.0	125.2	124.9	125.3	125.4	125.1	125.0
47	123.1	123.0	123.7	124.7	124.5	124.7	124.9	125.0	125.3	125.3	124.9	125.2	125.1

Table 5. Temperature Distribution (A_c = 37.5 in^2).

Probe Grid Number	Height Above Distributor Plate (in)												
	0.0	0.125	0.25	0.375	0.5	1.0	1.5	2.0	4.0	6.0	8.0	10.0	12.0
41	116.2	120.1	125.3	129.1	128.7	129.1	128.7	128.9	129.2	129.4	129.3	129.1	129.0
42	120.3	121.5	126.7	128.1	128.4	129.7	128.4	129.4	129.1	128.9	130.1	129.2	129.5
43	117.4	122.7	127.4	128.7	129.1	128.8	129.4	129.0	129.2	128.9	128.9	129.3	129.1
44	119.4	123.5	125.8	126.1	128.3	128.8	129.1	128.8	129.5	129.8	128.9	129.5	129.8
45	121.3	125.3	128.1	128.4	128.7	129.1	129.3	129.0	128.8	129.4	129.3	129.0	129.1
46	119.0	123.1	125.7	128.7	129.1	129.4	130.1	129.7	129.8	130.0	129.7	129.7	129.8
47	118.4	124.2	124.9	128.1	128.9	129.2	129.9	129.7	130.0	129.2	129.8	129.7	130.1
48	121.1	126.1	127.4	129.1	129.3	128.9	129.4	129.3	128.9	129.1	129.4	129.3	129.7
49	116.7	121.4	127.1	128.3	129.1	129.0	130.2	129.8	129.7	129.5	129.7	129.4	129.6
50	115.4	121.7	129.0	129.1	128.9	129.5	129.7	129.5	129.9	129.1	129.4	129.3	129.7
51	118.3	123.5	128.1	128.7	128.7	129.3	129.9	129.9	130.1	129.6	129.7	129.9	129.8
52	118.3	122.8	127.4	129.1	129.1	129.1	129.0	129.5	129.6	130.0	129.5	129.7	129.9
53	118.8	126.1	128.1	128.7	129.5	129.3	129.7	129.6	130.0	129.9	129.3	129.7	129.9
54	118.7	125.1	128.0	128.8	129.1	129.5	129.3	129.9	129.9	129.6	129.8	129.9	130.0
55	121.0	127.1	127.8	129.1	129.3	129.1	129.4	129.1	129.5	129.4	129.7	129.6	129.6

Table 6. Temperature Distribution (A_c = 72.0 in^2).

LIST OF REFERENCES

1. Agarwal, O.P. and Storrow, J.A., "Pressure Drop in Fluidization Beds," Society of Chemical Industry, v. 15, p. 278-286, April 1951.

2. Andeen, B.R. and Glicksman, L.R., Heat Transfer to Horizontal Tubes in Shallow Fluidized Beds, paper presented at ASME-AIChE Heat Transfer Conference, St. Louis, Missouri, 9-11 August 1976.

3. Baerg, A., Klassen, J. and Gishler, P.E., "Heat Transfer in Fluidized Solids Bed," Canadian Journal of Research Section F, v. 28, p. 287-307, August 1950.

4. Bartel, W.J., Genetti, W.E. and Grimmett, E.S., "Heat Transfer From a Horizontal Discontinuous Finned Tube in a Fluidized Bed," American Institute of Chemical Engineers Symposium Series Number 116, v. 67, p. 85-89, 1971.*

5. Bartholomew, R.N. and Katz, D.L., "Heat Transfer from Wall of Tube to Fluidized Bed," Chemical Engineering Progress Symposium Series Number 4, v. 48, p. 3-10, 1952.

6. Botterill, J.S.M., Fluid-Bed Heat Transfer, Academic Press, 1975.

7. Brazelton, W.T., Heat Transfer Studies in Fluidized Bed Region of Gas-Solid Systems, Ph.D. Thesis, Northwestern University, Evanston, Illinois, 1951.

8. Chechetkin, A.V., "High Temperature Carriers," Gosenergoizdat, 1962.*

9. Chekansky, V.V., Sheindlin, B.S., Galershtein, D.M. and Antonyuk, K.S., Tr. Spets. Konstr. Byuro Avtomat. Neftepererab Neftekhim, v. 3, p. 143, 1970.*

10. Chen, J.C. and Withers, J.G., "An Experimental Study of Heat Transfer from Plain and Finned Tubes in Fluidized Beds," American Institute of Chemical Engineers Symposium Series Number 174, v. 74, p. 327-333, 1978.

---

*Indicates supplementary reference.

11. Das, C.N. and Sarkar, S., "Heat Transfer in Dilute-Phase Fluidized Bed," Indian Journal of Technology, v. 5, p. 276-279, September 1967.

12. Davidson, J.F. and Harrison, D., Fluidized Particles, Cambridge University Press, 1963.

13. Dow, W.M. and Jakob, M., "Heat Transfer Between a Vertical Tube and a Fluidized Air-Solid Mixture," Chemical Engineering Progress, v. 47, p. 637-648, December 1951.

14. Einstein, V.G. and Gelperin, N.I., "Heat Transfer Between a Fluidized Bed and a Surface," International Chemical Engineering, v. 6, p. 67-73, January 1966.

15. Ergun, S. and Orning, A.A., "Fluid Flow through Randomly Packed Columns and Fluidized Beds," Industrial and Engineering Chemistry, v. 41, p. 1179-1184, June 1949.*

16. Frantz, J.F., "Minimum Fluidization Velocities and Pressure Drop in Fluidized Beds," Chemical Engineering Progress Symposium Series Number 62, v. 62, p. 21-31, 1966.

17. Gamson, B.W., "Heat and Mass Transfer - Fluid Solid Systems,"Chemical Engineering Progress, v. 47, p. 19-28, January 1951.

18. Gelperin, N.I. and Einstein, V.G., in Fluidization, (ed.) Davidson, J.F. and Harrison, D., p. 517-540, Academic Press, 1971.

19. Gelperin, N.I., Einstein, V.G. and Korotyanskaya, L.A., "Heat Transfer Between a Fluidized Bed and Staggered Bundles of Horizontal Tubes," International Chemical Engineering, v. 9, p. 137-142, January 1969.

20. Gelperin, N.I., Kruglikov, V.Y. and Einstein, V.G., Khimicheskaya Promyshlennost, v. 6, p. 358, 1958.*

21. Gelperin, N.I., Einstein, V.G. and Romanova, N.A., "Hydraulics and Heat Exchange in Fluidized Bed with Bundles of Vertical Pipes," Khimicheskaya Promyshlennost, v. 11, p. 23-30, November 1963.*

22. Gelperin, N.I., Einstein, V.G. and Zaikovski, A.V., Khimicheskoe Mashinostroenie, v. 3, p. 17, 1968.*

23. Genetti, W.E., Schmall, R.A. and Grimmett, R.A., "The Effect of Tube Orientation on Heat Transfer with Bare and Finned Tubes in a Fluidized Bed," American Institute of Chemical Engineers Symposium Series Number 116, v. 67, p. 90-96, 1971.

24. Glass, D.H. and Harrison, D., "Flow Patterns Near a Solid Obstacle in a Fluidized Bed," Chemical Engineering Science, v. 19, p. 1001-1002, December 1964.

25. Graf, E., Eidgenossische Technische Hochschule, Ph.D. Thesis, Zurich, Switzerland, 1955.*

26. Graf, E., Guyer, A. Jr. and Guyer, A., Helv. Chim. Acta., v. 28, p. 473-484, 1955.*

27. Grohse, E.W., "Analysis of Gas-Fluidized Solid Systems by X-ray Absorption," American Institute of Chemical Engineers Journal, v. 1, p. 358-365, September 1955.

28. Gutfinger, C. and Abuaf, N., "Heat Transfer in Fluidized Beds," Advances in Heat Transfer, v. 10, p. 167-218, Academic Press, 1974.

29. Huntsinger, R.C., "A Heat Transfer Correlation for Bed to Wall Heat Transfer in Gas-Solid Fluidized-Beds," Proceedings of South Dakota Academy of Science, v. 46, p. 185-201, 1967.

30. Jacob, A. and Osberg, G.L., "Effect of Gas Thermal Conductivity on Local Heat Transfer in a Fluidized Bed," Canadian Journal of Chemical Engineering, v. 35, p. 5-9, June 1957.

31. Korolev, V.N. and Syromyatnikov, N.I., "Heat Transfer From a Surface with Artificial Roughness to a Fluidized Bed," Journal of Engineering Physics, v. 28, p. 698-700, June 1975.

32. Krause, W.B., An Investigation of the Heat Transfer Mechanisms Around Horizontal Bare and Finned Heat Exchange Tubes Submerged in an Air Fluidized Bed of Uniformly Sized Particles, Ph.D. Thesis, University of Nebraska, Lincoln, Nebraska, 1978.

33. Kruglikov, V.Y., Dissertation, Mosk. Neft. Institute, 1951.*

34. Kunii, D. and Levenspiel, O., Fluidization Engineering, Wiley, 1969.

35. Lemlich, R. and Caldas, I. Jr., "Heat Transfer to a Liquid Fluidized Bed," American Institute of Chemical Engineers Journal, v. 4, p. 376-380, September 1958.

36. Leva, M., Fluidization, McGraw-Hill, 1959.

37. Leva, M. and Grummer, M., "A Correlation of Solids Turnover in Fluidized Systems - Its Relation to Heat Transfer," Chemical Engineering Progress, v. 48, p. 307-312, June 1952.

38. Leva, M., Grummer, M., Weintraub, M. and Pollchik, M., "Introduction to Fluidization," Chemical Engineering Progress, v. 44, p. 511-520, July 1948.

39. Leva, M., Grummer, M., Weintraub, M. and Pollchik, M., "Fluidization of Solid Non-Vesicular Particles," Chemical Engineering Progress, v. 44, p. 619-626, August 1948.

40. U.S. Bureau of Mines Bulletin 504, Fluid Flow Through Packed and Fluidized Systems, by Leva, M., Grummer, M., Weintraub, M., Pollchik, M. and Storch, H.H., p. 1-149, 1951.

41. Levenspiel, O. and Walton, J.S., "Bed-Wall Heat Transfer in Fluidized Systems," Chemical Engineering Progress Symposium Series Number 9, v. 50, p. 1-13, 1954.

42. Lewis, W.K., Gilliland, E.R. and Bauer, W.C., "Characteristics of Fluidized Particles," Industrial and Engineering Chemistry, v. 41, p. 1104-1117, June 1949.

43. Marsheck, R.M., A Study of Solid Particle Flow Patterns in a Fluidized Bed Using a Modified Thermistor Anemometer Probe, Ph.D. Thesis, University of Maryland, College Park, Maryland, 1962.

44. Maskayek, V.K. and Baskakov, A.P., "Characteristics of External Heat Transfer in a Fluidization Bed of Coarse Particles," Journal of Engineering Physics, v. 24, p. 411-414, 1973.

45. Massimilla, L. and Bracale, S., Ricerca Science, v. 26, p. 487, 1956.*

46. Matheson, G.L., Herbst, W.A. and Holt, P.H. 2ND, "Characteristics of Fluid-Solid Systems," Industrial and Engineering Chemistry, v. 41, p. 1099-1104, June 1949.

47. Mickley, H.S. and Fairbanks, D.F., "Mechanism of Heat Transfer to Fluidized Beds," American Institute of Chemical Engineers Journal, v. 1, p. 374-384, September 1955.

48. Mickley, H.S. and Trilling, T.A., "Heat Transfer Characteristics of Fluidized Beds," Industrial and Engineering Chemistry, v. 41, p. 1135-1147, June 1949.

49. Miller, C.O. and Logwinuk, A.K., "Fluidization Studies of Solid Particles," Industrial and Engineering Chemistry, v. 43, p. 1220-1226, May 1951.

50. Morse, R.D., "Fluidization of Granular Solids - Fluid Mechanics and Quality," Industrial and Engineering Chemistry, v. 41, p. 1117-1124, June 1949.

51. Olin, H.L. and Dean, O.C., "Heat Transfer and Fouling of Fluidized Beds," The Petroleum Engineer, v. 25, p. C23-C32, March 1953.*

52. Parent, J.D., Yagol, N. and Steiner, C.S., "Fluidizing Processes - Basic Observations from Laboratory Equipment," Chemical Engineering Progress, v. 43, p. 429-436, August 1947.

53. U.S. Atomic Energy Commission Report ANL-7353, by Patel, R.D., 1967.*

54. Petrie, J.C., Freeby, W.A. and Buckham, J.A., "In-Bed Heat Exchangers," Chemical Engineering Progress, v. 64, p. 45-51, July 1968.

55. Pillai, K.K., "Heat Transfer to a Sphere Immersed in a Shallow Fluidized Bed," Letters in Heat and Mass Transfer, v. 3, p. 131-145, March 1976.

56. Rao, S.P. and Kaparthi, R., "Heat Transfer in Semi-Fluidized Beds," Transactions Indian Institute of Chemical Engineering, p. 43-46, April 1969.

57. Richardson, J.F. and Mitson, A.E., "Sedimentation and Fluidization Part II - Heat Transfer from a Tube Wall to a Liquid-Fluidized System," Transactions Institution of Chemical Engineers, v. 36, p. 270-282, August 1958.

58. Rukenshtein, E., Zhurnal Prikladnoi Khimii, v. 35, p. 71, 1962.*

59. Rukenshtein, E., Heat Transfer Between a Non-Homogeneous Fluidized Bed, paper presented at Third International Heat Transfer Conference, Chicago, Illinois, 7-12 August 1966.*

60. Sarkits, V.B., Dissertation, LTI im. Lensoveta, 1959.*

61. Saxena, S.C., Grewal, N.S. and Gabor, J.D., "Heat Transfer Between a Gas Fluidized Bed and Immersed Tubes," Advances in Heat Transfer, v. 14, p. 149-247, Academic Press, 1978.

62. Toomey, R.D. and Johnstone, H.F., "Heat Transfer Between Beds of Fluidized Solids and Walls of Container," Chemical Engineering Progress Symposium Series Number 5, v. 49, p. 51-63, 1953.

63. Traber, D.B., Pomerantsev, V.M., Mukhlenov, I.P. and Sarkin, V.B., Zhurnal Prikladnoi Khimii, v. 35, p. 2386, 1962.*

64. Trivedi, R.C. and Rice, W.J., "Effect of Bed Depth, Air Velocity, and Distributor on Pressure Drop in an Air-Fluidized Bed," Chemical Engineering Progress Symposium Series Number 67, v. 62, p. 57-63, 1966.

65. van Heerden, C., Nobel, A.P.P. and van Krevelen, D.W., "Studies on Fluidization I - The Critical Mass Velocity," Chemical Engineering Science, v. 1, p. 37-49, October 1951.

66. van Heerden, C., Nobel, A.P.P. and van Krevelen, D.W., "Mechanism of Heat Transfer in Fluidized Beds," Industrial and Engineering Chemistry, v. 45, p. 1237-1242, June 1953.

67. Varygin, N.N. and Martyushin, I.G., Khimicheskoe Mashinostroenie, v. 5, p. 6, 1959.*

68. Vijayaraghavan, M.R. and Sastri, V.M.K., "Effect of Surface Roughness on Heat Transfer in Fluidized Beds," Future Energy Production - Heat and Mass Transfer Processes, v. 2, p. 571-578, 1976.

69. Vreedenberg, H.A., "Heat Transfer Between Fluidized Beds and Vertically Inserted Tubes," Journal of Applied Chemistry, v. 2, Supp. 1, p. S26-S33, 1952.

70. Vreedenberg, H.A., "Heat Transfer Between a Fluidized Bed and a Horizontal Tube," Chemical Engineering Science, v. 9, p. 52-60, August 1958.

71. Vreedenberg, H.A., "Heat Transfer Between a Fluidized Bed and a Vertical Tube," Chemical Engineering Science, v. 11, p. 274-285, January 1960.

72. Wen, C.Y. and Leva, M., "Fluidized-Bed Heat Transfer: A Generalized Dense-Phase Correlation," American Institute of Chemical Engineers Journal, v. 2, p. 482-488, December 1956.

73. Wen, C.Y. and Yu, Y.H., "Mechanics of Fluidization," Chemical Engineering Progress Symposium Series Number 62, v. 62, p. 100-111, 1966.

74. Wender, L. and Cooper, G.T., "Heat Transfer Between Fluidized-Solids Beds and Boundary Surfaces - Correlation of Data," American Institute of Chemical Engineers Journal, v. 4, p. 15-23, March 1958.

75. Wicke, E. and Fetting, F., "Heat Transfer in Turbulent Gas Flow," Chemie-Ingenieur-Technik, v. 26, p. 301-309, June 1954.

76. Wilhelm, R.H. and Kawauk, M., "Fluidization of Solid Particles," Chemical Engineering Progress, v. 44, p. 201-218, March 1948.

77. Yoshida, K., Ueno, T. and Kunii, D., "Mechanism of Bed-Wall Heat Transfer in a Fluidized Bed at High Temperatures," Chemical Engineering Science, v. 29, p. 77-82, January 1974.

78. Zabrodsky, S.S., "Hydrodynamics and Heat Transfer in Fluidized Beds," Gosenergoizdat, 1963, (English translation by Zenz, F.A., MIT Press, Cambridge, Massachusetts, 1966).

79. Zabrodsky, S.S., "Compound Heat Exchange Between a High Temperature Gas-Fluidized Bed and a Solid Surface," International Journal of Heat and Mass Transfer, v. 16, p. 241-247, February 1973.*

80. Zenz, F.A. and Othmer, D.F., Fluidation and Fluid Particle Systems, Reinhold, New York, 1960,*

INITIAL DISTRIBUTION LIST

		No. Copies
1.	Defense Technical Information Center Cameron Station Alexandria, Virginia 22314	2
2.	Library, Code 0142 Naval Postgraduate School Monterey, California 93940	2
3.	Department Chairman, Code 69 Department of Mechanical Engineering Naval Postgraduate School Monterey, California 93940	1
4.	Professor P.F. Pucci, Code 69Pc Department of Mechanical Engineering Naval Postgraduate School Monterey, California 93940	2
5.	Lieutenant Commander Michael C. Morgan 2305 Ahakapu Street Pearl City, Hawaii 96782	1

Thesis
M822655 Morgan
c.1

192540

Particle flow cell formation at minimum fluidization flow rates in a rectangular gas-fluidized bed.